

國立交通大學
材料科學與工程研究所
博士論文

利用微波加熱法純化奈米碳管與在碳管
上合成白金觸媒之探討

Investigation of Purification of Carbon Nanotubes
and Synthesis of Pt Catalysts on Carbon Nanotubes
by Using Microwave Heating Method

研 究 生：陳 建 銘

指 導 教 授：陳 家 富 博 士

呂 志 鵬 博 士

中 華 民 國 九 十 七 年 一 月

利用微波加熱法純化奈米碳管與在碳管上
合成白金觸媒之探討

Investigation of Purification of Carbon Nanotubes and
Synthesis of Pt Catalysts on Carbon Nanotubes by Using
Microwave Heating Method

研究生：陳建銘 Student: Chieng-ming Chen
指導教授：陳家富 博士 Advisor: Dr. Chia-Fu Chen
 呂志鵬 博士 and Dr. Jihperng Leu

國立交通大學
材料科學與工程研究所
論文初稿

A Thesis

Submitted to Institute of Materials Science and Engineering
College of Engineering

National Chiao Tung University

In Partial Fulfillment of the Requirements

For the Degree of Doctor of Philosophy

In Materials Science and Engineering

January 2008

Hsinchu, Taiwan, Republic of China

中華民國九十七年一月

利用微波加熱法純化奈米碳管與在碳管上 合成白金觸媒之探討

研究生：陳建銘

指導教授：陳家富、呂志鵬 博士

國立交通大學

材料科學與工程研究所

摘 要

奈米碳管具有獨特且優異的化學及物理特性，深具潛力應用於各個領域，例如：場發射顯示器、儲氫材料、化學感測器、奈米電子元件與複合材料等。合成奈米碳管主要的方法有：雷射蒸發法、電弧法與化學氣相沉積法，在這些方法中，過渡金屬(Fe, Co, Ni)常用來作為奈米碳管之成長之觸媒，觸媒存在奈米碳管中會降低奈米碳管的應用特性，本研究論文利用微波輔助酸處理製程去除多層管壁奈米碳管中之金屬觸媒。多層管壁奈米碳管試樣先經過超音波震盪分散後，再以微波輔助消化系統酸處理去除金屬觸媒，研究結果顯示，以熱重分析儀量測純化前後奈米碳管中殘存之金屬觸媒量。在 5M 硝酸中，微波消化 15 分鐘，金屬觸媒含量可由 10.39 wt% 快速減低至 1.52 wt%。利用穿透式電子顯微鏡來觀察純化前後碳管的結構與金屬觸媒，而拉曼光譜儀則探討奈米碳管之鍵結特性。結果顯示，硝酸可以快速吸收微波之熱與能，可以避免因碳管長時間浸泡於酸溶液中，而對管壁所造成的破壞，進而達到快速純化奈米碳管。另外，本論文研究並探討使用微波聚醇法有效且快速被覆白金粒子於奈米碳管上。結果顯示，添加分散劑與保護劑使白金粒子均勻有效被覆於奈米碳管表面，先對奈米碳管進行純化步驟，再利用微波聚醇法以使具有氯鉑酸之乙二醇溶液內之白金觸媒粒子被覆在奈米碳管上。為了快速形成具有高密度且均勻被覆白金粒子的奈米碳管，添加適當聚乙炔吡咯烷酮 (Polyvinylpyrrolidone, PVP) 與十二烷基硫酸鈉 (Sodium Dodecyl Sulfate, SDS) 當界

面活性劑與分散劑，結果顯示微波聚醇法所合成之白金粒子約 4.1nm，其粒徑分佈集中且均勻分散於奈米碳管表面。添加 SDS 可達到有效分散奈米碳管表面白金粒子，而不會產生聚集現象。微波聚醇法所需反應時間約 1.5min，白金被覆量約 54 wt%，所以微波聚醇法添加 SDS、PVP 可有效且快速均勻被覆白金粒子於奈米碳管上。



Investigation of Purification of Carbon Nanotubes and Synthesis of Pt Catalysts on Carbon Nanotubes by Using Microwave Heating Method

Student: Chieng-Ming Chen


Advisor: Dr. Chia-Fu Chen

and Dr. Jihperng Leu

Institute of Materials Science and Engineering

National Chiao Tung University

Abstract

The logo of National Chiao Tung University is a circular emblem with a gear-like border. Inside the circle, there is a stylized representation of a building or industrial structure, and the year '1896' is inscribed at the bottom.

Carbon nanotubes (CNTs) have excellent and unique performances and versatile applications, such as field emission display, hydrogen storage, chemical sensor, nano-electronic devices and composite materials. High-quality and well-aligned carbon nanotubes are essential to the potential applications. The synthesis methods of CNTs are arc-discharge, laser vaporization, and chemical vapor deposition. Transition metal (Fe, Co, Ni) are known to be catalysts for vapor grown CNTs synthesis. CNTs may found their limited applications as they contain metal catalysts in tubes. In this thesis, microwave-assisted acidic treatment process is used to purify multi-walled carbon nanotubes. Ultrasonic shaking was first applied to disperse CNTs samples. A acidic treatment with microwave-assisted digestion system was then used to dissolve metal catalysts. The result indicated that the amounts of catalyst metals reduced from 10.39 wt% to 1.52 wt% within 15 min of microwave digestion acid treatment with 5 M HNO₃. A thermo-gravimetric analysis (TGA) was used to estimate the amount of catalyst metal in CNTs. The structure of carbon nanotubes and catalyst before/after

purification is characterized and TEM. The bonding characteristics of CNTs are studied by using a Raman spectrometer. That HNO_3 can rapidly absorb microwave heat and energy to shorten the acid treatment time prevents the structures of CNTs from destruction. A high-yield of multi-walled carbon nanotubes with high purity is then obtained.

In the second part of the thesis, CNTs are first purified by microwave digestion and Pt nanoparticles in ethylene glycol solution with Pt precursor (H_2PtCl_6) are coated on CNTs by microwave polyol process. In order to briskly synthesize uniform Pt nanoparticles of high density dispersed on CNTs, poly(vinylpyrrolidone) (PVP) and sodium dodecyl sulfate (SDS) are adequately added in mixture reactants to act as the protective reagents and dispersants. The results show that Pt nanoparticles with narrow distribution and suitable diameter of about 4.1 nm were highly dispersed and loaded on the surface of CNTs by microwave digestion method. SDS was added to increase the dispersion of Pt on CNTs and to reduce the aggregation phenomenon. The microwave polyol processing duration was below 1.5min and the loading amount of Pt on CNTs was about 52 wt%. Pt nanoparticles can be uniformly and rapidly dispersed on CNTs by microwave polyol process with the addition of SDS and PVP.

致 謝

本論文能順利完成，要感謝的人實在太多了，首先感謝我的指導教授陳家富老師，陳老師在論文研究上的指導與鼓勵，使得這篇論文能順利完成。更重要的是陳老師對學生的照顧與愛護，讓我得以順利完成學業，開拓未來更寬廣的道路。感謝博士論文審查委員汪大永老師、薛富盛老師、張立老師、呂志鵬老師、陳密老師及許鈺宗老師對於本論文的指導與寶貴的建議，在此由衷的表示感謝。

接著要感謝如同家人們的實驗室同仁，感謝陳密學姐、林建良學長、蔡佳倫學長、施士塵學長、陳建仲學長、彭若慈學姐、吳良科學長等在研究上提供的建議與協助。感謝羅鴻鈞、許智勛、徐振航、王滋銘、曾靜怡同學以及施騰凱、劉厥揚、洪淙琦、王瑞豪學弟與李依璇學妹等實驗室的學弟妹們，不僅在研究上熱情相助，在校園生活中也留下許多寶貴的回憶與歡熱。另外感謝林智偉、蘇俊璋、胡晟民、林高照等由大學部至今的同學，感謝你們在實驗上的幫助。並感謝明新科技大學化學工程系的彭永旺、游宏偉學弟等在研究上的努力。

同時也感謝國科會在經費上的補助，國家奈米元件實驗室及交大奈米科技中心在分析設備上的支持。以及明新科技大學陳密老師允借的實驗設備，讓本論文能夠順利完成。

最後，我要感謝我的家人及親戚們在這段時間所給予的支持與鼓勵，感謝兄長陳木豪無私的付出支撐經濟重擔讓我無後顧之憂。僅以此論文獻給我最愛的親人與在天國的母親。

Contents

Abstract (Chinese).....	I
Abstract (English).....	II
Acknowledgement.....	V
Contents.....	VI
Table Captions.....	IX
Figure Captions.....	X
Chapter 1 Introduction.....	1
1.1 Carbon nanotubes.....	1
1.1.1 Structure and properties of carbon nanotubes.....	2
1.1.1.1 Structure of carbon nanotubes.....	2
1.1.1.2 Electronic properties of carbon nanotubes.....	4
1.1.1.3 Mechanical properties carbon nanotubes.....	7
1.1.2 Applications of carbon nanotubes.....	8
1.1.2.1 Energy storage.....	8
1.1.2.2 Hydrogen storage.....	9
1.1.2.3 Lithium intercalation.....	9
1.1.2.4 Electrochemical supercapacitors.....	10
1.1.2.5 Field emitting devices.....	10
1.1.2.6 Transistors.....	11
1.1.2.7 Nanoprobes and sensors.....	11
1.1.2.8 Composite materials.....	12
1.1.2.9 Templates.....	14
1.1.3 Carbon nanotube synthesis.....	14
1.1.3.1 Arc discharge.....	14
1.1.3.2 Laser ablation.....	15
1.1.3.3 Catalytic chemical vapor deposition (CVD).....	16
1.1.3.4 Catalytic growth mechanisms of carbon nanotubes.....	17
1.2 Fuel cell.....	18
1.2.1 Classification of fuel cells.....	19
1.2.1.1 Polymer electrolyte membrane fuel cell.....	20
1.2.1.2 Phosphoric acid fuel cell.....	21
1.2.1.3 Alkaline fuel cell.....	21
1.2.1.4 Molten carbonate fuel cell.....	22
1.2.1.5 Solid oxide fuel cell.....	23

1.2.2 Potential of direct methanol fuel cell	24
1.3 Microwave Chemistry	27
1.3.1 Microwave-assisted synthesis of metallic nanostructures	27
1.3.2 Possible effects of MW heating	29
1.3.2.1 Thermal effects	29
1.3.2.2 Effects of hot spots and hot surfaces.....	30
1.3.2.3 Superheating	30
1.3.2.4 Non-thermal effects	30
1.4 Motivation of this thesis.....	30
Chapter 2 Literature Review	34
2.1 Purification of carbon nanotubes	34
2.1.1 Thermal oxidation	34
2.1.2 Microfiltration and ultrasonically assisted filtration.....	34
2.1.3 Acid treatment.....	35
2.1.4 Thermal oxidation combined with acid treatment	36
2.2 Fundamental and structure of DMFC	37
2.2.1 The Proton Exchange Membrane (PEM).....	37
2.2.2 Electrodes Structure of DMFC	40
2.2.3 Anode structure and principle of DMFC	41
2.2.4 Cathode structure and principle of DMFC.....	42
2.2.5 Limits of DMFC	46
Chapter 3 Experimental Details.....	50
3.1 Experiment Procedures	50
3.1.1 Experiment flow chart of purification process.....	50
3.1.2 Experiment flow chart of Pt-synthesis process.....	51
3.2 Experiment equipments	52
3.2.1 Microwave system	52
3.3 Analysis instruments	53
3.3.1 Thermogravimetric Analyzer (TGA)	53
3.3.2 Scanning Electron Microscopy (SEM)	54
3.3.3 Transmission Electron Microscopy (TEM)	54
3.3.4 Raman Spectroscopy.....	55
3.3.5 Energy Dispersive X-ray Analysis (EDX).....	56
3.3.6 X-ray Diffraction (XRD)	56
3.3.7 Cyclic Voltammetry (CV)	57
Chapter 4 Purification of MWCNTs Using Microwave Heating Method	59
4.1 Purification of MWCNTs Synthesized by ECR-CVD.....	59
4.1.1 Sample Preparation and Experiment Procedures.....	59

4.1.2	Characterization of the Purified MWCNTs and Discussions	59
4.1.3	Summary	65
4.2	The effects of different experiment conditions on purification of MWCNTs	66
4.2.1	Experiment Conditions and Procedures	66
4.2.2	Characterizations of MWCNTs of various experiment conditions and discussions	67
4.2.3	Summary	76
4.3	Purification efficiency of multi-walled carbon nanotubes synthesized by thermal chemical vapor deposition	77
4.3.1	Experiment condition and procedures	77
4.3.2	Characterizations and discussion	77
4.3.3	Summary	83
4.4	Reaction Model of Microwave-Assisted Purification of MWCNTS.....	84
4.4.1	TEM analysis and tube opening.....	84
4.4.2	TGA analysis and purification efficiency	87
4.4.3	Microwave assisted technique and reaction model.....	88
4.4.4	Summary	93
Chapter 5	Coating Pt Particles on CNTs as DMFC Electrode Using Microwave Heating Method	95
5.1	Experiment Procedures to Synthesize Pt Catalyst on MWCNTs.....	95
5.2	The effects of solutions on Pt particles synthesis	96
5.3	The effect of PVP molecular weight on particle size and dispersion.....	107
5.4	The Effect of SDS on Pt particle dispersion	110
5.5	The effect of temperature on loading amount of Pt	119
5.6	The effect of time on Pt loading amount.....	128
5.7	Electrochemical properties of Pt/MWCNTs electrode	140
5.8	Conclusions of Microwave-assisted synthesis Pt/MWCNTs electrode.....	142
Chapter 6	Conclusions	143
References	145

Table Captions

Table 1-1 Isomers of carbon	2
Table 1-2 Mechanical properties of CNTs compared with other Materials	8
Table 1-3 Comparisons of various fuel cells.....	24
Table 1-4 Physical parameters of typical solvents used for microwave heating ...	29
Table 4-1 Experiment condition of nitric acid concentration, sonication time, and microwave-assisted purification time	66
Table 5-1 Summary of the experiment conditions	96



Figure Captions

Fig. 1-1 Isomers of carbon: diamond, fullerene, graphite, and CNTs	1
Fig. 1-2 Models of different CNTs structures	3
Fig. 1-3 TEM pictures of the ends of (a) a SWCNT, (b) a closed MWCNT, and (c) an open MWCNT. Each black line corresponds to one graphene sheet viewed edge-on	4
Fig. 1-4 Schematic diagram showing how a hexagonal sheet of graphite is rolled to form a CNT.....	5
Fig. 1-5 A single semi-conducting nanotube is contacted by two electrodes. The Si substrate, which is covered by a layer of SiO ₂ 300nm thick, acts as a back-gate	11
Fig. 1-6 Use of a MWNT as AFM tip. VGCF stands for Vapour Grown Carbon Fibre. At the centre of this fibre the MWNT forms the tip.....	12
Fig. 1-7 Schematic illustration of the arc discharge system and TEM micrograph of the grown CNTs.....	15
Fig. 1-8 Schematic illustration of the laser ablation apparatus	16
Fig. 1-9 Schematic illustration of the catalytic deposition and TEM micrograph of the grown CNT	17
Fig. 1-10 Schematics of tip-growth and base-growth for carbon filament growth	18
Fig. 1-11 Schematic diagram of a DMFC.....	25
Fig. 2-1 The structure of Nafion.....	38
Fig. 2-2 Yeager's three-phase model of Nafion; a fluorocarbon region (A), an interfacial zone (B) and an ionic cluster region (C)	39
Fig. 2-3 Membrane and electrode assembly (MEA).....	41
Fig. 2-4 Exploded view of a DMFC	41

Fig. 2-5 Bridge model of oxygen reduction on Pt (z represents the oxidation state)	42
Fig. 2-6 CV of a platinum electrode in 0.5M H ₂ SO ₄ (aq)	44
Fig. 3-1 Experiment flow charts of purification process	50
Fig. 3-2 Experiment flow charts of Pt particles synthesis process	51
Fig. 3-3 The microwave digestion system	52
Fig. 3-4 The Q500 Thermogravimetric Analyzer, TA Instruments	53
Fig. 3-5 Schematic diagram of a TEM	55
Fig. 3-6 Schematic diagram of Bragg's law	57
Fig. 3-7 Schematic diagram of a cyclic voltammetry experiment	58
Fig. 4-1 shows a low magnification TEM image of raw carbon nanotubes	60
Fig. 4-2 shows a low magnification TEM image of MWCNTs after purification by microwave digestion	61
Fig 4-3 The TEM image of acid treated MWCNTs	62
Fig. 4-4(a) TGA graphs of raw samples and purified MWCNTs	64
Fig. 4-4(b) TGA graphs of raw samples and purified MWCNTs	64
Fig. 4-5 The low magnification TEM image of raw MWCNTs	68
Fig. 4-6 The low magnification TEM image of purified MWCNTs	68
Fig. 4-7 The catalysts embedded in the tip of MWCNTs were removed	69
Fig. 4-8 The effect of acid concentration on purification ability for different processing time	70
Fig. 4-9 shows the effect of ultra-sonication time on purification efficiency of 5 M nitric acid	71
Fig. 4-10 shows the result of TGA analysis of (a) raw and (b) purified samples	72
Fig. 4-11 The catalyst contents after purification with 5 M acid for various treatment times	73

Fig. 4-12 The Raman spectroscopy of raw and purified samples.....	74
Fig. 4-13 The TEM image shows that raw sample contains multi-walled carbon nanotubes and catalyst	78
Fig. 4-14 The catalysts embedded in the tip were removed.....	78
Fig. 4-15 The TGA analysis of (a) raw and (b)120min-purified sample	80
Fig. 4-16 The residual catalyst content of different digestion time ranges from 10 to 120 min.....	80
Fig. 4-17 The catalyst covered by tens of graphene layer is difficult to remove...	81
Fig. 4-18 Raman analysis of raw and purified sample for 30, 60, 90, and 120 min treatment.....	82
Fig. 4-19(a)-(e) High resolution TEM image of the unpurified (a) and purified (b-e) carbon nanotubes at the tip	86
Fig. 4-20 Low magnification TEM image of tubular wall structure of the purified carbon nanotubes	86
Fig. 4-21 The relationship between the amount of residual catalysts in the CNTs and processing time	88
Fig. 4-22(a)-(f) The reaction model of purification assisted by microwave dielectric heating for the CNTs	93
Fig. 5-1 The SEM image of sample prepared at 40°C in EG	97
Fig. 5-2 The SEM image of sample prepared at 60°C in EG	98
Fig. 5-3 The SEM image of sample prepared at 80°C in EG	98
Fig. 5-4 The XRD spectrum of sample prepared at 40°C in EG	99
Fig. 5-5 The XRD spectrum of sample prepared at 60°C in EG	99
Fig. 5-6 The XRD spectrum of sample prepared at 80°C in EG	100
Fig. 5-7 The SEM image of sample prepared at 80°C in EG with the addition of D.I. water	101

Fig. 5-8 The XRD spectrum of sample prepared at 80°C in EG and D.I. water..	101
Fig. 5-9 The SEM images of Pt catalyst synthesized on MWCNTs at different temperature in ETOH/water with PVP. (a) 40°C (b) 60°C (c) 80°C.....	103
Fig. 5-10 The XRD spectrum of Pt catalyst synthesized on MWCNTs at 40°C in ETOH/water solution with PVP.....	104
Fig. 5-11 The XRD spectrum of Pt catalyst synthesized on MWCNTs at 60°C in ETOH/water solution with PVP.....	104
Fig. 5-12 The XRD spectrum of Pt catalyst synthesized on MWCNTs at 80°C in ETOH/water solution with PVP.....	105
Fig. 5-13 The SEM images of Pt catalyst synthesized on MWCNTs at different temperature in isopropyl-alcohol. (a) 40°C (b) 60°C (c) 80°C.....	106
Fig. 5-14 The SEM images of Pt nanoparticles synthesized on MWCNTs by heating the solution to 160°C for 30 min with different molecular weight of PVP (a) PVP MW=8000, (b) 58000 (c) 1300000.....	109
Fig. 5-15 The XRD spectrum of Pt nanoparticles synthesized on MWCNTs by heating the solution to 160°C for 30 min with different molecular weight of PVP.....	110
Fig. 5-16 The SEM images of Pt nanoparticles synthesized on MWCNTs with different molecular weight of PVP and the addition of SDS.(a) PVP MW=8000, (b) 58000 (c) 1300000	112
Fig. 5-17 The XRD spectrums of Pt nanoparticles synthesized on MWCNTs with different molecular weight of PVP and the addition of SDS.(a) PVP MW=8000, (b) 58000 (c) 1300000	113
Fig. 5-18 The TEM images of Pt nanoparticles synthesized on MWCNTs with different molecular weight of PVP and the addition of SDS.(a) PVP MW=8000, (b) 58000 (c) 1300000	114

Fig. 5-19 The TEM images of Pt nanoparticles synthesized on MWCNTs with different molecular weight of PVP and the addition of SDS. (a) 8000:58000=1:1, (b) 58000:1300000=1:1 (c) 1300000:8000=1:1	115
Fig. 5-20 The XRD spectrums of Pt nanoparticles synthesized on MWCNTs with different molecular weight of PVP and the addition of SDS. (a) 8000:58000=1:1, (b) 58000:1300000=1:1 (c) 1300000:8000=1:1	116
Fig. 5-21 The TEM images of Pt nanoparticles synthesized on MWCNTs with different molecular weight of PVP and the addition of SDS. (a) 8000:58000=1:1, (b) 58000:1300000=1:1 (c) 1300000:8000=1:1	117
Fig. 5-22 Mechanism between Pt particle, SDS, and PVP.....	119
Fig. 5-23 The SEM images of Pt particles synthesized on MWCNTs at different temperature for 30min. (a) 80°C (b) 100°C (c) 120°C.....	121
Fig. 5-23 The SEM images of Pt particles synthesized on MWCNTs at different temperature for 30min. (d) 140°C (e) 160°C (f) 180°C	122
Fig. 5-24 The TEM images of Pt particles synthesized on MWCNTs at different temperature for 30min. (a) 80°C (b) 100°C (c) 120°C.....	123
Fig. 5-24 The TEM images of Pt particles synthesized on MWCNTs at different temperature for 30min. (d) 140°C (e) 160°C (f) 180°C	124
Fig. 5-25 The XRD spectrums of Pt particles synthesized on MWCNTs at different temperature for 30min. (a) 80°C (b) 100°C (c) 120°C.....	125
Fig. 5-25 The XRD spectrums of Pt particles synthesized on MWCNTs at different temperature for 30min. (d) 140°C (e) 160°C (f) 180°C	126
Fig. 5-26 The Pt loading amounts at different reaction temperatures	127
Fig. 5-27 The SEM images of Pt particles synthesized on MWCNTs of different reaction time at 140°C. (a) 1.5min (b) 2min (c) 5min.....	129
Fig. 5-27 The SEM images of Pt particles synthesized on MWCNTs of different	

reaction time at 140°C. (d) 10 min (e) 30min (f) 90min	130
Fig. 5-28 The TEM images of Pt particles synthesized on MWCNTs of different reaction time at 140°C. (a) 1.5min (b) 2min (c) 5min	131
Fig. 5-28 The TEM images of Pt particles synthesized on MWCNTs of different reaction time at 140°C. (d) 10 min (e) 30min (f) 90min	132
Fig. 5-29 The XRD spectrums of Pt particles synthesized on MWCNTs of different reaction time at 140°C. (a) 1.5min (b) 2min (c) 5min	133
Fig. 5-29 The XRD spectrums of Pt particles synthesized on MWCNTs of different reaction time at 140°C. (d) 10 min (e) 30min (f) 90min	134
Fig. 5-30 The Pt loading amount of different reaction time.....	135
Fig. 5-31 The particle size distribution of Pt nanoparticles	136
Fig. 5-32 High magnification SEM image of Pt-dispersed spiral CNTs	137
Fig. 5-33 Cross section images of Pt-sputtered MWCNTs	138
Fig. 5-34 Cross section images of highly Pt-dispersed MWCNTs by microwave assisted polyol method.....	138
Fig. 5-35 The XPS spectrum of Pt Pt 4f peak of the microwave synthesized Pt particles on MWCNTs	139
Fig. 5-36 The electrocatalytic activity of Pt catalyst was tested by cyclic voltammetry (CV) in electrolyte of 1.0M H ₂ SO ₄	141
Fig. 5-37 Electrocatalytic activities of Pt/MWCNTs electrodes	141

Chapter 1 Introduction

1.1 Carbon nanotubes

Carbon is the sixth element in the periodic table and is listed at the top of column IV. Carbon can exist in various forms as diamond, graphite, carbon fibers, fullerenes and CNTs. Crystal structures of these carbons are shown schematically in Fig 1-1. Carbon shows a variety of stable forms ranging from 0D fullerenes [1] to 1D conducting or semiconducting CNTs to 2D semi-metallic graphite to 3D semiconducting diamond, as shown in Table 1-1 [2].

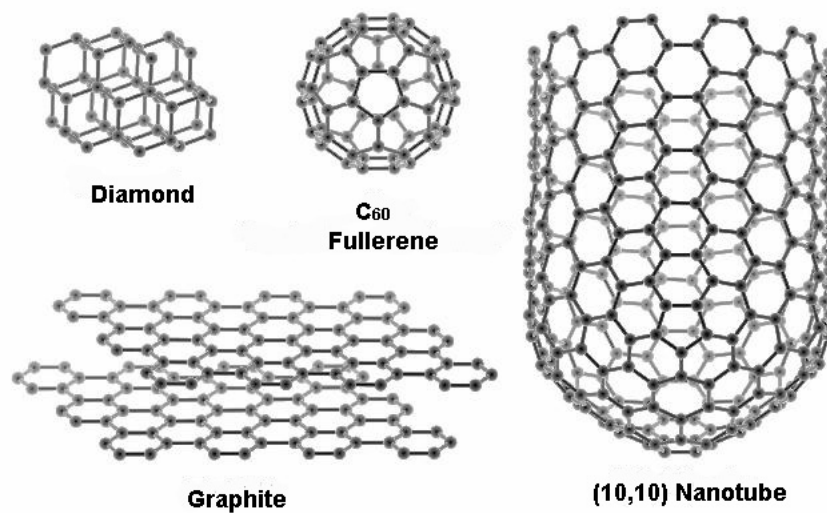


Fig. 1-1 Isomers of carbon: diamond, fullerene, graphite, and CNTs [3].

Table 1-1 Isomers of carbon [2].

Dimension	0-D	1-D	2-D	3-D
Isomer	C60 Fullerene	CNTs Carbyne	Graphite Fiber	Diamond Amorphous
Hybridization	sp^2	sp^2 (sp)	sp^2	sp^3
Density [g / cm ³]	1.72	1.2-2.0 2.68-3.13	2.26 ~2	3.515 2-3
Bond Length [Å]	1.4 (C=C) 1.46 (C-C)	1.44 (C=C)	1.42 (C=C) 1.44 (C=C)	1.54 (C-C)
Electronic Properties	Semiconductor $E_g = 1.9$ eV	Metal or Semiconductor	Semimetal	Insulator $E_g = 5.47$ eV

1.1.1 Structure and properties of carbon nanotubes

1.1.1.1 Structure of carbon nanotubes

CNTs consist of either one cylindrical graphene sheet (Single-walled nanotubes, SWCNTs) or several nested cylinders with inter-layer spacing of 0.34 - 0.36 nm, close to the typical spacing of turbostratic graphite, i.e. MWCNTs. There are many possibilities to form a cylinder with a graphene sheet [4]. A few configurations are shown in Fig. 1-2. Figure 1-2(a)-(c) are SWCNTs of (a) armchair, (b) zig-zag and (c) chiral type. Figure 1-2(d) represents MWCNTs formed by four tubes of increasing diameter with layer spacing of 0.34 nm. Rolling up the sheet along one of the symmetry axis gives either a zig-zag tube or an armchair tube. It is also possible to roll up the sheet in a direction different from a symmetry axis to obtains a chiral CNT. Besides the chiral angle, the circumference of the cylinder can also be varied.

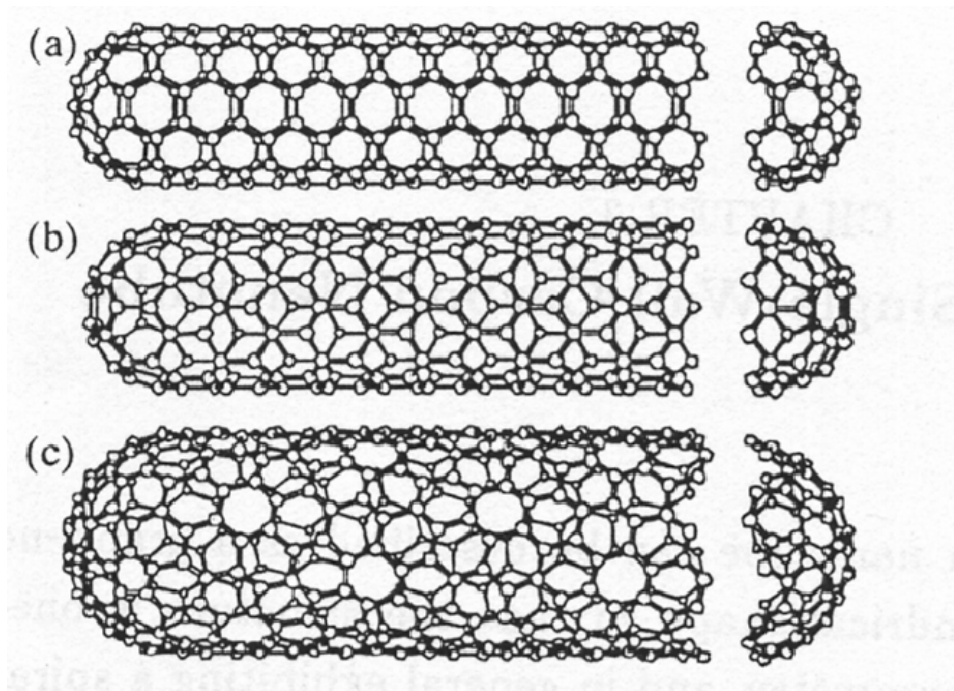


Fig. 1-2 Models of different CNTs structures [5].

Pristine SWCNTs are usually closed on both ends by fullerene-like halfspheres that contain both pentagons and hexagons [4]. SWCNTs with well-defined spherical tip are shown in Fig. 1-3(a). MWCNTs in which the cap shape is more polyhedral than spherical are presented in Fig. 1-3(b). The opened MWCNTs in which the ends of graphene layers and the tube internal cavity are exposed are shown in Fig 1- 3(c). Defects in the hexagonal lattice are usually present in the form of pentagons and heptagons. Pentagons make a positive curvature of the graphene layer and are generally found at the cap as shown in Fig. 1-3(b), where each kink in the graphene layers points to the presence of pentagons in the carbon network. Heptagons give rise to a negative curvature of the tube wall [6]. Defects consisting of several pentagons and/or heptagons have also been observed. A simple model indicates that the diameter and/or chirality of the tube varies from one side of the defect to the other [7]. Such an arrangement forms a link between two different tubes and is accordingly called a junction.

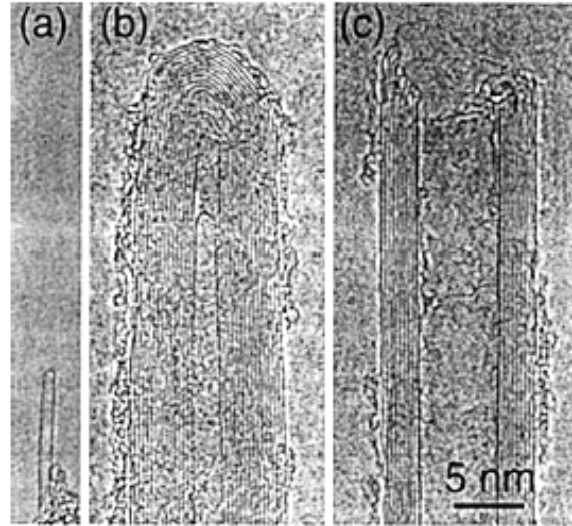


Fig. 1-3 TEM pictures of the ends of (a) a SWCNT, (b) a closed MWCNT, and (c) an open MWCNT. Each black line corresponds to one graphene sheet viewed edge-on [8].

1.1.1.2 Electronic properties of carbon nanotubes

Figure 1-4 shows the cutting graphite sheet along the dotted lines which connects two crystalline graphite equivalent sites on a 2-D [9]. Each carbon atom has three nearest neighbors, rolling sheet of graphite into cylinder to form CNTs. The circumference of CNTs can be expressed in term of the chiral vector, C_h , and chiral angle, θ . The chiral vector is given by Eq. (1):

$$C_h = na_1 + ma_2 \equiv (n, m) \quad (1)$$

(n, m are integers, $0 \leq |m| \leq n$),

where a_1 and a_2 are primitive vector lengths both equal to $\sqrt{3} l_{C-C}$ and l_{C-C} is C-C bond length. The chiral angle determines the amount of twist in the tube. Chiral angles exist in two limiting cases at 0° and 30° . The chiral angle is defined in Eq. (2) as

$$\cos \theta = \frac{C_h \cdot a_1}{|C_h| \cdot |a_1|} = \frac{2n + m}{2\sqrt{nm + m^2 + n^2}} \quad (2)$$

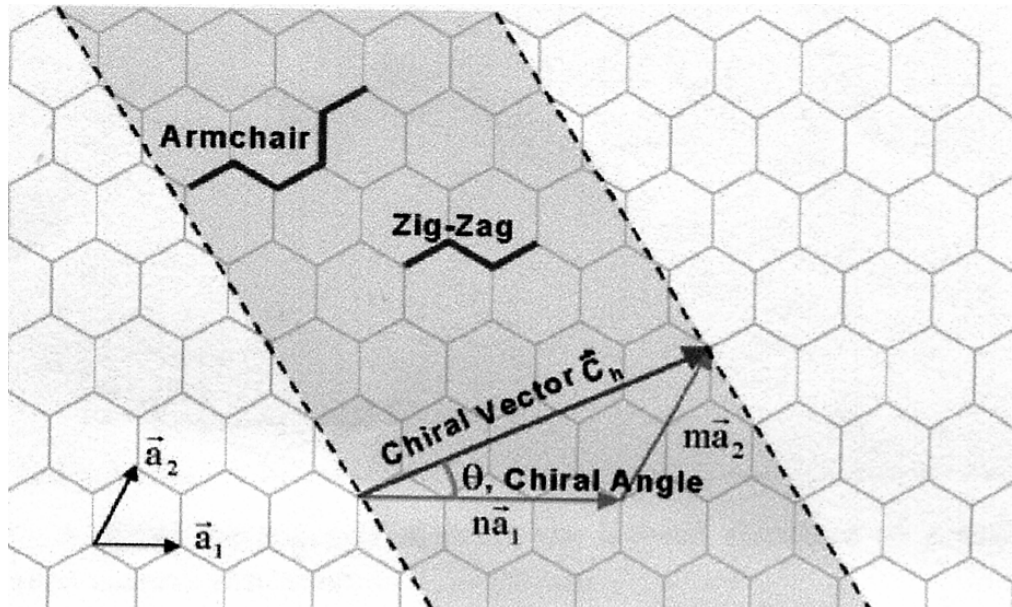


Fig. 1-4 Schematic diagram showing how a hexagonal sheet of graphite is rolled to form a CNT [9].

The zig-zag CNTs correspond to the case of $m = 0$, and the armchair CNTs correspond to the case of $n = m$. The chiral CNT corresponds to the other (n, m) chiral vectors. The zig-zag CNT $(n, 0)$ is generated from hexagon with $\theta = 0^\circ$, and armchair CNT (n, n) is formed from hexagon with $\theta = 30^\circ$. The chiral CNTs are formed from hexagon with $0^\circ < \theta < 30^\circ$. The inter-atomic spacing of carbon atom is known so that the rolled up vector of CNT can define the CNTs diameter. The properties of carbon CNTs depend on the atomic arrangement, diameter, length and the morphology [10]. This diversity of possible configurations is indeed found in practice, and no particular type is preferentially formed. In most cases, layers of MWCNTs are chiral [11,12] different helicities [13]. The lengths of SWCNTs and MWCNTs are usually well over $1 \mu\text{m}$ and diameters range from $\sim 1 \text{ nm}$ (for SWCNTs) to $\sim 50 \text{ nm}$ (for MWCNTs).

The electronic properties of SWCNTs have been studied in a large number of theoretical researches [4,14-17]. These models show that the electronic properties vary between calculable metallic ways and semiconducting approaches, depending on the tube chirality (n, m) given by [1]

Metallic properties: $n-m = 0$ or $(n-m)/3 = \text{integer}$

Semiconducting properties: $(n-m)/3 \neq \text{integer}$

The study shows that about 1/3 of SWCNTs are metallic, while the other 2/3 of SWCNT are semiconductor with a band gap inversely proportional to the tube diameter. This is due to the very unusual band structure of graphene and is absent in systems that can be described by traditional free electron theory. Graphene is a zero-gap semiconductor with energy bands of p-electrons crossing the Fermi level at the edges of the Brillouin zone, leading to a Fermi surface made up of six points [18]. Graphene should show a metallic behavior at room temperature since electrons can easily cross from the valence to the conduction band. However, it behaves as a semi-metal because the electronic density at the Fermi level is quite low [1,18]. Rolling up the graphene sheet into a cylinder imposes periodic boundary conditions along the circumference and only a limited number of wave vectors are allowed in the direction perpendicular to the tube axis. When such wave vectors cross the edge of the Brillouin zone, and thus the Fermi surface, the CNT is metallic. This is the case for all armchair tubes and for one out of the three zig-zag and chiral tubes. Otherwise, the band structure of the CNT shows a gap leading to semiconducting behavior, with a band gap that scales approximately with the inverse of the tube radius. Band gaps of 0.4-1 eV can be expected for SWCNTs (corresponding to diameters of 1.6-0.6 nm) [4,14,16]. This simple model does not take into account the tube curvature which induces hybridization effects for very small tubes [15] and generates a small band gap for most metallic tubes [17]. The exceptions are armchair tubes that remain metallic due to their high symmetry.

These theoretical predictions proposed in 1992 were confirmed in 1998 by scanning tunneling spectroscopy [19,20]. The scanning tunneling microscope has since then been used to image the atomic structure of SWCNTs [21,22] and the

electron wave function [23] and to characterize the band structure [22,24]. Numerous conductivity experiments on SWCNTs and MWCNTs have yielded additional informations [25-36]. At low temperature, SWCNTs behave as coherent quantum wires where conduction occurs through discrete electron states over large distances. Transport measurements revealed that metallic SWCNTs show extremely long coherence lengths [29,36,37]. MWCNTs also show such effects in spite of their larger diameter and multiple shells [38,39].

1.1.1.3 Mechanical properties carbon nanotubes

It has been indicated by growing experimental evidences that both MWCNT and SWCNT have certainly extraordinary mechanical properties. Yakobson et al [40,41] inspected the instability of CNTs beyond linear response. Their simulation results show that CNTs are remarkably resilient due to the sustaining extreme strain with no signs of brittleness or plasticity. Besides, some experimental measurements of Young's modulus of CNTs have been reported. Treacy et al. [42] obtained a relation between tip oscillation amplitude and Young's modulus. Through TEM observations of some CNTs, they defined the amplitude of those oscillations and obtained an average value of 1.8 TPa for the Young's modulus. Another way to probe the mechanical properties of CNTs is to use the tip of AFM to bend anchored CNT. Young's modulus can be extracted with simultaneous recording of the force exerted by the tube as a function of the displacement from its equilibrium position. By this way, Wong et al. [43] reported a mean value of 1.28 ± 0.59 TPa with no dependence on tube diameter for MWCNT. Walters et al. [44] investigated the elastic strain of CNT bundles with the AFM. An experimental strain measurement and an elastic modulus of 1.25 TPa was assumed. Yield strength of 45 ± 7 GPa was then calculated.

Yu et al. [45,46] reported the tensile of SWCNT and MWCNT ropes. For MWCNT ropes, tensile strengths of the outermost layer ranged from 11 to 63 GPa and elastic

modulus ranged from 27 to 950 GPa. For SWCNT ropes, tensile strengths from 13 to 52 GPa and average elastic modulus from 320 to 1470 GPa were obtained.

In terms of mechanical properties, CNTs are among the strongest and most elastic materials known to exist in nature [47]. Table 1-2 shows the mechanical properties of CNTs with other materials. It indicates that MWCNTs are of the most superior mechanical characteristics. The hollow structure and close topology of CNTs form a distinct mechanical response in CNT compared to other graphitic structures.

Table 1-2 Mechanical properties of CNTs compared with other Materials [47].

Materials	Young's modulus (GPa)	Tensile strength (GPa)	Density (g/cm ³)
SWCNT	1054	~150	
MWCNT	1200	~150	2.6
(10,10) Nanorope	563	~75	1.3
Type I carbon fiber	350	2.5	2.6
Steel	208	0.4	7.8
Epoxy	3.5	0.05	1.25
Wood	16	0.08	0.6

1.1.2 Applications of carbon nanotubes

1.1.2.1 Energy storage

Graphite carbonaceous materials and carbon fiber electrodes are commonly used in fuel cells, batteries and other electrochemical applications. Advantages of considering nanotubes for energy storage are their small dimensions, smooth surface topology and perfect surface specificity. The efficiency of fuel cells is determined by the electron transfer rate at carbon electrodes, which is fastest on nanotubes following the ideal Nernstian behavior [48]. Electrochemical energy storage and gas phase intercalation will be described more thoroughly in the following.

1.1.2.2 Hydrogen storage

The advantage of hydrogen as energy source is water as the combustion product. In addition, hydrogen can be easily regenerated. For this reason, a suitable hydrogen storage system is necessary to satisfy both volume and weight limitations. Two common means to store hydrogen are gas phase and electrochemical adsorption. Because of their cylindrical and hollow geometry and nanometre-scale diameters, it has been predicted that carbon nanotubes can store liquids or gases in inner cores through capillary effects. As a threshold for economical storages, the storage requirements of 6.5 % by weight as the minimum level for hydrogen fuel cells has been set. It is reported that SWNTs were able to meet and sometimes exceed this level by using gas phase adsorption (physisorption). Yet, most experimental reports of high storage capacities are rather controversial so that it is difficult to assess the application potential. What lacks is a detailed understanding of the hydrogen storage mechanism and the effect of material processing on this mechanism. Another possibility for hydrogen storage is electrochemical storage. In this case H atoms instead of hydrogen molecules are adsorbed. This is called chemisorption.

1.1.2.3 Lithium intercalation

The basic principle of rechargeable lithium batteries is the electrochemical intercalation and deintercalation of lithium in both electrodes. An ideal battery requires high-energy capacity, fast charging and long cycle time. The capacity is determined by the lithium saturation concentration of the electrode materials. For Li, this is highest in nanotubes if all interstitial sites (inter-shell van der Waals spaces, inter-tube channels and inner cores) are accessible for Li intercalation. SWNTs have shown to possess both highly reversible and irreversible capacities. Because of the large voltage hysteresis observed, Li-intercalation in nanotubes is still unsuitable for battery application. This feature can potentially be reduced or eliminated by

processing, i.e. cutting nanotubes to short segments.

1.1.2.4 Electrochemical supercapacitors

Supercapacitors have high capacitance and potentially applicable in electronic devices. Typically, they are comprised of two electrodes separated by an insulating material that is ionically conducting in electrochemical devices. The capacity of the electrochemical supercap inversely depends on the separation between the charge on the electrode and the counter charge in the electrolyte. Because this separation is about a nanometre for nanotubes in electrodes, very large capacities result from the high nanotube surface area accessible to the electrolyte. In this way, a large amount of charge injection may occur if only a small voltage is applied. This charge injection is used for energy storage in nanotube supercapacitors [49]. Generally speaking, most interest is laid upon the double-layer supercapacitors and redox supercapacitors with different charge-storage modes.

1.1.2.5 Field emitting devices

If a solid is subjected to a sufficiently high electric field, electrons near the Fermi level can be extracted from the solid by tunneling through the surface potential barrier. This emission current depends on the strength of the local electric field at the emission surface and its work function, which denotes the energy necessary to extract an electron from its highest bounded state into the vacuum level. The applied electric field must be very high in order to extract an electron. This condition is fulfilled for carbon nanotubes, because their elongated shape ensures a very large field amplification [48].

For technological applications, the emissive material should have a low threshold emission field and large stability at high current density. Furthermore, an ideal emitter is required to have a diameter in nanometer size, a structural integrity, a high electrical conductivity, a small energy spread and a large chemical stability. Carbon

nanotubes possess all these properties. However, the application bottleneck of nanotubes is the dependence of conductivity and emission stability on fabrication processes and synthesis conditions. Examples of potential applications of nanotubes as field emitting devices are flat panel displays, gas discharge tubes in telecom networks, electron guns for electron microscopes, AFM tips and microwave amplifiers.

1.1.2.6 Transistors

The field-effect transistor – a three-terminal switching device – can be constructed of only one semiconducting SWNT. By applying a voltage to a gate electrode, nanotubes can be switched from conducting to insulating state [49]. A schematic representation of such a transistor is given in Fig. 1-5. Such carbon nanotube transistors can be coupled together to work as a logical switch, which is the basic component of computers [50].

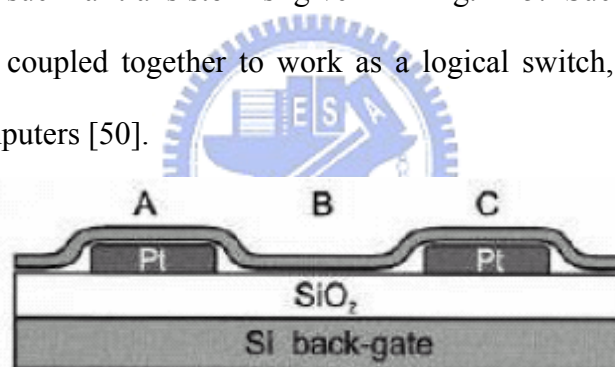


Fig. 1-5 A single semi-conducting nanotube is contacted by two electrodes. Si substrate covered by a layer of SiO₂ 300nm thick acts as a back-gate.

1.1.2.7 Nanoprobes and sensors

Because of their flexibility, nanotubes can also be used in scanning probe instruments. Since MWNT tips are conducting, they can be used in STM and AFM instruments (Fig. 1-6). Advantages are the improved resolution in comparison with conventional Si or metal tips. Tips do not suffer from crashes with surfaces because of their high elasticity. However, nanotube vibration, due to their large length, is still an important issue unless shorter nanotubes can be grown under control.

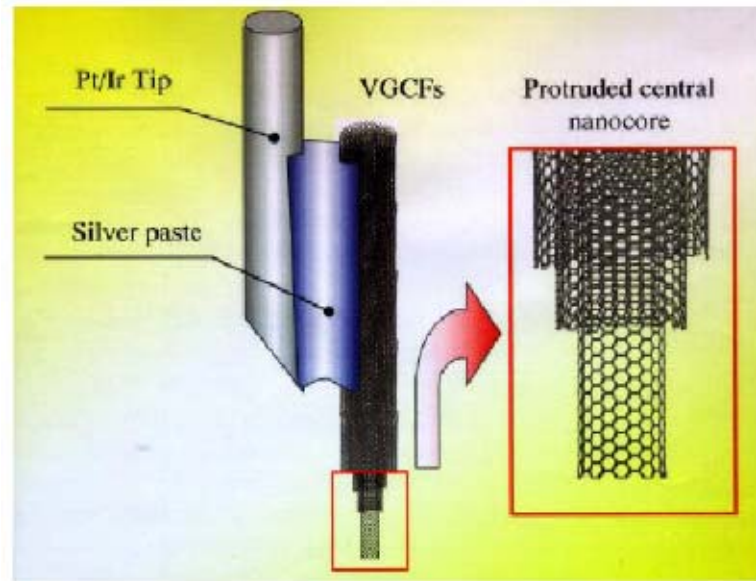


Fig. 1-6 Use of a MWNT as AFM tip. VGCF stands for Vapour Grown Carbon Fibre. At the centre of this fibre MWNT forms the tip [48].

Nanotube tips can be modified chemically by the attachment of functional groups. Nanotubes can be used as molecular probes with potential applications in chemistry and biology. Described below are the further applications. A pair of nanotubes can be used as tweezers to move nanoscale structures on surfaces [49]. Sheets of SWNTs can be used as electromechanical actuators, mimicking the actuator mechanism present in natural muscles SWNTs may be used as miniaturised chemical sensors. On exposure to environments containing NO_2 , NH_3 or O_2 , the electrical resistance changes.

1.1.2.8 Composite materials [48]

Because of the stiffness of carbon nanotubes, they are ideal for structural applications. For example, they may be used as reinforcement composites of high strength, low weight and high performance. Theoretically, SWNTs have Young's Modulus of 1 TPa. MWNTs are weaker because the individual cylinders slide with respect to each other. Ropes of SWNTs are also less strong. The individual tubes can pull out by shearing and at last the whole rope breaks. This happens at stresses far below the tensile strength of individual nanotubes. Nanotubes also sustain large

strains in tension without fracture. In other directions, nanotubes are highly flexible [48]. One of the most important applications of nanotubes based on their properties is the reinforcement in composite materials. However, there have not been enough successful experiments to prove the better filler performance over traditional carbon fibers. The main problem is to create a good interface between nanotubes and the polymer matrix, because nanotubes are too smooth and too small in diameter, which is nearly the same as that of a polymer chain. Next, nanotubes are quite different from the individual nanotube in mechanical properties because of the easy aggregation. Limiting factors for good load transfer are sliding of cylinders in MWNTs and shearing of tubes in SWNT ropes. To solve this problem the aggregates need to be broken up and dispersed or cross-linked to prevent slippage. A main advantage of using nanotubes for structural polymer composites is that nanotube reinforcements increase the toughness of the composites by absorbing energy due to their highly flexible elasticity. Other advantages are the low density of nanotubes, increased electrical conduction and better performance during compressive load. Another possibility, which is an example of a non-structural application, is the filling of photoactive polymers with nanotubes. PPV (Poly-p-phenylenevinylene) filled with MWNTs and SWNTs is a composite, which has been used in several experiments. These composites show a large increase in conductivity with only a little loss in photoluminescence and electro-luminescence yields. Another benefit is that the composite is more robust than pure polymers. Of course, nanotube-polymer composites could also be used in other areas. For instance, they could be used in the biochemical field as membranes for molecular separations or for osteointegration (growth of bone cells). However, these areas are less explored. The most important thing we have to know about nanotubes for their efficient usage as reinforcing fibers is the knowledge on how to manipulate surfaces chemically to enhance interfacial

behavior between individual nanotubes and the matrix material.

1.1.2.9 Templates [48]

Because of the small channels, strong capillary forces exist in nanotubes. These forces are strong enough to hold gases and fluids in nanotubes and it is possible to fill cavities in nanotubes to build nanowires. The critical issue is the wetting characteristics of nanotubes. Because of their smaller pore sizes, filling of SWNTs is more difficult than filling of MWNTs. If it becomes possible to keep fluids inside nanotubes, it could also be possible to run chemical reactions inside cavities. Though special organic solvents wet nanotubes easily to make nanoreactor available, that nanotubes are normally closed cannot meet the application requirement. This is accessible through a simple chemical reaction, oxidation. Pentagons in the end cap of nanotubes are more reactive than sidewalls and during oxidation, caps are easily removed while sidewalls stay intact.

1.1.3 Carbon nanotube synthesis

There are three major methods to synthesize CNTs: arc discharge, laser ablation and catalytic chemical vapor deposition.

1.1.3.1 Arc discharge

Arc discharge is the first available method to produce both MWCNTs [51,52] and SWCNTs [53,54]. This is the classic method to prepare MWCNTs. The method has been put in use for a long time for carbon fiber production. Therefore, it is very possible that CNTs were observed but not recognized until Iijima synthesized CNTs by this approach in 1991 [55,56].

Figure 1-7 shows the schematic of arc discharge system [8]. The arc discharge apparatus involves two graphite rods as anode and cathode. The rods are brought together under a gas atmosphere (usually He, but H₂ [57] and Ar have also been used) and a voltage is applied until stable arc is achieved. As the anode is consumed, a gap

(~ 1mm) between cathode and anode is maintained by adjusting the position of anode. Carbons are deposited on the cathode to form CNTs and other carbon particles.

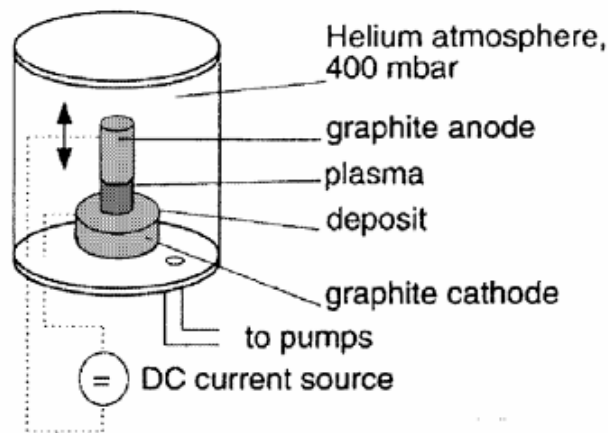


Fig. 1-7 Schematic illustration of arc discharge system and TEM micrograph of the grown CNTs [8].

1.1.3.2 Laser ablation

Laser ablation was first used to synthesize C_{60} in 1985 by Kroto et al. [58] and was demonstrated to grow SWCNTs and MWCNTs in 1995 by Smalley's group at Rice University [59,60]. Thess et al. [61] showed that the synthesis could be carried out in a horizontal flow tube under inert gas flow at controlled pressure. In this setup the flow tube is heated to $\sim 1200^{\circ}\text{C}$ by a tube furnace as displayed in Fig. 1-8. Laser pulses enter the tube and strike a target consisting of a mixture of graphite and metal catalyst such as Co or Ni. SWCNTs condense from the laser vaporization plume and deposit on a collector outside the furnace zone [62]. The size of carbon sources limited the sample volume. Besides, purifications are necessary to separate the tube from undesirable by-products.

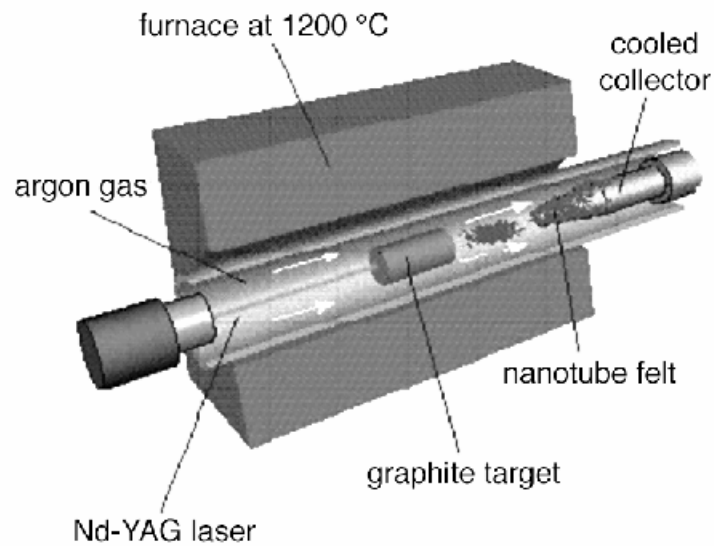


Fig. 1-8 Schematic illustration of laser ablation apparatus [63].

1.1.3.3 Catalytic chemical vapor deposition (CVD)

The catalytic growth of CNTs is an alternative of arc discharge and laser ablation. It is based on the decomposition of hydrocarbon gases over transition metals to grow CNTs by using chemical vapor deposition (CVD). Since 1960s [64], carbon filaments and fibers have been produced by thermal decomposition of hydrocarbons. Catalysts are usually necessary to promote the growth [65]. A similar approach was used to grow MWCNTs from the decomposition of acetylene over iron particles in 1993 [66]. A tube produced by catalytic growth is shown in Fig. 1-9. In general, the diameter of CNTs grown by catalytic growth is larger than that of arc discharge but imperfect in graphitized crystalline structure. To grow MWCNTs, acetylene is usually used as carbon source between 600 and 800°C. To grow SWCNTs, the temperature has to be significantly higher (900-1200°C) because of the higher energy of formation. In this case carbon monoxide or methane must be used due to their high stability at higher temperatures as compared to acetylene.

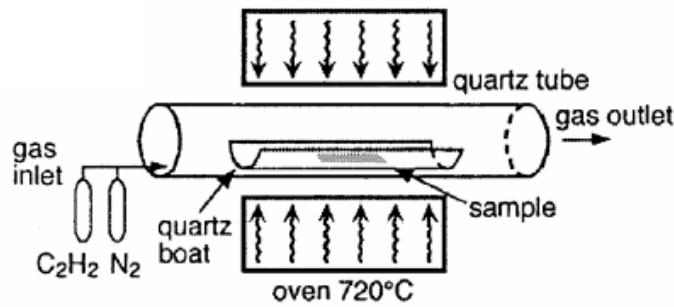


Fig. 1-9 Schematic illustration of catalytic deposition and TEM micrograph of the grown CNT [8].

Up to now, the catalytic CVD has undergone many improvements. Co catalysts supported on silica particles produced straight as well as coiled MWCNTs [67], and the yield of CNTs was significantly increased by using zeolites as catalyst supports [68,69]. It was also reported that in the continuous production of SWCNTs, both carbons and catalysts are supplied in gas phase. Besides, the yield and average diameter of SWCNTs could be varied by controlling process parameters [70]. In addition, catalyst support types were found to control the formation of individual or bundled SWCNTs [71]. Transition metal (Fe, Co, Ni) particles are catalysts for vapor grown CNTs synthesis with hydrocarbons as the carbon source. Metal catalysts are generally necessary to activate CNTs growth. A variety of other catalysts, hydrocarbons and catalyst supports have been used successfully by numerous groups in the world to synthesize CNTs [72,73].

1.1.3.4 Catalytic growth mechanisms of carbon nanotubes

Many growth mechanisms have been proposed to explain the relation between the growth condition and the structure of CNTs. According to the position of metal particles on the filament, two growth modes, base-growth and tip-growth, were reported [74]. The ‘base-growth’ mode means that the filament grows upward from metal particles, which attach to the substrate. If metal particles detach and move to the

head of the growing filament, it is the ‘tip-growth’ mode. These mechanisms were illustrated graphically in Fig. 1-10 by Sinnott et al. [75] (after Baker and Harris [74]).

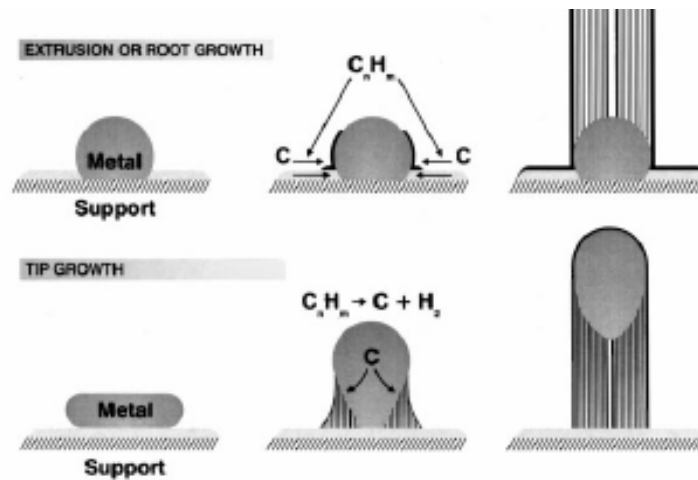


Fig. 1-10 Schematics of tip-growth and base-growth for carbon filament growth [75].

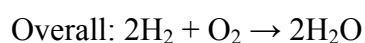
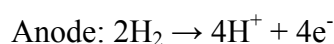
Andrews et al. suggested [76] that the catalyst particle size determines the size of the ‘filament’. When the particle diameter is in the range of tenths of a micron, the carbon is produced as filaments of similar diameter [74,77]. As the particle diameter is reduced, the filament curvature increases to impose an increasing strain on the basal planes of the crystallites. Finally, a continuous surface is energetically favorable to form MWCNTs.

1.2 Fuel cell

Fuel cell can be traced back to the 1800's discovery by Sir William Robert Grove. Grove realized that if electrolysis could split water into hydrogen and oxygen by electricity then the reverse would also be true. Combining hydrogen and oxygen with the correct method would produce electricity. To prove his hypothesis, Sir William Robert Grove built a device that would combine hydrogen and oxygen to produce electricity, the world's first fuel cell. His invention was a success, and Grove's work advanced the idea of the conservation of energy and its reversibility. In 1899, a fuel

cell with power density of 104 km/h was assembled in an electric vehicle, the “Jamais Contente”.

Nowadays, to discover a new power source with less pollution and lower price to replace fossil oil is a noteworthy topic among resource industry. With the high efficiency and less pollution, fuel cells have become the most possible and popular power source in the next generation. Fuel cells generate electricity from a simple electrochemical reaction in which oxygen and hydrogen combine to form water and generate electrons. The reactions are



In 1960s, the fuel cell was initially applied as an auxiliary power source in the Gemini space flights. Subsequently, advances in this technology were stagnant until the late 1980s when the fundamental design underwent significant reconfiguration. Even though there are challenges and obstacles to develop fuel cells, scientists never cease devoting their energies and efforts on fuel cell fields.

1.2.1 Classification of fuel cells

Fuel cells are classified primarily according to the types of electrolyte employed. This determines the types of chemical reactions that take place in the cell, the types of catalysts required, the temperature range in which cell operates, the fuel required, and other factors. These characteristics, in turn, affect the appropriate applications of these cells. There are several types of fuel cells currently under development, each with its own advantages, limitations, and potential applications. According to electrode types, several most promising types include proton exchange membrane fuel cell (PEMFC), alkaline fuel cell (AFC), phosphoric acid fuel cell (PAFC), molten carbonate fuel cell (MCFC), and solid oxide fuel cell (SOFC). Details of these fuel cells are described as

followed.

1.2.1.1 Polymer electrolyte membrane fuel cell

Polymer electrolyte membrane (PEM) fuel cells, also called proton exchange membrane fuel cells, deliver high power density and have the advantages of low weight and volume, compared to other fuel cells. PEM fuel cells use a solid polymer as an electrolyte and porous carbon electrodes containing platinum catalysts. They need only hydrogen, oxygen from the air, and water to operate and do not require corrosive fluids as some other fuel cells. They are typically fueled with pure hydrogen supplied from storage tanks or onboard reformers.

Polymer electrolyte membrane fuel cells operate at relatively low temperatures, around 80°C. Low temperature operation initiates quickly and results in less wear on system components and better durability. However, the necessity of noble-metal catalysts to separate electrons and protons of hydrogen costs high for systems. The platinum catalyst is also extremely sensitive to CO poisoning, and it is necessary to employ an additional reactor to reduce CO in the fuel gas if hydrogen are derived from alcohol or hydrocarbon fuels. This also increases the cost. Developers are currently exploring Pt-Ru catalysts that are more resistant to CO. PEM fuel cells are used primarily for transportation applications and some stationary applications. Due to the fast startup, low sensitivity to orientation and favorable power-to-weight ratio, PEM fuel cells are particularly suitable for passenger vehicles, such as cars and buses. A significant barrier of using these fuel cells in vehicles is hydrogen storage. Most fuel cell vehicles powered by pure hydrogen must store hydrogen onboard as compressed gases in pressurized tanks. Due to the low energy density of hydrogen, it is difficult to store enough hydrogen onboard to allow vehicles to travel the same distance as gasoline-powered vehicles before refueling, typically 300-400 miles. Higher-density liquid fuels such as methanol, ethanol, natural gas, liquefied petroleum

gas and gasoline seem to be available, but vehicles must have an onboard fuel processor to reform methanol to hydrogen. This increases costs and maintenances. The reformer also releases carbon dioxide, though less than that emitted from current gasoline-powered engines.

1.2.1.2 Phosphoric acid fuel cell

Phosphoric acid fuel cells use liquid phosphoric acid as an electrolyte with the acid contained in a Teflon-bonded silicon carbide matrix and porous carbon electrodes containing platinum catalysts. Chemical reactions that take place in the cell are shown in the diagram to the right. Phosphoric acid fuel cell (PAFC) is considered the "first generation" of modern fuel cells. It is one of the most mature cell types and the first to be used commercially with over 200 units in current use. This type of fuel cell is typically used for stationary power generation, but some PAFCs have been used to power large vehicles such as city buses. PAFCs are more tolerant of impurities in the reformat than PEM cells, which are easily poisoned by CO_2 — CO_2 attaching to the platinum catalyst at the anode as a result of decreasing fuel cell's efficiency. They are efficient by 85% for co-generations of electricity and heat, but less efficient for electricity generation only. This is slightly more efficient than combustion-based power plants with typical operation efficiency of 33 to 35%. PAFCs are also less powerful than other fuel cells, given the same weight and volume. As a result, these fuel cells are normally large and heavy. PAFCs are also expensive. Like PEM fuel cells, PAFCs require an expensive platinum catalyst, which raises the cost of the fuel cell.

1.2.1.3 Alkaline fuel cell

Alkaline fuel cells (AFCs) were one of the first fuel cell technologies developed, and were the first type widely used in the U.S. space program to generate electrical energy and water onboard spacecraft. These fuel cells use the aqueous solution of

potassium hydroxide as the electrolyte and use a variety of non-precious metals as catalysts at the anode and cathode. High-temperature AFCs operate at temperatures between 100°C and 250°C. However, more-recent AFC designs operate at lower temperatures from 23°C to 70°C.

AFCs are high-performance fuel cells due to the rate at which chemical reactions take place in the cell. They are also very efficient, reaching efficiencies of 60% in space applications. The disadvantage of this fuel cell is that it is easily poisoned by carbon CO₂. In fact, even a little CO₂ in the air can affect the cell's operation, and it is necessary to purify both hydrogen and oxygen in the cell. This purification process is expensive. Susceptibility to poisoning also affects the cell's lifetime and raises further the cost. Cost is less of a factor for remote locations such as space or under the sea. However, for effective competition in most mainstream commercial markets, these fuel cells have to become more effective in cost. AFC stacks have been shown to maintain sufficiently stable operation for more than 8,000 operating hours. To be economically viable in large-scale utility applications, these fuel cells need to reach operating time exceeding 40,000 hours. This is possibly the most significant obstacle in commercializing this fuel cell technology.

1.2.1.4 Molten carbonate fuel cell

Molten carbonate fuel cells (MCFCs) are currently being developed for natural gas and coal-based power plants for electrical utility, industrial and military applications. MCFCs are high-temperature fuel cells that use electrolytes composed of molten carbonate salt mixture suspended in a porous and chemically inert ceramic lithium aluminum oxide (LiAlO₂) matrix.

Since they operate at extremely high temperatures of 650°C and above, non-precious metals can be used as catalysts at the anode and cathode to reduce costs. Improved efficiency is another reason why MCFCs offer significant cost reductions

over phosphoric acid fuel cells (PAFCs). Molten carbonate fuel cells can reach efficiencies of 60%, considerably higher than the 37-42% efficiencies of a phosphoric acid fuel cell plant. When waste heats are utilized, overall fuel efficiencies can be as high as 85%. Unlike alkaline, phosphoric acid and polymer electrolyte membrane fuel cells, MCFCs don't require an external reformer to convert more energy-dense fuels to hydrogen. Due to the high operation temperatures, these fuels are converted to hydrogen within the fuel cell itself by a process called internal reforming, which also reduces the cost. Molten carbonate fuel cells are not prone to CO or CO₂ poisoning, making them more attractive for fueling with gases made from coals. Although they are more resistant to impurities than other fuel cell types, scientists are looking for ways to make MCFCs resistant enough to impurities from coals, such as sulfurs and particulates. The primary disadvantage of current MCFC technology is durability. The high temperatures at which these cells operate and the corrosive electrolyte used accelerate component breakdown and corrosion, decreasing cell life. Scientists are currently exploring corrosion-resistant materials for components and fuel cell designs to increase cell life without decreasing performances.

1.2.1.5 Solid oxide fuel cell

Solid oxide fuel cells (SOFCs) use hard non-porous ceramic compounds as electrolytes. Since the electrolyte is a solid, the cell does not have to be constructed in the typical plate-like configuration of other fuel cell types. SOFCs are expected to be around 50-60% efficient at converting fuel to electricity. In applications designed to recover and utilize the system waste heat, overall fuel efficiencies could top 80-85%. Solid oxide fuel cells operate at very high temperatures. Cost reduction is valid because it is unnecessary to use precious metal catalysts at high temperatures. SOFCs also reform fuels internally and can use a variety of fuels to reduce the cost associated with adding a reformer to the system. SOFCs are the most sulfur-resistant fuel cell

type and tolerate more sulfurs than other cell types by several orders in magnitude. In addition, they are not poisoned by CO, which can even be used as fuel. This allows SOFCs to use gases made from coals. High-temperature operation has disadvantages. It results in a slow startup and requires considerable thermal shielding to retain heat and to protect personnel. This may be acceptable for utility applications but not for transportation and small portable applications. High operating temperatures also place stringent durability requirements on materials. The development of low-cost materials with high durability at cell operating temperatures is the key technical challenge. Scientists are currently developing lower-temperature SOFCs operating at or below 800°C that have fewer durability problems and cost less. Lower-temperature SOFCs produce less electrical power, however, and stack materials that will function in this lower temperature range have not been identified. The differences and features of these fuel cells are summarized in Table 1-3.

1.2.2 Potential of direct methanol fuel cell

Direct methanol fuel cell (DMFC) is a kind of PEMFCs and is separated from PEMFC for detail discussion. Most fuel cells are powered by hydrogen, which can be fed to the fuel cell system directly or can be generated within the fuel cell system by reforming hydrogen-rich fuels such as methanol, ethanol and hydrocarbon fuels. Direct methanol fuel cell, however, is powered by pure methanol, which is mixed with steam and fed directly to the fuel cell anode. Direct methanol fuel cells do not have the fuel storage problems typical of some other fuel cells since methanol is higher than hydrogen in energy density. Methanol is also easier to transport and supply to the public using our current infrastructure since it is a liquid, like gasoline. Fig.1-11 shows the schematic diagram of a DMFC.

Table 1-3 Comparisons of various fuel cells.

	MCFC	PAFC	PEMFC	SOFC
Electrolyte	Molten carbonate salt	Liquid phosphoric acid	Ion exchange membrane	Solid metal oxide
Operating tempt.	600~1000°C	150~200°C	60~100°C	600~1000°C
Reforming	External/Internal	External	External	External/Internal
Oxidant	CO ₂ /O ₂ /Air	O ₂ /Air	O ₂ /Air	O ₂ /Air
Efficiency	45~60%	35~50%	35~50%	45~60%
Max. Efficiency	85%	80%	60%	85%
Max. power output	2MW	1MW	250kW	220kW
Waste heat uses	High pressure stream	Space heating or water heating	Space heating or water heating	Heating water or stream

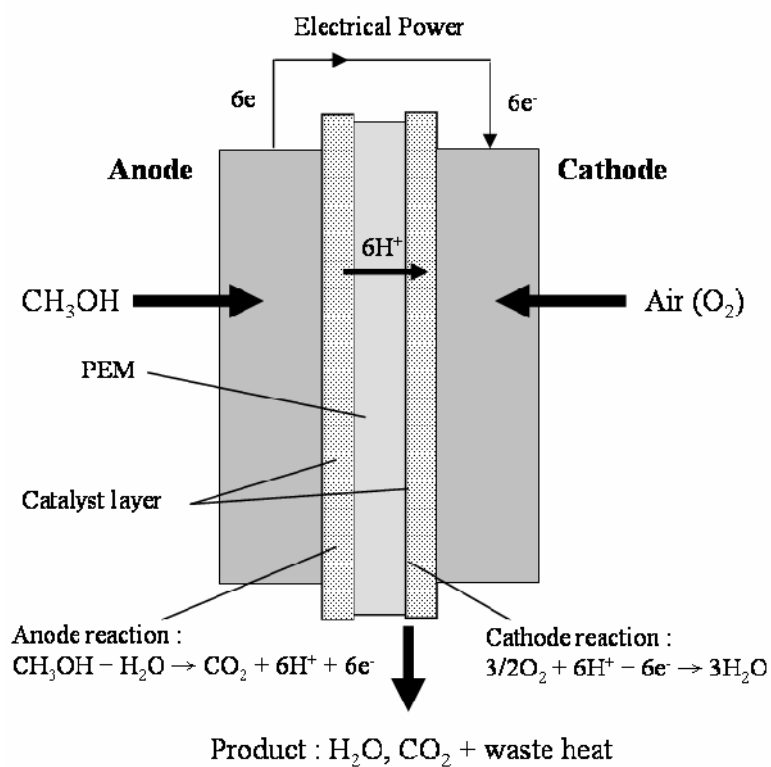
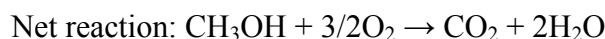
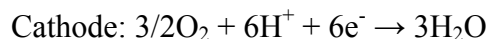
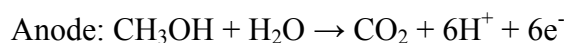


Fig. 1-11 Schematic diagram of a DMFC.

The anode, the negative post of the fuel cell, does several jobs. It conducts the electrons freed from hydrogen molecules so that they can be used in external circuits. It has channels etched into it that disperse hydrogen gases uniformly over catalyst surfaces. The cathode, the positive post of the fuel cell, has channels etched into it that distribute the oxygen to the surface of the catalyst. It also conducts electrons back from external circuits to catalysts, where they can recombine hydrogen ions and oxygen to form water. The electrolyte is the proton exchange membrane. This specially treated material only conducts positively charged ions and blocks electrons. The catalyst is a special material that facilitates the reaction of oxygen and hydrogen. It is usually made of platinum powder thinly coated onto carbon paper or cloth. The catalyst is rough and porous so that maximum surface area of the platinum can be exposed to the hydrogen or oxygen. The platinum-coated side of the catalyst faces the proton exchange membrane.

Because methanol is fed directly into the fuel cell, complicated catalytic reforming is unnecessary, and storage of methanol is much easier than that of hydrogen since methanol is a liquid and does not require high pressure operation. The energy density of methanol is greater than compressed hydrogen by orders of magnitude. However, efficiency is low, due to the high permeation of methanol through the membrane and the sluggish dynamic behavior. Methanol is also poisonous. As a result, DMFCs are limited in the power production but still can store much energy in a small space. This means they can produce a small amount of power over a long period of time which makes them well suited to power consumer electronics such as cell phones and laptops but rules them out of automotive applications. DMFC relies upon the oxidation of methanol on a catalyst layer to form carbon dioxide. Water is consumed at the anode and is produced at the cathode. Protons (H^+) are transported across the proton exchange membrane to the cathode where they react with oxygen to produce

water. Electrons are transported via an external circuit from anode to cathode to provide power to external devices. The half reactions are:



Because water is consumed at the anode in the reaction, pure methanol cannot be used without provision of water via either passive transport such as back diffusion, or active transport such as pumping. The need for water limits the energy density of the fuel.

1.3 Microwave Chemistry

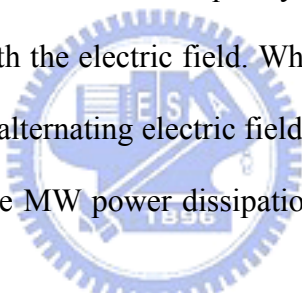
Considerable knowledge of microwave radiation was obtained during the development of radar before and during the second world war. In the late 1960s it was used as a heating mode for temperature-jump experiments [78]. The first application in chemical research was reported in the early 1970s, when gas-phase discharge was applied to realize decomposition of simple organic compounds [79]. By the early 1980s, two patents concerning polymer chemistry appeared and one was related to starch derivatisation. However, when significant rate accelerations for reactions carried out in a conventional microwave oven were observed in 1986, considerable attention on reactions was laid upon dielectric heating [80,81]. In addition, more advanced microwave ovens were designed. Moreover, ensued are discussions on the causes of microwave reaction rate enhancements, apprehensions about temperature monitoring and control as well as trials of large-scale reactions in microwave ovens.

1.3.1 Microwave-assisted synthesis of metallic nanostructures

Microwave (MW) rapid heating has received considerable attention as a new promising method for the one-pot synthesis of metallic nanostructures in solutions. A variety of metallic nanostructures, including spherical particles, sheets, plates, rods,

wires, tubes and dendrites have generated significant scientific and technological interests because of their unique optical as well as novel chemical and catalytic properties. These nanostructures have been synthesized by various techniques, including chemical reduction of metallic ions in aqueous or organic solvents [82-84]. In general, chemical reduction has been carried out by heating reagent solutions at 65–200°C in an oil bath. In the oil-bath heating, the solvent is heated by conduction and convection, so that there is a large temperature distribution within the solvent.

Recently, microwave dielectric heating has been applied to the rapid synthesis of metallic nanostructures [85-112]. MWs are a portion of the electromagnetic spectrum with frequencies in the range from 300 MHz to 300 GHz. The commonly used frequency is 2.45 GHz. In the microwave frequency range, polar molecules such as H₂O undertake to orientate with the electric field. When dipolar molecules attempt to re-orientate with respect to an alternating electric field, they lose energy in the form of heat by molecular friction. The MW power dissipation per unit volume in a material (P) is given by equation:


$$P = c|E|^2 f \epsilon'' = c|E|^2 f \epsilon' \tan \delta$$

where c is a constant, E is an electric field in the material, f is the radiation frequency, and ϵ' and ϵ'' are the dielectric and dielectric loss constants, respectively. ϵ' represents the relative permittivity, which is a measure of the ability of a molecule to be polarized by an electric field and $\tan \delta = \epsilon''/\epsilon'$ is the energy dissipation factor or loss tangent. Equation indicates that ϵ'' is the most important physical parameter that describes the ability of a material to heat in the MW field. The physical parameters of typical solvents used in MW heating for synthesis of metallic nanostructures are listed in Table 1-4.

Table 1-4 Physical parameters of typical solvents used for microwave heating [113].

	B.p. [°C]	ϵ'	ϵ''	$\tan \delta$
water	100	78.3	12.3	0.157
methanol	65	32.7	20.9	0.639
ethanol	78	24.3	6.08	0.200
N,N-dimethylformamide(DMF)	153	36.71	–	–
ethylene glycol (EG)	198	41.0	41.0	1.00
N-methylpyrrolidone (NMP)	202	32.0	8.855	0.277

Water, alcohols, DMF and ethyleneglycol (EG) have high dielectric losses and high reduction abilities and are ideal solvents for MW rapid heating. The MW heating in these solvents in the presence of surfactants has been used to synthesize nanoparticles of various metals (Ni, Ru, Rh, Pd, Ag, Ir, Pt, Au.), [85-104] metallic compounds (PtRu, TiO₂, CdS, CdSe, MoSe₂, PbS, HgS, CuInTe₂, CuInSe₂) and Au/Pd core-shell structures [105-112].

1.3.2 Possible effects of MW heating

There are two effects of MW dielectric heating, thermal and non-thermal [114]. Thermal effects arise from different temperature regimes under MW heating, whereas non-thermal effects result from effects inherent to the MWs. These effects lead to different morphologies and sizes of metallic nanostructures under MW heating from those in the conventional oil-bath heating.

1.3.2.1 Thermal effects (effects of rapid and uniform heating)

MW provides rapid and uniform heating of reagents, solvents, intermediates and products. Fast heating accelerates the reduction of metal precursors and the nucleation of the metal cluster, and results in mono-dispersed small nanostructures. When MWs are incident perpendicular to the solvent surface, their intensity is attenuated in the direction of incidence. However, for most materials, the distance is quite long in the direction of penetration at which the incident power is reduced to half of its initial

value. Therefore, the power dissipation is fairly uniform throughout the solvent. This homogeneous MW heating also provides uniform nucleation and growth conditions, and leads to uniform nanomaterials of small size. Due to the rapid and homogeneous MW heating, a better crystallinity can be obtained. Therefore, such single-crystalline nanostructures as polygonal plates, rods and wires could be synthesized efficiently in many cases.

1.3.2.2 Effects of hot spots and hot surfaces

When solids heated by MW are involved in the reaction system, hot spots are created on the solid–liquid surface. The uniform formation of hot spots and hot surfaces also accelerates the reduction of metal precursors and the nucleation of the metal cluster, and leads to uniform nanostructures of small size.

1.3.2.3 Superheating

Superheating of solvents over boiling points of solvents often occurs as a consequence of the MW dissipation over the whole liquid volume [113]. This effect is especially significant in the presence of a large amount of ions.

1.3.2.4 Non-thermal effects

Non-thermal effects are defined as those that occur under the same temperature profiles of solvents between MW and oil-bath heatings during the reaction. Formation of hot spots and hot surfaces are typical non-thermal effects for the preparation of metallic nanostructures. MW heating induces various thermal and non-thermal effects described above.

1.4 Motivation of this thesis

Since the discovery of CNTs, relevant research fevers and developments of commercial applications such as hydrogen storage, atomic force microscope probe, microelectronic transistor, electrical field emitter of flat panel display and scanning tunneling microscope tip have been stimulated tremendously and discussed in

previous chapters. Carbon nanotubes may find their limited use in some applications as they contain a small fraction of metal catalysts in tubes and tend to have defects along the graphene tube wall. Defects within the multi-walled carbon nanotubes would reduce electrical and structure properties. High-quality and well-aligned carbon nanotubes are essential to the potential applications of microelectronic industries. In this thesis, a microwave-assisted heating system was used to dissolve the metal catalyst. Inorganic acids such as H_2SO_4 , HNO_3 and HCl can rapidly absorb microwave heat and energy and completely dissolve metals that reside in carbon nanotubes. Since Environmental Protection Agency (EPA) recommended the microwave-assisted method with nitric acid, this leaching procedure of metals has been widely applied in sediments of soils and sludges. Nitric acid is strong enough to solubilize metals from materials. In closed microwave digestion system, metal catalysts are dissolved in acid solution rapidly without agitation. Therefore, lower concentration of acids and acid immersing time are available to completely retain walls of carbon nanotubes.

After purification, morphology of carbon nanotubes and purification degree are evaluated and the amount of residual catalyst metals in samples is estimated. A high-yield and no destructive multi-walled carbon nanotubes in high purity are obtained.

Discussed in the second are effects of purification time, acidic concentration and ultrasonification time on purification efficiency of the as-synthesized MWCNTs. According to previous results, a one-step process to produce opened and catalyst-free carbon nanotubes with high purity was well established. And in the third part, the model describing the purification process of CNTs in microwave system is introduced. In the first step, the tips of nanotubes might be attacked and opened selectively by nitric acid, while in the second step in acid dissolution most metal catalysts in the tips

are eliminated. Finally, highly pure and opened carbon nanotubes without damage to the wall structure were obtained. These results are different from those mentioned in other approaches to destroy both tips and walls and reveal that the microwave-assisted acidic treatment might have selectivity between tips and walls of CNTs. The purification of the as-synthesized MWCNTs could be processed by microwave digestion treatment for short duration and is expected to investigate and formulate a reaction mechanism to realize why this processing technique could result in a high purification efficiency of the as-synthesized MWCNTs with no remarkable structure damages during processing.

After the purification of CNTs, platinum nanoparticles with uniform diameter (about 4.3 nm) were efficiently dispersed on multi-walled carbon nanotubes (MWCNTs) with temperature-controlled, microwave-assisted polyol method.

In recent years, due to environmental protection concerns, greenhouse effect, and the energy crisis, fuel cells have become a subject of great interest. Worldwide interests in fuel cells have the basis on the prospect of fulfilling energy needs with less environmental impact, greater efficiency, and lower cost compared with traditional fossil fuels. Fuel cells have been proposed as a major energy source because of their portability and the potential application in electric vehicles. The Pt/C catalyst is known one of the effective factors affecting the transformation reaction of hydrogen or methanol to water. The catalytic activity of Pt/C catalyst is strongly related to the particle size of Pt, the degree of particle size distribution, and the dispersion of Pt on carbon support.

In the final part of thesis, a temperature-controlled microwave heating system was used to disperse Pt catalyst with suitable size, narrow size distribution, and highly dispersion on CNTs which could provide high electro-catalytic activity in fuel cell applications. And the effect of temperature on Pt reduction rate in microwave-assisted

polyol process is demonstrated. Besides, the effects of additives and reaction time on Pt reduction were also studied. Other characteristics such as Pt particle size, size distribution, loading amount, and dispersion on MWCNTs were also investigated under temperature-controlled microwave heating process to obtain dense Pt clusters on CNTs.



Chapter 2 Literature Review

2.1 Purification of carbon nanotubes

Many kinds of synthetic techniques have been developed, and metal catalysts are generally necessary to activate carbon nanotube growth. Carbon nanotubes may find their limited use in some applications as they contain a small fraction of metal catalyst in tubes and tend to have defects along the graphene tube wall. Defects within the multi-walled carbon nanotubes would reduce electrical and structure properties. Recently, many purified methods have been investigated and have been used successfully to remove impurities from carbon soots [115-120].

2.1.1 Thermal oxidation

One of the efficient purification methods reported by Tsang et al. [121] was oxidation in air at 750°C. Due to the small difference in reactivity between Multi-walled carbon nanotubes (MWCNTs) and carbon nanoparticles, pure MWCNTs were obtained after prolonged oxidation. Many following up researchers [122-124] adopted thermal annealing and similar thermal oxidation method to purify CNTs but with low yield.

2.1.2 Microfiltration and ultrasonically assisted filtration

In addition to thermal oxidation, Shelimov and coworkers [125] proposed a method to purify single walled carbon nanotubes by ultrasonically assisted filtration. These methods were based on physical phenomena. In this method, sample sonication during filtration prevents filter contamination and provides a fine nanotube-nanoparticle suspension through purification. Amorphous and crystalline carbon impurities and metal particles are removed from single walled carbon nanotube samples by ultrasonically-assisted microfiltration. The process generates SWNT material with purity above 90% and yields of 30-70%. Although this method

could separate coexisting carbon nanospheres, metal nanoparticles, polyaromatic carbons and fullerenes from the carbon nanotube fraction, metal catalysts embedded in the tip and wall structure could not be eliminated by this method. One advantage of microwave digestion method was that the embedded metal catalyst would be eliminated and the purity of carbon nanotubes could be higher.

2.1.3 Acid treatment

A two step process of thermal annealing in air and acid treatment, proposed by Moon et al. [126], was used to purify single walled carbon nanotubes. This purification process used an acid treatment with HCl for 24 h to etch away the catalytic metals and obtained SWCNTs with metals below 1%. The result showed that the reproducible optimal purification process provided a total yield of about 25~30 wt % with transition metals less than 1%.

Zhang et al. [127] investigated the effect of PMMA and MCB on the purification and cutting of SWCNTs by thermogravimetric analyses. Chattopadhyay et al. [128] proposed a method of complete elimination of metal catalysts from single walled carbon nanotubes. Chen and coworkers [129] investigated a three steps purification of MWCNTs by which the raw material can be purified completely without damage. Various acids such as HF, H₂SO₄, HNO₃ and HCl have been used to remove metal catalysts mostly. These processes involved repeated steps of filtering and ultra-sonication in acid solution, for example, stirred in 3M nitric acid and refluxed for 24 h at 60°C, and then suspended and refluxed in 5M HCl solution for 6 h at 120°C. After acid treatment, samples were calcined in static air at 510°C for about 60 min. The total acid treatment processing time was above 30 hours. While metals are dissolved in solution, CNTs are cut into small length and even cause destruction. Walls of CNTs are always damaged by strong acid. Kajiura et al. [130] reported a three-step purification process consisting of soft oxidation with 2.8 N HNO₃ for 6-24

h, air oxidation for 10 min at 550°C and a high-temperature vacuum treatment for 3h at 1600°C. After the final step, about 20 % of the weight of the initial raw soot remained and the final product contained metals less than 1%. Bandow et al. [131] investigated a purification method of microfiltration which could separate carbon nanospheres, metal nanoparticles, polyaromatic carbons and fullerenes from single-walled carbon nanotube (SWNTs) fraction. Ando et al. [132] reported that MWCNTs were ground and boiled with 20% H₂O₂ in a reflux condenser for 45 h. Then the residual material was refluxed for 24h in a mixture of sulfuric acid (96%) and nitric acid (61%) with the ratio of 3:1.

2.1.4 Thermal oxidation combined with acid treatment

Another purification method to eliminate metal catalyst was proposed by Chiang et al. [133]. This method suggests a purification strategy to oxidize Fe and then dissolve the oxide. Raw material was heated in static air at 200°C for 24 h and followed by sonication in concentrated HCl (37%) in 80°C water bath for 15 min. Although the HCl treatment time was 15 min, the total purification time was obviously higher than 24 h. In this report, the total acid treatment time was below two hour. It was apparently that microwave digestion could effectively eliminate catalysts from carbon nanotubes and would not introduce structure defect.

In this work, a microwave-assisted digestion system was used to dissolve the metal catalyst. Inorganic acids such as H₂SO₄, HNO₃ and HCl can rapidly absorb microwave heat and energy and completely dissolve metals in carbon nanotubes. Since Environmental Protection Agency (EPA) recommended the microwave-assisted method with nitric acid [134], this leaching procedure of metals has been widely applied in sediments of soils and sludges. Nitric acid is strong enough to solubilize metals from materials. In closed microwave digestion system, metal catalysts are dissolved in acid solution rapidly without agitation. Therefore, lower concentration of

acids and acid immersing time are available to completely retain walls of carbon nanotubes. After purification, morphology of carbon nanotubes and purification degree are evaluated by SEM and TEM. The amount of residual catalyst metals in samples is estimated by thermogravimetric analysis (TGA). A high-yield and no destructive multi-walled carbon nanotubes in high purity are obtained. Metal content is less than 5 wt%

2.2 Fundamental and structure of DMFC

2.2.1 The Proton Exchange Membrane (PEM)

Direct methanol fuel cell is a kind of Proton Exchange Membrane fuel cells. As the name implies, PEMFC employs a proton exchange membrane (PEM). PEM serves as a physical barrier between anode and cathode gases and also as the electrolyte (hence it is also known as a solid polymer electrolyte). Today, the most common PEM is Nafion, a perfluorosulfonic acid membrane developed by E.I. DuPont de Nemours & Co. The structure of Nafion is shown in Fig. 2-1. Values of x and y can be varied to produce materials with different equivalent weights. The most common equivalent weight is 1100. Although Nafion is similar in structure to polytetrafluoroethylene (PTFE or Teflon), it has excellent mechanical strength, water insolubility and chemical and thermal stability. The sulfonated side chains endow Nafion with high proton conductivity and cation exchange capacity. Nafion has found numerous applications, such as liquid and gas separations, fuel cells and the chloro-alkali industry.

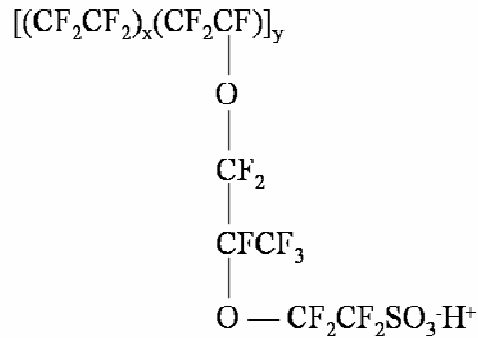


Fig. 2-1 Structure of Nafion.

Nafion is in structure a fascinating polymeric material. The exact structure of Nafion is not known but there have been several models proposed to describe the way how ionic groups aggregate within Nafion membranes. These models include the Mauritz-Hopfinger Model [135], the Yeager Three-Phase Model [136], the Eisenberg-Hird-More Model of Hydrocarbon Ionomers [137] and the Gierke Cluster Network Model [138]. Each model attempts to predict the fundamental features of equilibrium ionic selectivities and ionic transports. Electrostatic interactions cause the ionic groups to aggregate and form tightly packed regions referred as clusters [139]. These electrostatic interactions enhance intermolecular forces and considerably influence the properties of the parent polymer. Small angle X-ray scattering (SAXS) and neutron scattering clearly indicate that ionic clustering is present in Nafion [140]. Although no one model has been found to provide a complete explanation of the properties and selectivities found, several models base these properties and selectivities on an extensive micro-phase separated morphology [141,142]. Yeager's model describes Nafion as consisting of three regions: fluorocarbon region (A), interfacial zone (B) and ionic cluster region (C). These regions are depicted in Fig.2-2. Region A consists of the fluorocarbon backbone and is quite hydrophobic. Region (C) consists of clusters of pendant sulfonate groups. This region is quite hydrophilic and

most absorbed water and counterions exist in this region. Gierke has proposed that these ionic clusters are spherical and exist as a network interconnected by smaller channels [143]. Region (B) is an interfacial region containing the pendant side chain material and sulfonate groups that are not clustered. Hence, only part of the absorbed water and counterions exist in this region.

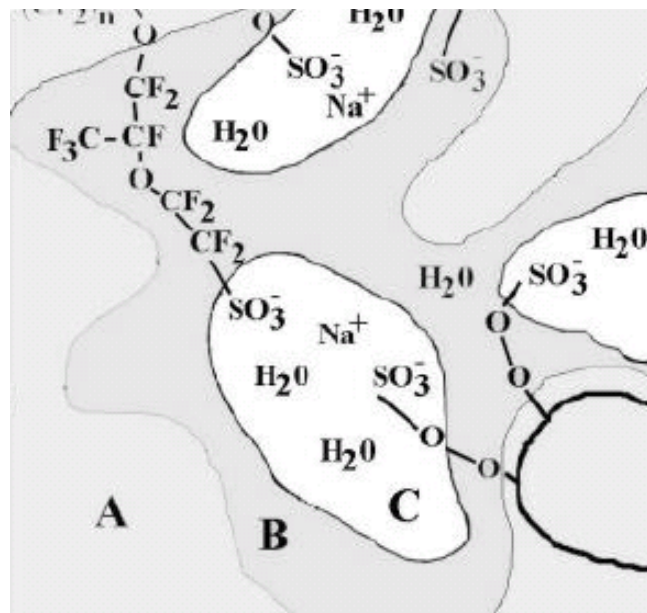


Fig. 2-2 Yeager's three-phase model of Nafion; a fluorocarbon region (A), an interfacial zone (B) and an ionic cluster region (C).

The proton conductivity of Nafion is dependant on its hydration state. In the dry state, Nafion is a poor ion conductor, but ionic conductivity increases sharply with water content [144] and reactant gases are therefore often humidified before entering a PEMFC. However, this induces water management at the cathode and limits the operational temperature of Nafion based PEMFCs to under around 100°C since sufficient liquid water must be present for good conductivity. However, if too much water is present, electrode pores and flow fields filled with water leads to mass transport problem referred as flooding. Therefore, water management is often a delicate balance that is critical to good performance. Companies such as Dow, Aciplex,

Gore and Ballard have developed other membranes. The scientific community has studied these membranes in less detail since they are proprietary to the companies that developed them. Generally, they have similar sulfonated perfluorocarbon structures.

2.2.2 Electrodes Structure of DMFC

DMFC electrodes are complex three-dimensional structures consisting of a number of different materials in a heterogeneous mixture. Much skill and art have been developed to produce structures with improved performances. Usually a 10-50 μm thick layer, consisting of carbon-supported Pt catalyst bonded with recast Nafion and/or PTFE is applied onto a gas diffusion backing. The backing is typically carbon fiber paper or carbon cloth that serves as a current collector and gas conduit. The backing is often treated to aid water management within the cell. The recast Nafion in the catalyst layer originates from a Nafion solution that can be mixed with the catalyst before electrode preparation or added once the catalyst layer has been formed. Its primary purpose is to provide a medium for proton conduction within the catalyst layer, because only those Pt sites that are in ionic contact with the membrane can be active for oxidation or reduction of fuels or oxidants. PTFE binds together the electrode particles and aids in water management. The catalyst, Nafion and PTFE are typically mixed together with water and alcohol(s) to form an ink. This ink is then spray-applied, brush-applied or even screen printed onto the backing [145]. Several proprietary methods have been reported where the catalyst mixture is applied directly onto the membrane [146,147]. Typically, electrodes are hot-bonded to each side of the membrane to form the membrane and electrode assembly (MEA). An MEA is shown in Fig.2-3. The thin size and low mass of the MEA is the main advantage of a DMFC. This allows the formation of compact lightweight stacks. A fuel cell stack consists of several MEAs electrically connected in series by bipolar plates. The bipolar plate serves as an electrical connection between MEAs and also physically separates

reactant gases. A schematic diagram of a single cell DMFC is shown in Fig. 2-4. Bipolar plates have flow fields machined onto each side to distribute reactant gases throughout the entire area of the electrode. The most common flow field shapes are serpentine and interdigitated.

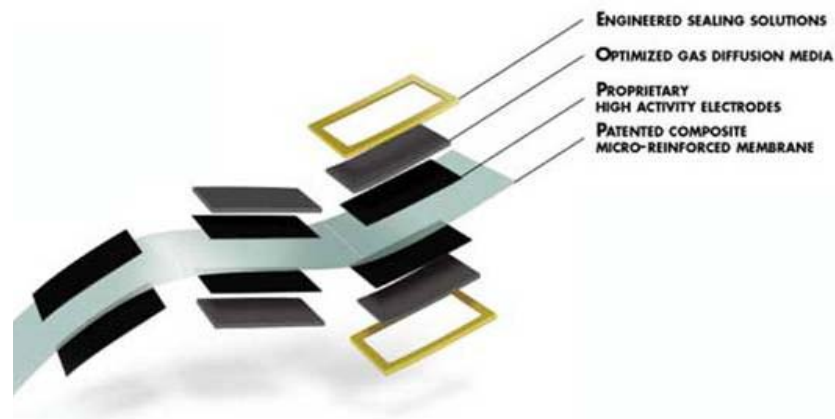


Fig. 2-3 Membrane and electrode assembly (MEA).

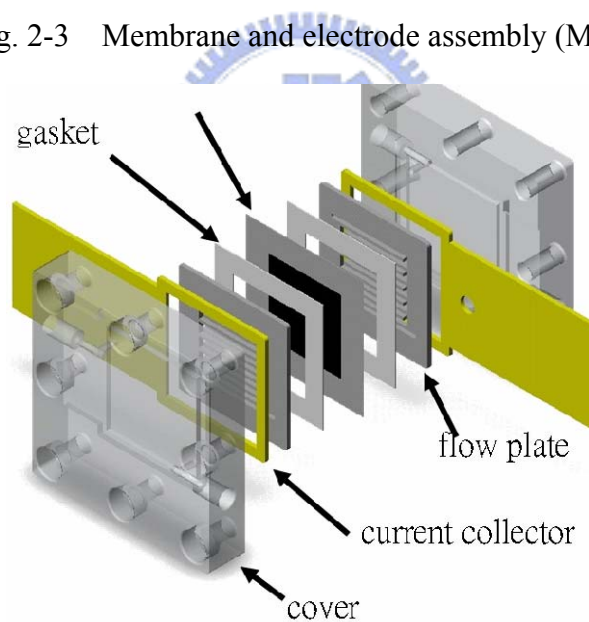


Fig. 2-4 Exploded view of a DMFC.

2.2.3 Anode structure and principle of DMFC

DMFC anodes typically consist of Pt catalyst, either Pt black or Pt on a carbon support. These anodes perform very well when pure hydrogen is used, but storage and infrastructure make hydrogen an inconvenient fuel to supply. To circumvent these

issues, hydrogen can be replaced by methanol. However, DMFC has a major drawback, that is, CO poison. When CO is absorbed and poisons Pt catalyst strongly onto its surface, active sites for hydrogen electro-oxidation are blocked to result in electrical current losses. The performance loss is unacceptable when CO of as little as 10 ppm is present in the fuel mixture. Obviously, a CO tolerant catalyst is expected. Pt is easily poisoned but bi-metallic Pt/X co-catalysts (X = Ru, Mo, Sn) have been shown to be more tolerant to CO. The second metal is deposited with Pt and will either reduce poisoning or decrease the potential by which CO is removed. Ru has been shown to be most effective. However, Ru addition further increases the cost of the anode. Higher temperature operation can also decrease the effect of CO poisoning.

2.2.4 Cathode structure and principle of DMFC

The oxygen reduction reaction (ORR) is a multi-electron process consisting of numerous elementary steps, involving both series and parallel pathways. It is generally accepted that oxygen reduction on Pt occurs via dissociative adsorption of O₂ followed by protonation of the adsorbed species, with the former being the rate-determining step. There have been several models that attempt to describe these pathways [148-150]. Several models successfully interpret the same data due to their similarity. One such model, illustrated in Fig. 2-5, is the bridge model of the ORR on Pt in acid. Because of the bridging oxygen system, it is obvious that optimal Pt particle spacing is of critical importance.

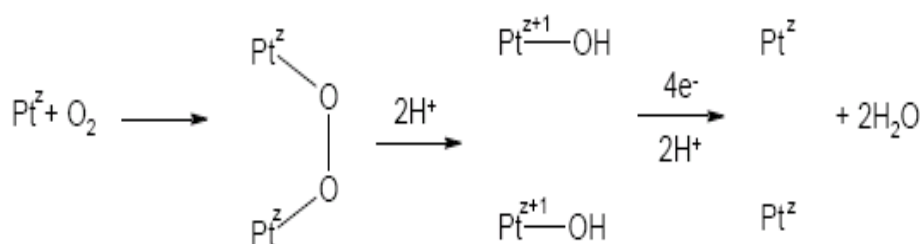


Fig. 2-5 Bridge model of oxygen reduction on Pt (z represents the oxidation state).

The complicated pathway of the ORR results in slow electrochemical kinetics. One measure of the rate of an electrochemical reaction is its exchange current density, j_0 . The j_0 of ORR on Pt is 10⁵ less than j_0 of hydrogen oxidation at Pt. This huge difference accounts for the chief influence of the cathode activity on hydrogen/air cell fuel performance. Therefore, cathode activity enhancement has been a major focus for PEMFC electrode development. In order to increase cathode activity, one must increase catalyst utilization. This will not only increase performance but can also lead to a lowering of the Pt loading required. In order to activate a catalyst site electrochemically, pathways for electron, proton and gas transports must all be present. The active area of Pt is typically measured by using cyclic voltammetry (CV) in acid electrolytes. Specifically, the area under the hydrogen adsorption/desorption peaks is determined as shown in Fig. 2-6. Regions of oxide formation (Q_A) and reduction (Q_C) as well as formation of hydrogen (H_A) and its reduction (H_C) are indicated. A larger area per mass of Pt indicates a larger active area. One very successful method to increase catalyst utilization is to employ carbon supported Pt catalyst. Typically, Pt particles (3-10 nm) are dispersed onto the electronically conducting carbon particles, about 30-50 nm. The ideal carbon support should possess high chemical stability, good electronic conductivity and high surface area for suitable pore size distribution. The best type of carbon for fuel cell catalyst support is carbon black. There are several types of commercial carbon blacks under study to be used in fuel cells, and Vulcan XC72 is the most common. Although carbon is an excellent electronic conductor, it is a very poor proton conductor because carbon is hydrophobic. However, the carbon surface does consist of hydrophilic moieties. Carbon-oxygen complexes, such as phenol, carbonyl, carboxyl, quinone and lactone groups can all be found on the carbon surface. In general, exposing the carbon to an oxidizing agent forms these complexes.

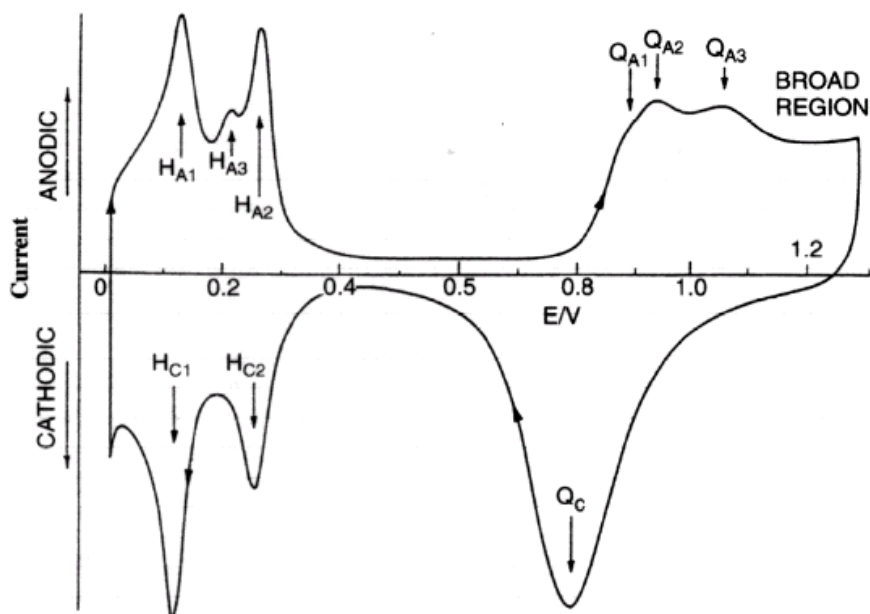


Fig. 2-6 CV of a platinum electrode in 0.5M H₂SO₄(aq).

One serious issue with Pt/carbon catalysts is the sintering of Pt particles [151]. Sintering occurs when Pt particles become larger over their lifetime. This decreases the Pt surface area, and ultimately leads to a decline in performance throughout the operation lifetime. An ideal catalyst support material that is both electronically and ionically conductive is desired. Pickup et al. have studied such a material, a conducting polymer composite [152]. The composite consists of polypyrrole and polystyrenesulfonate, which are electronically conductive and proton conductor, respectively. This material was tested as a replacement of carbon and reasonable performance was achieved. However, low Pt utilization and polymer stability are still issues [153]. Another method to increase catalyst utilization is to add a proton-conducting polymer (such as Nafion) into the catalyst layer. Pt catalyst near or directly in contact with the Nafion membrane is utilized most efficiently. However, utilization drops off deeper into the catalyst layer, largely due to the limited proton conductivity of the catalyst layer. Nafion solution can be applied onto preformed

electrodes or directly mixed with the catalyst during ink preparation. This increases the proton conductivity of the catalyst layer. In 1986, Raistrick was able to demonstrate that carbon-supported Pt catalyst mixed with Nafion could outperform conventional Pt black electrodes that had ten times the Pt loading [154]. This was a major breakthrough in fuel cell development in that it made the cost of Pt required much more feasible. To design an electrode with carbon-supported catalyst and Nafion, they must be mixed in proper proportions to form a stable three-phase boundary where the gas, ion conductor and electronically conducting phase with catalytical activity are all present. This requirement limits the amount of Nafion that can be added since the morphology, low gas permeability and poor electronic conductivity of Nafion disrupts this boundary and adversely affects cell performances. Because of this and the high cost of Nafion, alternative methods to provide proton conductivity in the catalyst layer are of interest. Another approach to increase Pt utilization is to simply deposit Pt only in the areas of the electrode where it would be electroactive. This can be done by sputter deposition where layers as thin as 2 nm can be deposited. There have been many studies that use sputter deposition to localize Pt catalyst at the front surface of the electrode or even directly onto the membrane surface. Srinivsan et al. applied a 50 nm thick layer of Pt onto an uncatalyzed gas diffusion layer (GDL) by sputter deposition and achieved a 10-fold reduction in Pt loading (from 4 mg/cm² to 0.4 mg/cm²) without performance loss [155]. Hirano et al. later showed that electrodes prepared by sputter deposition with Pt loading of 0.1 mg/cm² could perform the same as those prepared by using standard materials (Pt/C) at Pt loading of 0.4 mg/cm² [156]. Cha and Lee further reduced the Pt loading to 0.04 mg/cm² by alternating sputter deposited Pt layers and painted Nafion/Carbon ink layers with successively lower amounts of Pt in each layer [157]. This leads to very efficient utilization of Pt. Sputter deposition is promising for fuel cells since a larger

percentage of Pt is electrochemically active. It also allows the fabrication of very thin active layers to decrease ohmic and mass transport overpotentials in catalyst layers. Sputter deposition is a well established industrial technique in areas such as thin films and integrated circuits and it is anticipated that this technique could be readily applied to micro-fuel cell applications.

2.2.5 Limits of DMFC

One of the most important limitations of direct methanol fuel cell is the low catalytic activity of electrodes, especially anodes and at present, there is no practical alternative to Pt based catalysts. High noble metal loadings on the electrode [158,159] and the use of perfluorosulfonic acid membranes significantly contribute to the cost of devices. An efficient way to decrease the loadings of precious platinum metal catalysts and higher utilization of Pt particles is to better disperse the desired metal on suitable supports [160]. In general, small particle size and high dispersion of platinum on the support will result in high electrocatalytic activity. Carbon materials possess suitable properties for the design of electrodes in electrochemical devices. Carbon is an ideal material to support nano-sized metallic particles in the electrode for fuel cell applications. No other material except carbon has the essential properties of electronic conductivity, corrosion resistance, surface properties and the low cost required for fuel cell commercialization. In general, the conventional supports namely carbon black is used for the dispersion of Pt particles.

To improve the catalyst utility, the material with high surface area and high electron conductivity is required for the catalyst support. However, the high chemical resistance to acid or alkaline media, the possibility to control up to certain limits, the porosity and the surface chemistry made carbon based materials preferred for catalyst supports. Carbon possesses unique electrical and structural properties to be used in fuel cells. Various forms of carbon, such as graphite, carbon black and other

composite materials have been chosen for catalyst supports. Among them, carbon nanotubes represent a distinctive class of catalyst supports, exhibiting high surface area and many available adsorption sites. In single-walled carbon nanotubes, bundle adsorption sites are represented either by the grooves formed between adjacent tubes or by the nanotube interior, the interstitial channels between tubes and the outer bundle surface. For multi-walled carbon nanotubes, adsorption occurs in aggregated pores inside the tube or on the external walls. Besides these catalyst-related structural properties, carbon nanotubes are more stable to oxidation, feature an increased wear-resistance and possess a good thermal stability. Their metallic characteristics promotes them as good support for metal particles, but chemically functionalized nanotubes can support other catalysts as well, such as bimetallic nanoparticles and organo-metallic complexes. There are three other advantages for carbon nanotubes as catalyst supports. First, the high purity of the material prevents self-poisoning, a common problem of conventional catalysts. Next, the mere nature of these supports can be of interest for liquid-phase reactions and thus limits the mass transfer. Finally, the catalytic activity and its selectivity can directly benefit from specific metal–support interactions. An overall result of the above features tells that catalytic studies on carbon nanotube-based systems have confirmed increased loadings and good dispersion of catalyst particles with respect to other supports. When used as a catalyst support, carbon nanotubes lead to a typical activity and selectivity in several catalytic reactions such as hydrogenation of olefins and nitrobenzene into anilines or selective hydrogenation of double carbon bonds in unsaturated aldehydes. Also of interest are hydroformylation of olefins to aldehydes and partial dehydrogenation reactions. Another applications target catalysts for redox reactions and catalytic decompositions.

2.2.6 Synthesis of Pt catalyst by more efficient method

In recent years, some research teams have reported the synthesis of Pt catalysts by using microwave-assisted heating polyol process [161,162]. The reactant mixture of Pt or other metal precursor, support materials, ethylene glycol and different kinds of additives in a beaker was placed in the center of a household microwave oven and heated for 5s irradiation on and 60s irradiation off for six times (so called “intermittent microwave heating”, IMH), or heated only for tens of seconds. These studies showed that microwave synthesized metal nanoparticles were very uniform in size and well dispersed on support material. The process indeed has advantages of simplicity, short reaction time and high energy efficiency. However, the most important key factor of a chemical reaction is still unknown, that is, the actual reaction temperature of metal precursor to precipitate as metallic nanoparticles in a household microwave oven is hard to be controlled or only be recorded during experiments. Besides, the loading amount (<20 wt%) and the dispersion density of Pt particles on support, carbon black, are still lower than that (about 40~60 wt%) of convention methods.

There are many factors that affect the efficiency of proton exchange membrane fuel cell (PEMFC). Direct methanol fuel cell (DMFC) with Pt/C catalyst is one effective factor for the transformation of hydrogen in methanol to water [163,164]. It is well known that the catalytic activity of Pt/C catalyst is strongly related to the Pt particle size, the particle size distribution degree and the dispersion of Pt on carbon support [165]. Therefore, Pt catalyst with suitable size, narrow size distribution and high dispersion should have high electro-catalytic activity in fuel cell application. As a result, considerable attention has been laid upon the synthesis and characterization of catalyst nanoparticles [166-168]. The simplest method, wet impregnation, used to synthesize Pt nanoparticles on electro-catalyst support is to impregnate the support

(usually carbon black) with a platinum precursor, and then heat the support above 300°C in the hydrogen atmosphere. However, the control of particle size and size distribution by this method is rather limited [169]. Hence, there are continuing efforts to investigate alternative methods to synthesize highly dispersed supported Pt particles with size-control and uniform size, such as micro-emulsions [170], supercritical fluid [171], sono-chemistry [172,173], polyol process [174,175] and sputtering[176]. All these methods generate colloids and clusters on the nanoscale and with greater uniformity. However, these methods are either time-consuming and complex in multi-step process, or low loading of Pt nanoparticles dispersed on supports.

In this present work, temperature-controlled microwave heating system was used to demonstrate the temperature effect on polyol process, and the effects of additives, reaction-time and other parameters on particle size, size distribution, loading amount and dispersion were also investigated under temperature controlled microwave heating process to obtain high dense Pt clusters on CNTs.

Chapter 3 Experimental Details

3.1 Experiment Procedures

3.1.1 Experiment flow chart of purification process

Fig 3.1 shows the experiment procedures of purification of MWCNTs. Raw MWCNTs were characterized by SEM, TEM, TGA, and Raman before purification and then purified by microwave heating system. After purification, samples were dried and characterized to investigate the effect of microwave heating method.

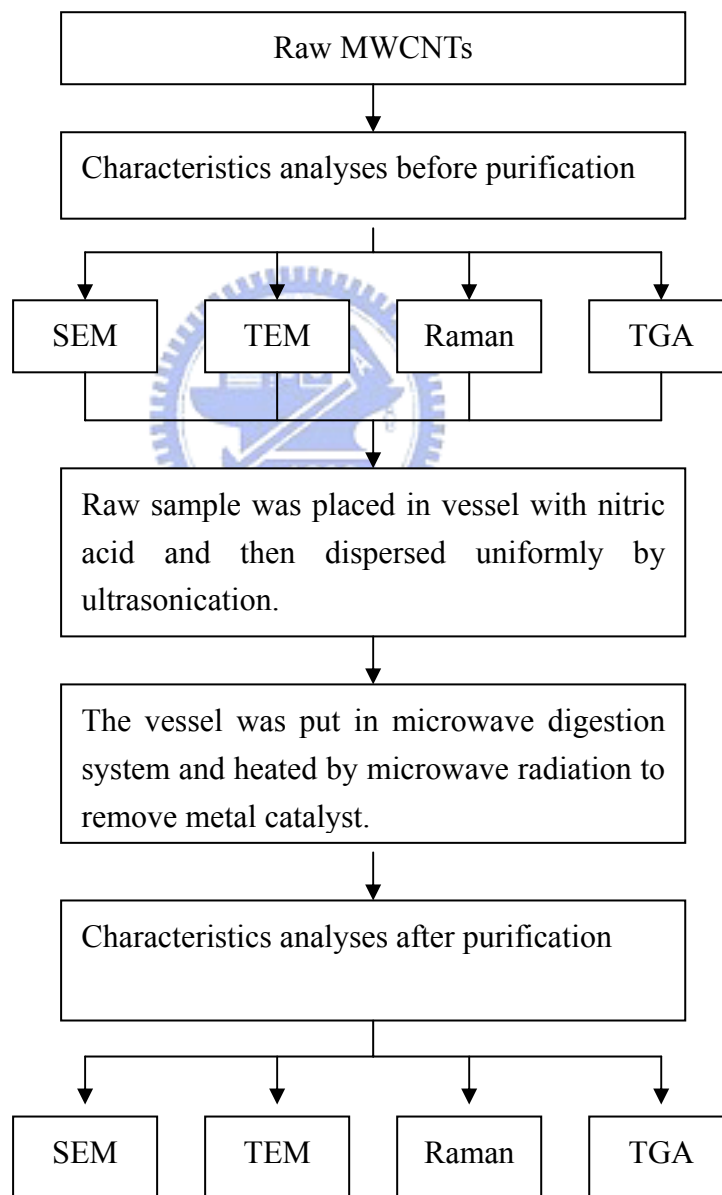


Fig. 3-1 Experiment flow charts of purification process.

3.1.2 Experiment flow chart of Pt-synthesis process

Fig 3.2 shows the experimental procedures of Pt particles synthesis on MWCNTs.

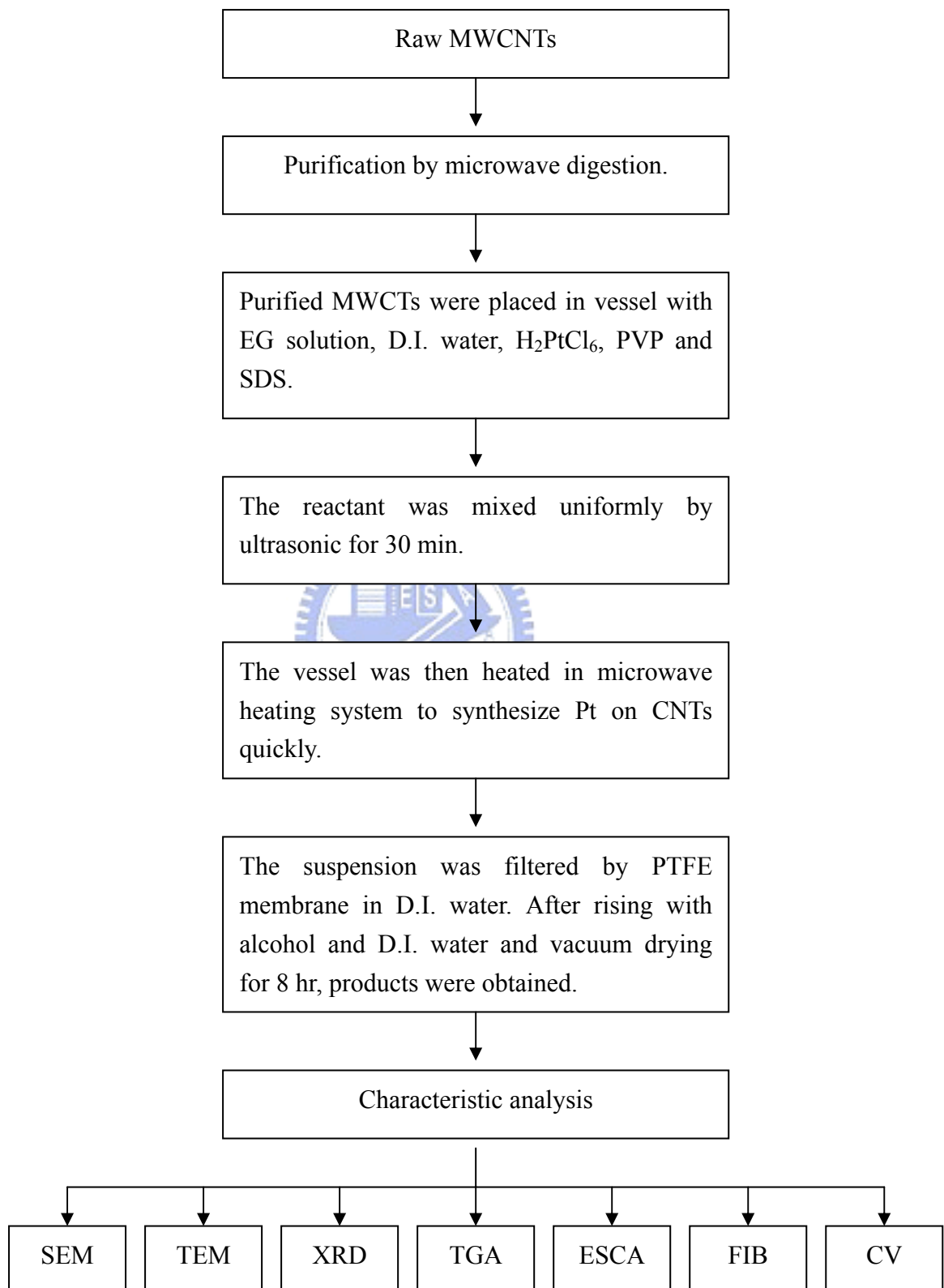


Fig. 3-2 Experiment flow charts of Pt particles synthesis process.

3.2 Experiment equipments

3.2.1 Microwave system

The microwave digestion system (Milestone Microwave Labstation ETHOSD), shown in Fig. 3-3, has dual magnetrons (1600 Watt) that can create a homogeneous microwave field with no cold or hot spots for incomplete digestions. The advantages of this method are high temperature, closed vessel, acid digestion samples, less acid consumption and volatile elements available.



Fig. 3-3 Microwave digestion system [177].

3.3 Analysis instruments

3.3.1 Thermogravimetric Analyzer (TGA)



Fig. 3-4 Thermogravimetric Analyzer, TA Instruments [178].

Q500 is a top-of-the-line research grade thermogravimetric analyzer, as shown in Fig. 3-4. Its efficient low mass furnace, ultra-reliable thermobalance, unique purge gas system (with mass flow control) and advanced automation provide superior TGA performances. Q500 offers the highest sensitivity (0.1mg) with very low baseline drift over the temperature range from ambient to 1,000°C. Sample pan loading and furnace movement are totally automated, and the touch screen data display of operating parameters makes increased convenience for users. TGA autosampler is a programmable multi-position sample tray accessory for Q500. It allows the routine unattended analysis of up to 16 samples but can be programmed for up to 64 samples. Sample trays are easily mounted and dismantled from Q500. In addition to increased productivity, the autosampler has flexibility sufficient to satisfy experimental requirements of both analytical and QC laboratories. High precision TGA experiments require constant purge gas flow rates. Control of the flow rate is especially important for high conductivity gases such as helium. Mass flow controllers with integrated gas

switching capability provide this control as part of an individual programmed method. Purge gas flow rates are settable from 0 to 240 mL/min in the increment of 1 mL/min. The system is pre-calibrated for helium, nitrogen, air and oxygen with calibration factors available for other non-corrosive gases.

3.3.2 Scanning Electron Microscopy (SEM)

Scanning electron microscopy is used to observe the object surface morphology over a wide varieties. It has the advantage of rather easy sample preparation, high image resolution, large field depth and high magnification. A common SEM contains an electron gun to generate electron beams accelerated under 0.4-40kV voltage. By deflecting incident beams with focusing coils, a two dimensional image can be obtained by detecting reflected secondary electrons and backscatter electrons. The model used here is JEOL 6500 with field emission electron source and 15kV accelerate voltage.

3.3.3 Transmission Electron Microscopy (TEM)

Transmission electron microscopy (TEM) is by far the most important technique to study defects in great detail. Theories of previous defect statements would be speculative or would never have been conceived without TEM. In a typical TEM, a static electron beam at 100-400kV accelerating voltage illuminates a region of electron transparent specimen immersed in the objective lens of the microscope. Transmitted and diffracted electrons are recombined by objective lens to form a diffraction patter in the back focal plane of those lens and a magnified image of the sample in its image plane. A number of intermediate lenses are used to project either the image or the diffraction patter onto a fluorescent screen for observation. The screen is usually lifted and the image is formed on photographic film for recording. A simple diagram of typical TEM instrument is shown in Fig. 3-5.

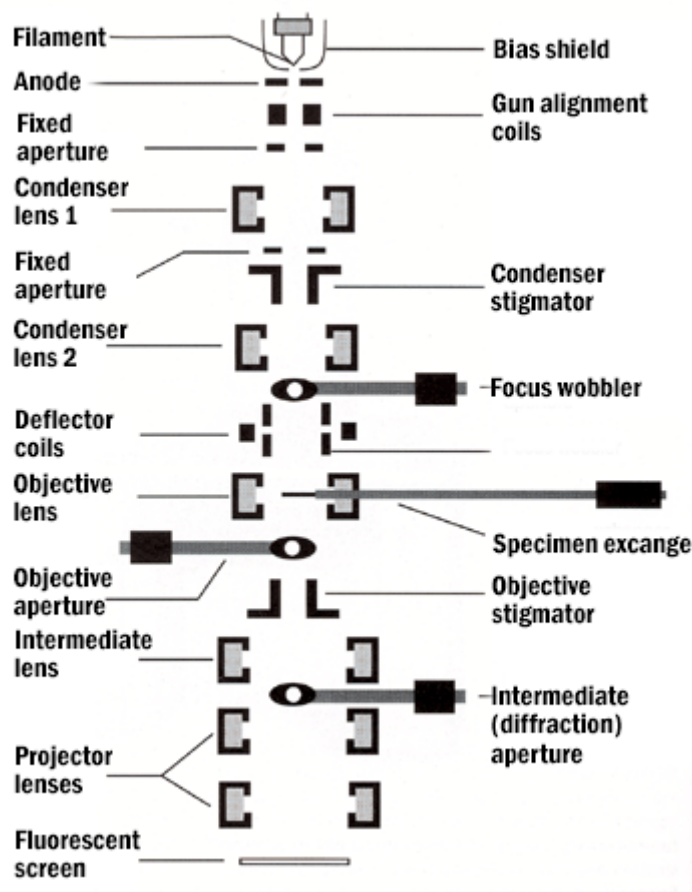


Fig. 3-5 Schematic diagram of a TEM.



3.3.4 Raman Spectroscopy

A powerful and nondestructive method to determine the nanotube structure is Raman spectroscopy, which is widely used to study the vibrational modes of carbon-based graphitic nanostructures. While photons illuminate a molecule or a crystal, the reaction with atoms is accompanied with momentum change or energy exchange. Collection of scatter photons brings about a sequence of spectrums, including Raman scattering (inelastic scattering) and Reyleigh scattering (elastic scattering). The photon of Raman scattering can be classified into two kinds, Stoke side in which photons lose energy or molecules gain energy, and anti-Stoke side, in which photons gain energy or molecules lose energy. Stoke side is used to characterize the material. As Raman spectrum provides information of crystallinity

and bonding, it has become the most direct and convenient way to identify carbon related materials. The instrument used is HORIBA Jobin Yvon, HR800. The source is Ar laser with wavelength of 514.3nm and power of 12mW. The spectral slit width is 0.4 cm^{-1} .

3.3.5 Energy Dispersive X-ray Analysis (EDX)

EDX is a micro-analytical technique that uses the characteristic spectrum of x-rays emitted by the specimen after high-energy electron excitation to obtain its elemental composition information. Elements detectable by EDX and electron energy loss spectroscopy (EELS) are somewhat complementary; EDX is generally suitable to detect elements of high atomic number (Z) whereas EELS can readily detect low-Z elements. Unlike EELS, EDX does not provide chemical information (except through quantitative analysis in some cases). Compared to EELS, EDX is a relatively simple technique and provides rapid qualitative microanalysis of the specimen.

3.3.6 X-ray Diffraction (XRD)

XRD is a useful tool to analyze the crystallography of specimen and to determine the mean size of particles. When X-ray radiation passes through matter, the radiation interacts with electrons in atoms and result in radiation scattering. If atoms are organized in planes and distances between atoms are of the same magnitude as the wavelength of X-rays, constructive and destructive interferences occur and result in diffraction by which X-rays are emitted at characteristic angles according to the spaces between atoms organized in crystalline structures called planes. Most crystals have many sets of planes through their atoms. Each set of planes has a specific interplanar distance and gives rise to a characteristic angle of diffracted X-rays. The relationship among wavelength, atomic spacing (d) and angle was solved by the Bragg Equation. If the illuminating wavelength is known and the angle can be measured, the interplanar distance can be calculated from the Bragg equation: $n\lambda =$

$2d\sin\theta$. A set of 'd-spaces' obtained from a single compound represents the set of planes that pass through atoms and is used to compare with d-space sets obtained from standard compounds.

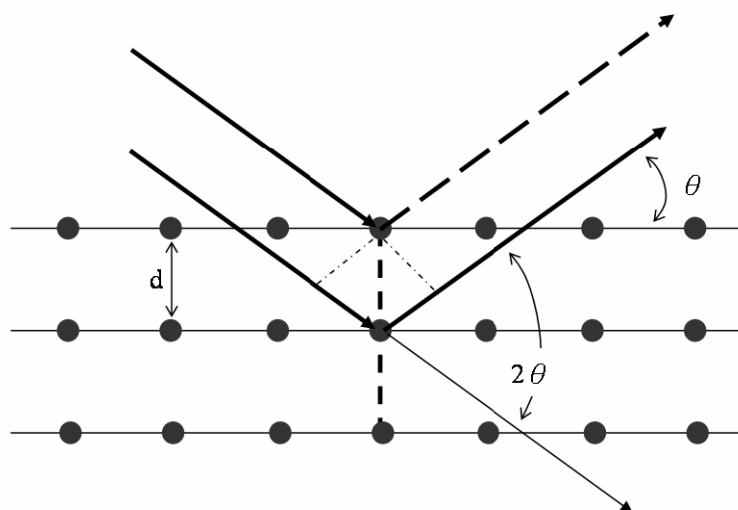


Fig. 3-6 Schematic diagram of Bragg's law.

3.3.7 Cyclic Voltammetry (CV)

Cyclic voltammetry is the most widely used technique for acquiring qualitative information about electrochemical reactions. The power of cyclic voltammetry results from its ability to rapidly provide considerable information on thermodynamics of redox processes and kinetics of heterogeneous electron-transfer reactions, and on coupled chemical reactions or adsorption processes. A simple potential wave form that is often used in electrochemical experiments is the linear wave form in which the potential varies continuously as a linear function of time. The rate of change of potential with time is referred to as the scan rate (v). A more commonly used variation of the technique is cyclic voltammetry, in which the direction of the potential is reversed at the end of the first scan. Thus, the waveform is usually of the form of an isosceles triangle. This has the advantage that the product of the electron transfer reaction in

the forward scan can be probed again in the reverse scan. In addition, it is a powerful tool to determine formal redox potentials, to detect chemical reactions preceding or following electrochemical reactions and to evaluate electron transfer kinetics. Fig. 3-7 is the experimental setup of the cyclic voltammetry measurement. Cyclic voltammograms were recorded by CH Instrument 614B potentiostat using a three-electrode cell. Platinum wire served as the counter electrode and saturated calomel electrode (SCE) was used as the reference electrode. The working electrode is a Pt wire attached with a thin Pt foil, used to contact with the testing sample.

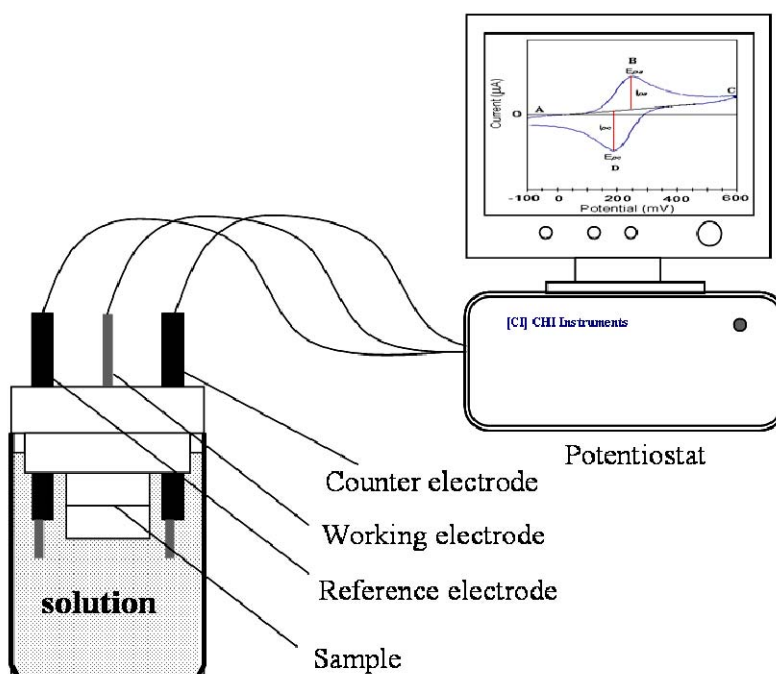


Fig. 3-7 Schematic diagram of a cyclic voltammetry experiment.

Chapter 4 Purification of MWCNTs Using Microwave

Heating Method

4.1 Purification of MWCNTs Synthesized by ECR-CVD

4.1.1 Sample Preparation and Experiment Procedures

Co catalyst nanoparticles were deposited on P-type Si (111) wafer by sputtering. Co catalyst was 7.5nm in thickness. Experiments were engaged by electron cyclotron resonance chemical vapor deposition (ECRCVD). Mixture of CH₄ and H₂ was used as sources gas. Gas flow rates of CH₄ and H₂ were 18 sccm and 2 sccm respectively. Power was set at 800W. The reaction temperature was 600°C. After deposition, a scanning electron microscope (Hitachi S-4700I) was used to examine the morphology of MWCNTs. High resolution transmission electron microscope (Philips Tecnai-20) was then used to investigate the microstructure of MWCNTs.

Acidic treatment in microwave digestion system (Milestone Microwave Labstation ETHOSD) was used to dissolve the metal catalyst. In this procedure, raw sample of MWCNTs were placed in a 100 ml Pyrex digestion tube. The first digestion step run at 210°C for 20 min with a 1:1 mixture of 5M HNO₃ and 5M HCl. The microwave power was set at 100W. The second digestion step was carried out at 210°C for 30min. After digestion, the suspension was filtered with 0.1µm PTFE (poly-(tetrafluoroethylene)) membrane in deionized water. After rinsing with alcohol and drying the sample, a black thin mat composed of MWCNTs was obtained.

4.1.2 Characterization of the Purified MWCNTs and Discussions

After purification, the morphology of MWCNTs and purification degree were observed by TEM The amount of residual catalyst metals in samples will be estimated with thermogravimetric analysis (TGA) by using a thermal analysis system of PERKIN ELMER 1020 Series TGA 7 with a rate of 20°C /min from 30°C to 900°C at

the air flow rate of 10 sccm. Acid treated MWCNTs were oxidized by air at the temperature determined by TGA for 45 min.

Figure 4-1 shows a low magnification TEM image of raw carbon nanotubes. In this image, there appeared impurities such as amorphous carbons, graphite and metals in multi-walled carbon nanotubes. Metal particles were evidently embedded in the tip or in tube core of MWCNTs. Many bundles with diameters ranging from 10 to 30 nm can be observed in the TEM image.

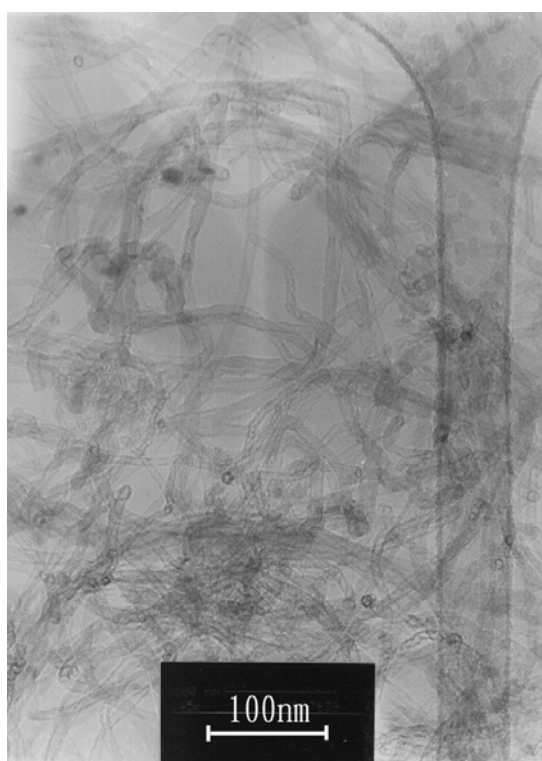


Fig. 4-1 A low magnification TEM image of raw carbon nanotubes.

Figure 4-2 shows a low magnification TEM image of MWCNTs after purification by microwave digestion. It indicated that most of the metal particles were removed. The structure and wall of MWCNTs were not destroyed. It is well known that HNO_3 is very efficient in solving metal particles and HCl is good in solving metal oxide. Amorphous carbon can be removed by nitric acid because it is a strong oxidant.

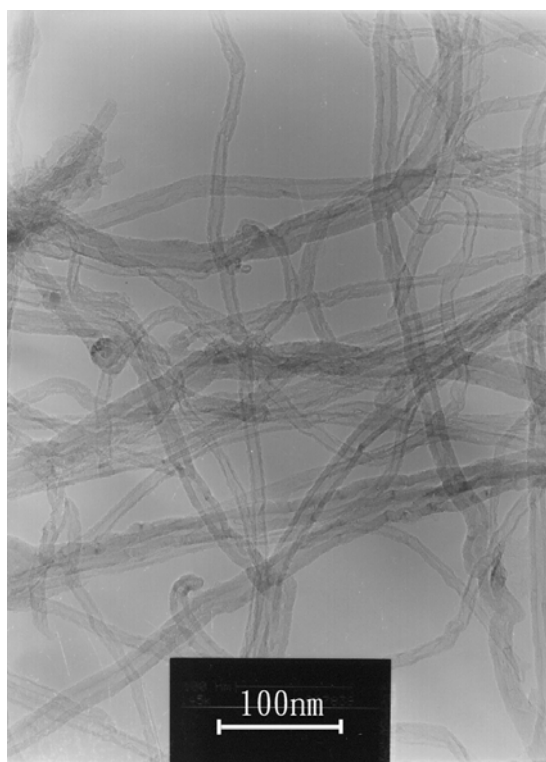


Fig. 4-2 A low magnification TEM image of MWCNTs after purification by microwave digestion.

However, in the microwave system, inorganic acid such as HNO_3 and HCl rapidly absorbed microwave heat and energy without agitation and rapidly dissolved metals. The processing time of the two step microwave-assisted and acid treated approach to dissolve metals in the MWCNTs was less than one hour. In a microwave digestion system without agitation, heat was absorbed rapidly so that metal catalysts could be eliminated from MWCNTs rapidly without damage.

Chen et al. [129] reported a three step non-destructive purification of MWCNTs by which the raw material can be purified completely without damage. But their procedure was crudely stirred in 3M nitric acid and refluxed for 24 h at 60°C , and then suspended and refluxed in 5M HCl solution for 6 h at 120°C . The total acid treatment processing time was above 30 hours. Moon et al [126] proposed a two step process of thermal annealing in air and acid treatment to purify single walled carbon nanotubes. This purification process used an acid treatment with HCl for 24 h to etch

away the catalytic metals and obtained SWCNTs with metals less than 1%. Kajiura et al. [130] reported a three-step purification process consisting of soft oxidation with 2.8 N HNO₃ for 6-24 h, air oxidation for 10 min at 550°C and a high-temperature vacuum treatment for 3h at 1600°C. After the final step, about 20 % weight of the initial raw soot remained and the final product contained metals less than 1%. Most purification methods removed metal catalysts with acid for more than 24 h. Too long nitric acid treatment will break down CNTs to small pieces [126].

Figure 4-3 shows a TEM image of MWCNTs treated by acids. It indicates the open end of MWCNTs and reveals that the cap is etched off and the wall of the graphite structure is not damaged. The tube diameter is about 20 nm. So, lower acid concentration and immersing time are available to completely retain carbon nanotube walls.

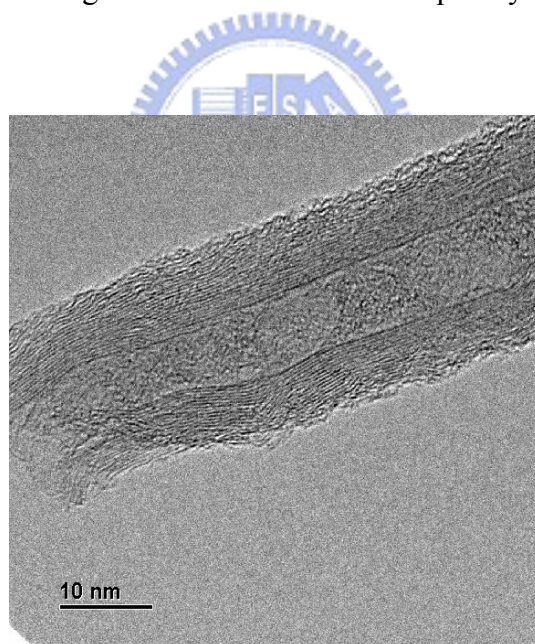


Fig 4-3 TEM image of acid treated MWCNTs.

Microwave-assisted digestion system was used in this research to dissolve metal catalysts. Since the total acid treatment time of the two steps digestion system was less than 1h, microwave digestion is effective and fast to remove metal particles from carbon nanotubes.

Combustion of acid treated samples proceeds to purify CNTs according to the

oxidation temperature difference between non-carbon nanotubes and CNTs. The burning temperature of CNTs is related to pre-treatment process and graphitization degree, so there is no general combustion temperature of CNTs. TGA is an effective method to detect the combustion temperature in air.

Figure 4-4 shows TGA graphs of raw samples and purified MWCNTs. Figure 4-4(a) shows the TGA of raw samples and indicates that the weight starts to reduce near 410°C. MWCNTs are completely evaporated at 730°C. The remaining materials are metal catalysts, the amount of which is about 30 % of the whole weight. The TGA graph indicates the existence of three phases in the sample. A peak at 520°C in the differential TGA suggests the presence of amorphous carbons and the other small peak at 630°C indicates that high temperature oxidation damages MWCNTs.

Figure 4-4(b) is the TGA graph of the sample after microwave digestion and acid purification treatment. It shows the correspondence between the slow weight loss from 30 to 450°C and the loss of water and amorphous carbon. In the temperature range from 450 to 650°C, the weight decreases sharply to 5.25 wt %. The broad peak at 520°C in the differential TGA is assumed to be amorphous and another peak at 610°C indicates the damage of MWCNTs due to high oxidation. Combustion temperature of MWCNTs begins at 600°C. The curve slope keeps almost constant in the temperature range between 490°C and 650°C. It shows a constant combustion speed. After 650°C the weight of MWCNTs remains constant, and the remainders may be metals and metal oxides which reside inside the tube before combustion. So, the optimum amorphous combustion temperature is about 520°C. The burning temperature of CNTs is related to pre-treatment process and graphitization degree, so it has little in common. TGA is an effective method to detect the combustion temperature in air. Dillon et al. [179] reported that the combustion temperature of carbon nanotubes is 785°C by TGA.

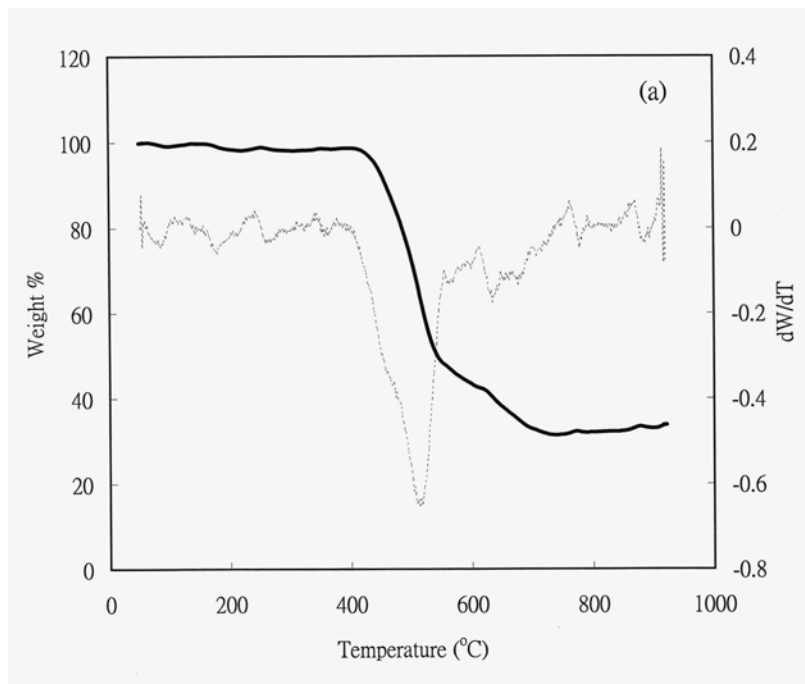


Fig. 4-4(a) TGA graphs of raw samples and purified MWCNTs.

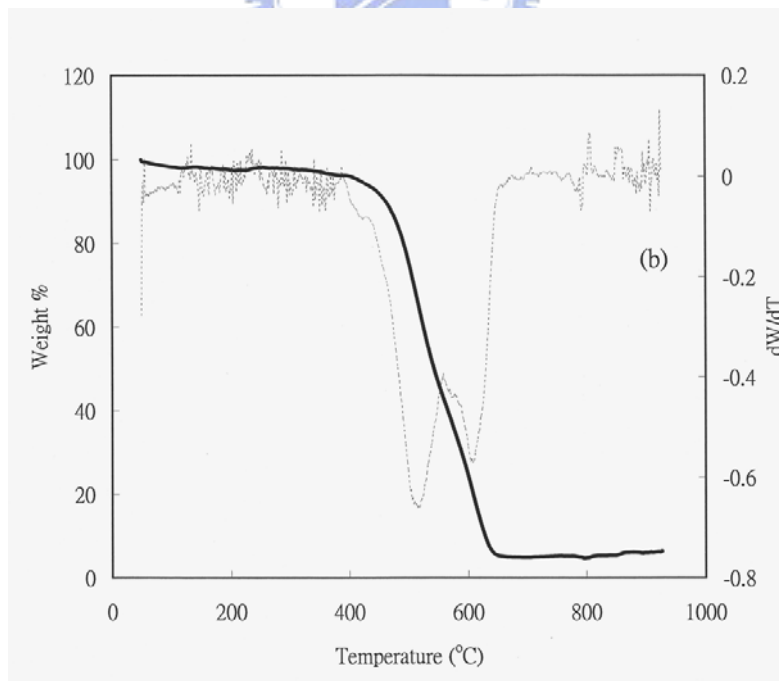


Fig. 4-4(b) TGA graphs of raw samples and purified MWCNTs.

In their procedure, carbon nanotubes were synthesized by using laser vaporization method. Colomer and coworkers [180] proposed that the optimum reaction temperature in air is 500°C for CNTs synthesized by catalytic chemical vapor deposition. Chen et al. [129] reported that raw materials of CNTs produced by different catalyst and synthesis methods are different in component and in graphitization degree. Therefore, the combustion temperature of raw carbon nanotubes synthesized by ECRCVD in our purification procedure begins at 520°C. This conclusion matches that of Colomer et al. [180]. They reported the burning temperature in air is 500°C for CNTs synthesized by catalytic chemical vapor deposition.

While microwave digestion purification procedure for MWCNTs synthesized by catalyzed CVD is an effective purification process, TGA is a good and accurate approach to evaluate the purity of MWCNTs on a weight percentage basis.

4.1.3 Summary

Presented in the research are MWCNTs of high yield and no damage by a two step microwave digestion system with acid treatment. In the microwave system, HNO₃ and HCl rapidly absorb microwave heat and energy and completely dissolve metals for purification without damage and of high quality. The processing time of the two step microwave-assisted and acid treated system to dissolve metals in MWCNTs is below one hour. After purification, the amounts of residual catalyst metals in samples reduced from 30wt% to 5.15 wt %. The results show that multi-walled carbon nanotubes of no damage and with metals about 5% are obtained. Conclusion is attained that microwave digestion method is an effective purification procedure for MWCNTs.

4.2 The effects of different experiment conditions on purification of MWCNTs

4.2.1 Experiment Conditions and Procedures

In the experiment of group A, as-prepared commercial multi-walled carbon nanotubes with diameters of 40-60 nm were dispersed in 25 ml deionized water with ultrasonic agitation for 1, 2 and 3 h. The weight of each sample was 0.6 g. After sonication, each sample was dried and then divided into three parts for microwave purification for 30, 60 and 90 min in 1M nitric acid and the weight of each part became 0.2 g. Procedures were the same for group B and group C, but different in acid concentration. Group B was purified by microwave-assisted purification with 3M nitric acid and group C with 5M nitric acid as shown in Table 4-1.

Table 4-1 Experiment condition of nitric acid concentration, sonication time, and microwave-assisted purification time.

Experiment groups	Group A	Group B	Group C
Concentration of nitric acid	1M	3M	5M
Sonication time	1 h, 2 h, 3 h		
Microwave-assisted acid-treatment time	30, 60, 90 min		
Microwave power	100 W		
Temperature	210 °C		

In purification, samples were placed in 100 ml TFM (thermally resistant form of Teflon by Milestone) vessels filled with nitric acid and then put on the sample rotor made of Teflon and available for 12 vessels. The power of microwave was set at 100 W. At the first step, temperature ramped up from room temperature to 210°C in 30 min. The temperature was controlled by temperature control system (ATC-400CE)

with continuous monitoring and $\pm 1^\circ\text{C}$ control of the internal temperature in a standard Milestone reference vessel. The maximum operating temperature of ATC-400CE is 300°C . The second step was carried out isothermally at 210°C for 30, 60 and 90 min respectively. After digestion, the suspension was filtered with $0.1\ \mu\text{m}$ PTFE (poly-(tetrafluoroethylene)) membrane in deionized water. After rinsing with alcohol and vacuum drying for 8 h, there appeared a black thin mat.

The morphology of MWCNTs and the wall structure of nanotubes before and after purification were observed by high resolution transmission electron microscopy (HRTEM, Philips TECNAI 20). The amount of metal catalysts in the raw sample and purified sample was estimated by thermo-gravimetric analysis (TGA, PERKIN ELMER 1020 Series TGA 7) at the heating rate of 20°C per minutes from 30°C to 900°C under the air flow rate of 10 sccm. The bonding structure of carbon nanotubes in raw and purified samples was analyzed by Raman spectroscopy (Renishaw system 200).

4.2.2 Characterizations of MWCNTs of various experiment conditions and discussions

Figure 4-5 is a low magnification TEM image, which shows that raw samples contain multi-walled carbon nanotubes and metal catalysts. In this image, metal catalysts of various sizes can be found in the tip or tube wall of MWCNTs. MWCNTs with diameters from 40 to 60 nm can also be displayed by TEM. In Figure 4-6, the image shows that most of metal particles were removed from MWCNTs after purification. As shown in Figure 4-7, catalysts embedded in the tip of MWCNTs were removed. Obviously, the closed tube tip was opened by acid treatment in microwave digestion. It seems that closed tip was opened first and then the metal catalyst was eliminated by nitric acid. This high resolution TEM image also shows that the tube wall structure was not damaged by acid treatment.

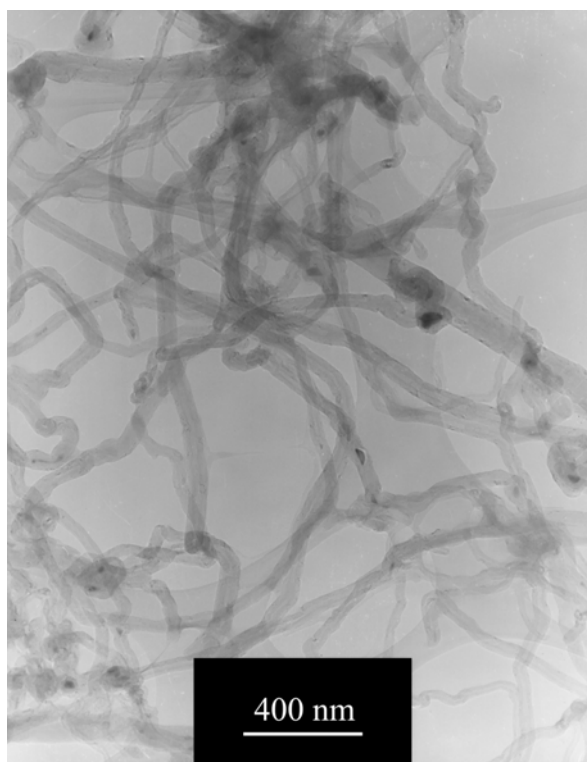


Fig. 4-5 Low magnification TEM image of raw MWCNTs.



Fig. 4-6 Low magnification TEM image of purified MWCNTs.

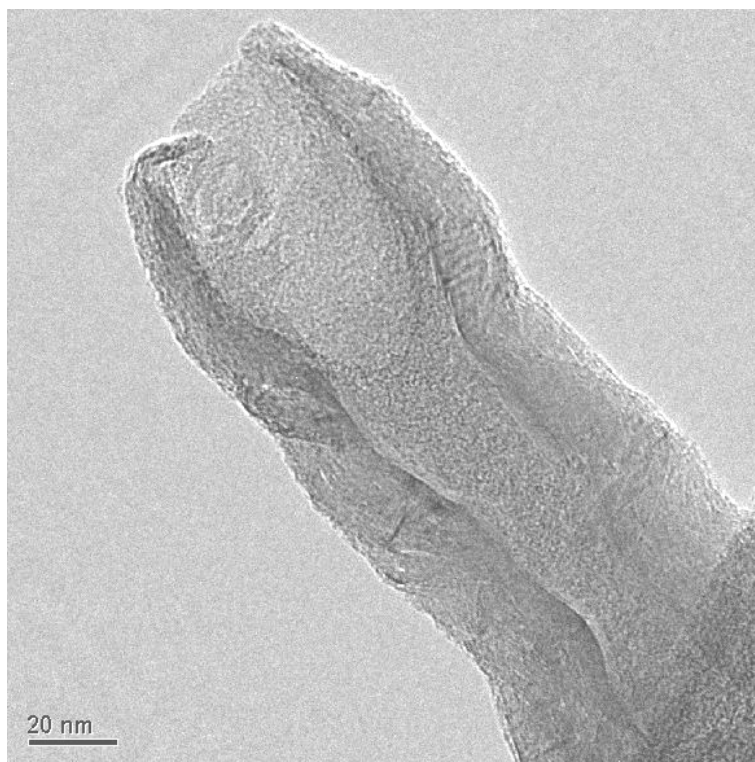


Fig. 4-7 Catalysts embedded in the tip of MWCNTs were removed.

Figure 4-8 shows the effect of acid concentration on purification for various processing time. The TGA measurement of the amount of residual catalyst is effective to evaluate the key features of purification. Behavior of the weight-temperature curve reveals that by-products during acid treatment such as carbonaceous appear in as-purified samples [126]. Curves a and b show that the purification for shorter microwave-digestion time is not strong enough no matter how high the acid concentration is. However, curve c shows that catalyst elimination increases with increasing acid concentration for 90 min treatment. This result could be that it takes time for the tube-open process to take place. In excess of the critical time, metal could be etched away quickly. In this experiment, 5 M nitric acid and 90 min might be appropriate parameters to purify carbon nanotubes.

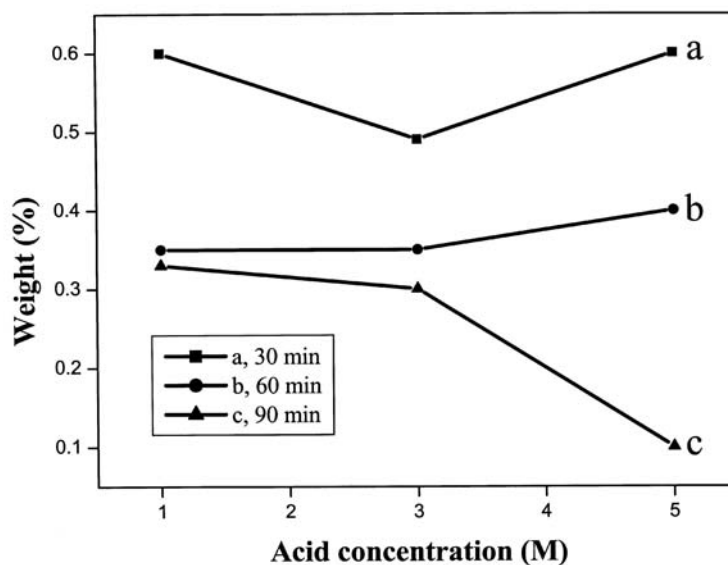


Fig. 4-8 Effect of acid concentration on purification ability for different processing time.

Figure 4-9 shows the effect of ultra-sonication time on purification efficiency with 5 M nitric acid for various treatment time. In curves d and e, increases of sonication time result in the decrease of residual metal amount. In samples with 60 min purification treatments, catalyst amount measured by TGA decreases from 0.49% to 0.31% with increasing treatment time from 1 h to 3 h. It seems that raw samples are more dispersed in ultrasonic treatments for longer acid treatments. However, acid treatment time of 90 min (Curve f) reveals almost the same amount of residual catalyst. The results could be that acid treatment time might dominate purification efficiency and long sonication time, which might induce the defect of tubes wall [125], is unnecessary.

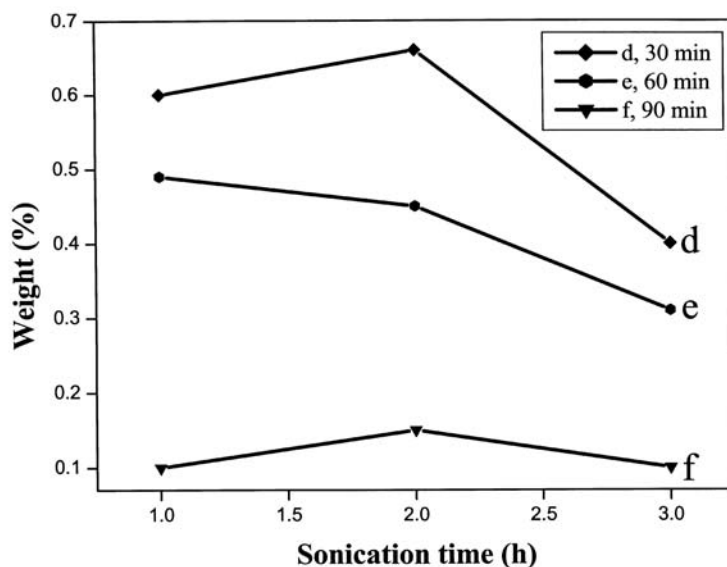


Fig. 4-9 Effect of ultra-sonication time on purification efficiency of 5 M nitric acid.

Figure 4-10 shows the results of TGA analysis of raw and purified samples. In Figure 6(a), the TGA analysis shows that metal catalyst content in the raw sample was 1.34%. The early slight weight gain in the raw sample might be due to the oxidation of metal catalysts. Raw sample weight starts to reduce near 515°C and MWCNTs completely evaporate above 712°C. The decomposition temperature at 673°C is defined as the inflection point during the oxidation of tubes [126]. Different from the raw sample, purified MWCNTs start to lose weight by burn-off from 550°C and completely burn-out near 758°C, as shown in Figure 6(b). The amount of residual catalyst dropped to 0.1 wt% in purified sample of group C for 90 min purification. The decomposition temperature in this purified sample was 703°C, which was slightly higher than that in the raw sample. This result reveals that residual metal embedded in raw samples acted as oxidation site and initiated oxidations [179]. It was also reported that metal impurities in the sample would lower the decomposition temperature and increase the decomposition rate [179]. The purified sample is thermally more stable towards oxidative destruction than raw MWCNTs. In Figures 6(a) and 6(b), there are

evidently no other separate regimes except the main combustion regime. This points out that microwave digestion does not introduce carboxyl, aldehyde and other oxygen-containing functional groups on the surface of the non-nanotubes carbonaceous fractions. These groups, by report, were extremely hygroscopic and reactive towards oxidation.

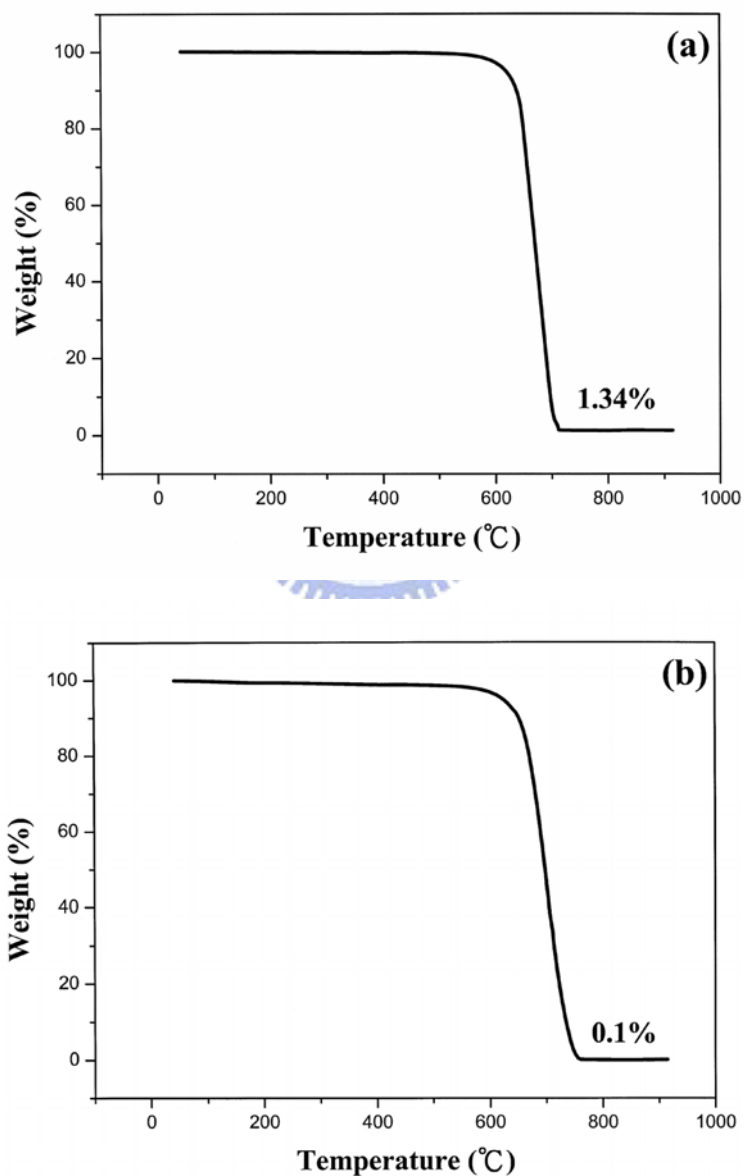


Fig. 4-10 Results of TGA analysis of (a) raw and (b) purified samples.

Figure 4-11 reported the catalyst contents after purification with 5 M acid for various treatment time. The amount of catalyst decreases form 1.34% to 0.6% at the processing time of 30 minutes and to 0.49% at 60 min treatment. After treated for 90 min, the total amount of catalyst dropped to 0.1%. This result clearly indicated that nitric acid could eliminate more catalysts under sufficient treatment time. The purity of purified MWCNTs could reach 99.9% only in 90 min acid processing time without damaging the wall structure.

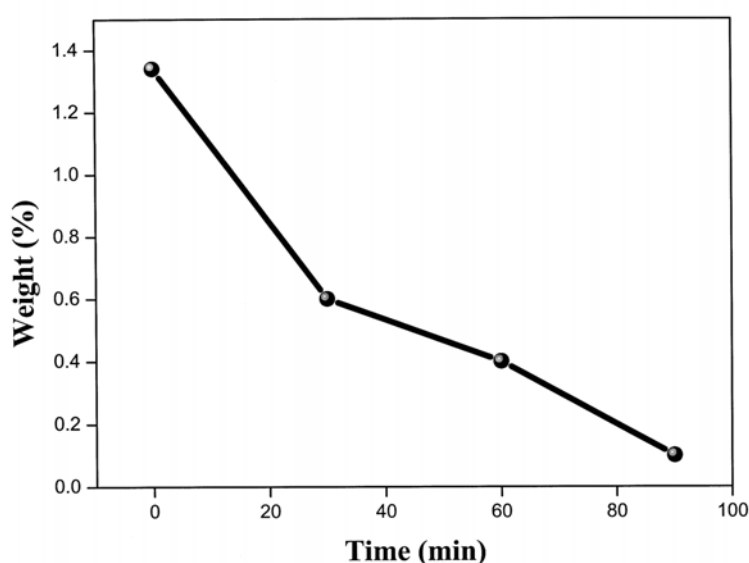


Fig. 4-11 Catalyst contents after purification with 5 M acid for various treatment time.

The Raman spectroscopies of raw and purified samples in Fig. 4-12 are composed of two characteristic peaks for nanotubes. The G band near 1580 cm^{-1} is related to the graphite E_{2g} symmetry of the interlayer mode, which reflects the structural intensity of the sp^2 -hybridized carbon atoms of the nanotubes. Another peak at 1350 cm^{-1} , the D band, indicates disordered carbon atoms. The extent of defect in carbon nanotubes can be evaluated with these two peaks. Raman analysis shows that ratios of I_G/I_D before and after purification are almost the same. This means that the bonding structure of

tube walls was not damaged by microwave-assisted purification. Some studies [120,179] have suggested that the I_G/I_D ratio would increase after purification, because of the improvement in nanotubes content by eliminating amorphous carbon. In this study the amount of carbonaceous materials was low (<3%) and the purification process did not damage bonds, so Raman curves of raw and purified sample are almost the same.

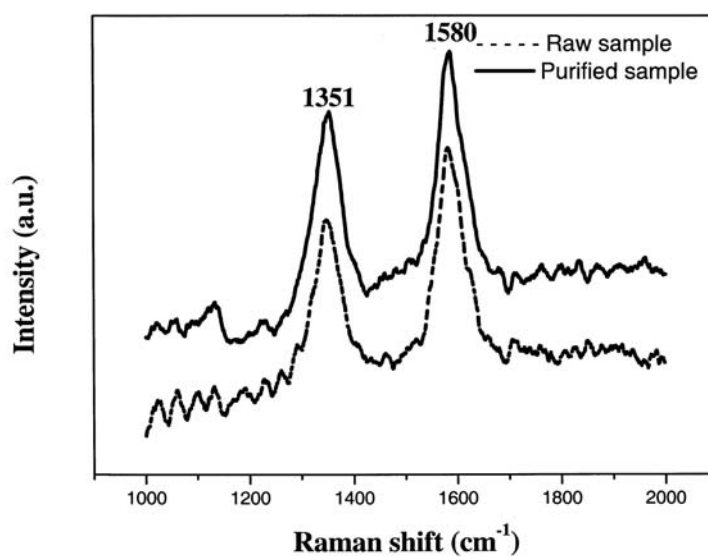


Fig. 4-12 Raman spectrums of raw and purified samples.

Research has been reported to obtain purified carbon nanotubes. Ando et al. [132] reported that MWCNTs were ground and boiled with 20% H_2O_2 in a reflux condenser for 45 h. Then the residual material was refluxed for 24h in a mixture of sulfuric acid (96%) and nitric acid (61%) with the ratio of 3:1. Chen et al. [129] proposed that MWCNTs were stirred in 3 M nitric acid and refluxed in 5 M HCl solution for 6 h at 120°C. After acid treatment, samples were calcined in static air at 510°C for about 60 min. Moon et al. reported a two step process of thermal annealing in air with acid treatment to purify single walled carbon nanotubes. In this study, the acid treatment with HCl for 24h was to etch away the metal catalyst [126]. Evidently most acid

treatments removed metal catalysts for more than 24 h. It was reported that carbon nanotubes would break into short pieces for too long acid treatments [179]. This is because oxygen containing mineral acid, HNO_3 for example, is very efficient in dissolving metal particles and polyaromatic solids such as graphites or amorphous carbons. However, in the microwave digestion system, nitric acid can rapidly absorb microwave energy without agitation in solution. Owing to the high efficiency of heat adsorption and no agitation, the processing time of microwave digestion to dissolve catalyst in MWCNTs can be reduced to 2 hours and metals could be eliminated from MWCNTs rapidly without destruction in wall structure.

In addition to the acid treatment, Shelimov et al. [125] also proposed a method of ultrasonically assisted filtration. In this method, sample sonication during filtration prevents filter contamination and provides a fine nanotube-nanoparticle suspension through purification. The process generates SWNTs with purity higher than 90%. Although this method could separate coexisting carbon nanospheres, metal nanoparticles, polyaromatic carbons and fullerenes from carbon nanotube fractions, metal catalysts embedded in the tip and wall could not be eliminated by this method. One advantage of microwave digestion method was that the embedded metal catalyst would be eliminated and the purity of carbon nanotubes could be higher.

Another purification method to eliminate metal catalysts was proposed by Chiang et al. [133]. This method suggests a purification strategy based on oxidizing Fe and then dissolving the oxide. Raw material was heated in static air at 200°C for 24 h and followed by sonication in concentrated HCl (37%) in 80°C water bath for 15 min. Although treated in HCl for only 15 min, the total purification time was obviously above 24 h. In this report, the total acid treatment time was below two hours. It was apparent that microwave digestion could effectively eliminate catalysts from carbon nanotubes and would not introduce structure defects.

4.2.3 Summary

Microwave digestion method was developed in our previous work with the advantages of high efficiency, easy operation, short time, damages free on CNTs and little consumption in reagents. However, residual catalyst amount of ECR-synthesized MWCNTs after purification was still high, because of the high catalyst content in raw samples. Investigated in this work is the purification efficiency of MWCNTs synthesized by thermal chemical vapor deposition with different parameters by using TGA, SEM, TEM and Raman spectroscopy and MWCNTs of high purity are expected. The results show that the purification efficiency increases with increasing acid treatment time. The amount of residual catalysts in purified samples was reduced to 0.1% after digestion for 90 min at 210°C. In conclusion, microwave digestion may have great potential in mass purification. High quality and large amount of purified CNTs would be applied to more intrinsic studies and industrial applications.



4.3 Purification efficiency of multi-walled carbon nanotubes synthesized by thermal chemical vapor deposition

4.3.1 Experiment condition and procedures

Sample after weighed and placed in 100 ml Teflon vessels filled with nitric acid was put on sample rotor made of Teflon. The power of microwave was set at 100 W and purification proceeded at two steps. First, the temperature ramped up to 210°C in 30 min. The second step was carried out isothermally at 210°C for 10, 20, 30,-120 min. After digestion, the suspension was filtered with 0.1 μm PTFE (poly-(tetrafluoroethylene)) membrane in deionized water. After rinsing with alcohol and vacuum drying for 8 h, there appeared a black thin mat.

4.3.2 Characterizations and discussion

Figure 4-13 is a TEM image, which shows that the raw sample contains multi-walled carbon nanotubes and catalyst. In this image, metal catalysts of various sizes can be found in the tip or on the tube wall. The diameters from 40 to 60 nm can also be displayed by TEM.

As shown in Figure 4-14, catalysts embedded in the tip were removed. Obviously, the closed tip was opened by acid treatment in microwave digestion. It seems that closed tip was opened first and the catalyst was eliminated by the acid. Another point is that the wall structure was not damaged by acid treatment.

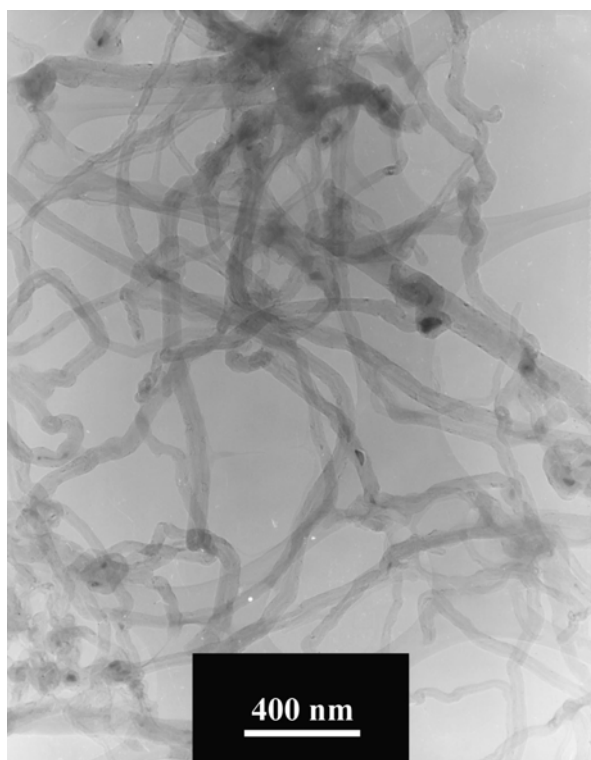


Fig. 4-13 TEM image shows that raw sample contains multi-walled carbon nanotubes and catalysts.

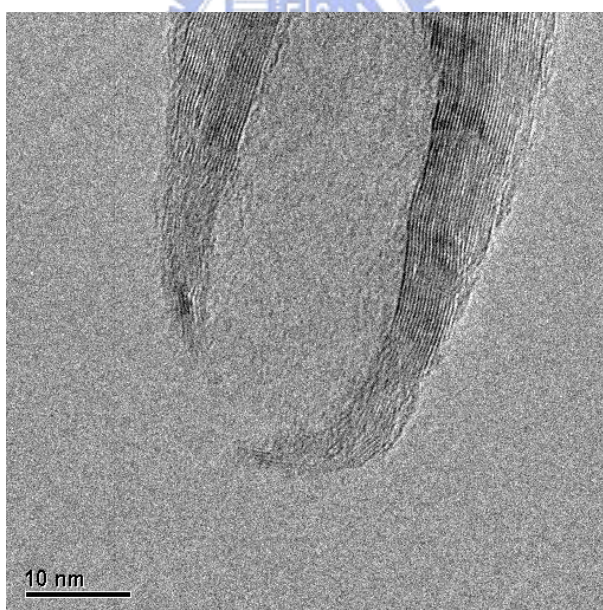


Fig. 4-14 Catalysts embedded in the tip were removed.

Figure 4-15 shows TGA analyses of raw and 120min-purified samples. Curve (a) shows that the original catalyst content is 10.39 wt%. The weight starts to reduce near 478°C and completely evaporate above 773°C. The decomposition temperature at

622°C is defined as the inflection point during oxidation. Besides, there appeared two region at 601°C and 642°C. The former might be carbonaceous particles or amorphous carbon, and the latter is MWCNTs. In curve (b), the weight loss of purified MWCNTs starts from 550°C and completely burn-outs at 728°C. The amount of residual catalysts dropped to 1.03% in 120min-purified samples. The decomposition temperature now is 701°C, which is slightly higher than that of the raw. The reason might be that the embedded metal catalyst in nanotubes acts as oxidation site and initiated oxidation [179]. It was also reported that the metal impurity would lower the decomposition temperature and increase the decomposition rate [179]. So, the purified sample is thermally more stable towards oxidative destruction than the raw. Another reason is carbonaceous materials contained in raw samples. Carboxyl, aldehyde and other oxygen-containing function groups on the surface of carbonaceous fractions are extremely hygroscopic and reactive towards oxidation. However, in curve (b), there is no any separate region except the main combustion region. This result points out that microwave digestion not only removes catalysts but also has potential to eliminate carbonaceous materials.

As shown in Figure 4-16, digestion time of the residual catalyst content ranges from 10 to 120 min. It is obvious that the content suddenly falls to 1.75% only in 10 min digestion. With increasing purification time the catalyst content slowly decreases to 1.03% in 120 min treatment.

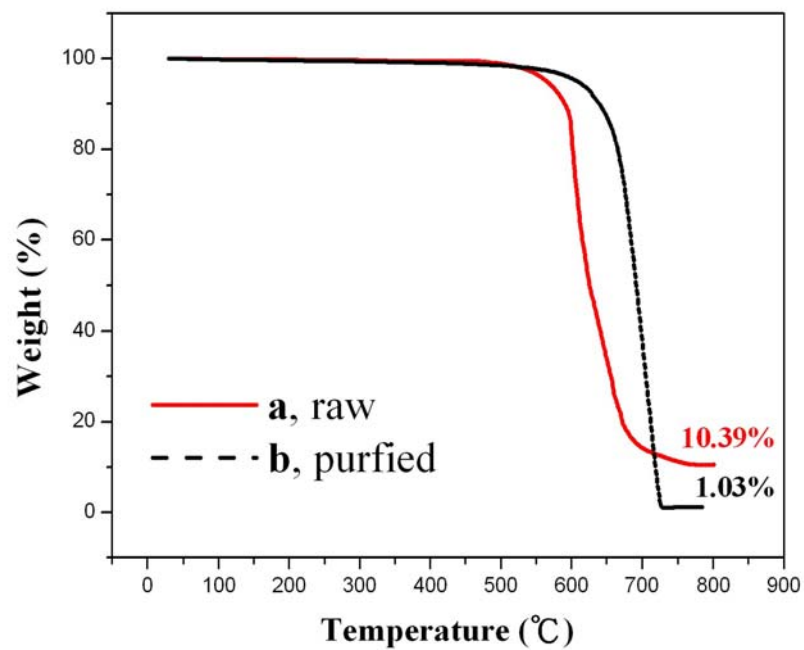


Fig. 4-15 TGA analyses of (a) raw and (b) 120min-purified samples.

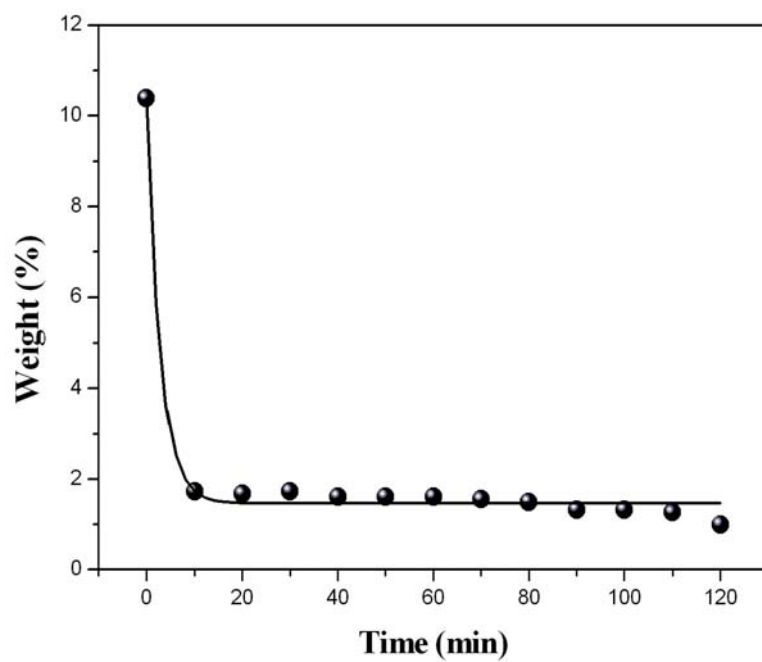


Fig. 4-16 Residual catalyst content of different digestion time ranges from 10 to 120 min.

The effect of time on purification efficiency may not be significant. The reason might be that most of metal particles were eliminated within the first few minutes, but other catalysts covered by tens of graphene layer is difficult to remove (Fig. 4-17). So, it is not a genius way to raise the digestion time, but to lower the diameter of carbon nanotubes. The efficiency of microwave digestion could be increased if the diameter of nanotubes is small and uniform.

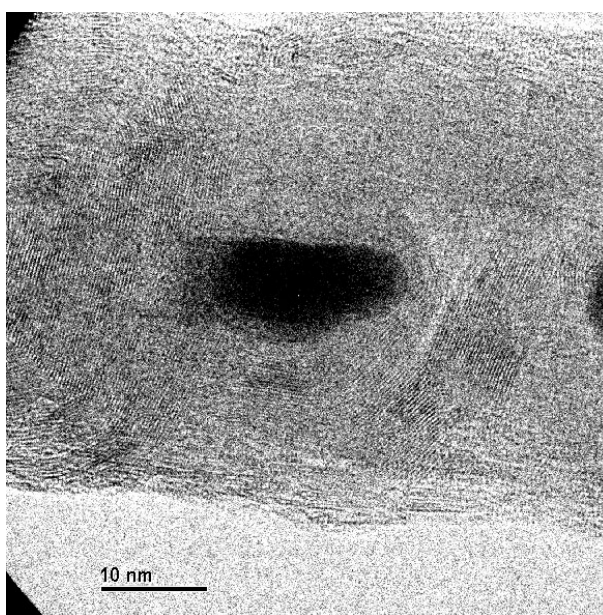


Fig. 4-17 Catalyst covered by tens of graphene layer is difficult to remove.

Figure 4-18 is Raman analyses of raw and purified samples for 30, 60, 90 and 120 min treatments. The results of Raman analyses show that the ratios of I_G/I_D increase after purification. Some studies [120,179] have also suggested that the I_G/I_D ratio would increase after purification because of the improvement in nanotube percentage by eliminating amorphous carbons. TGA analysis proves the existence of some amorphous carbons in raw samples, and there is no such feature in cure b of Fig. 4-15. Raman spectra and TGA analysis could prove each other that microwave digestion can eliminate both metal catalysts and carbonaceous materials without structure damages.

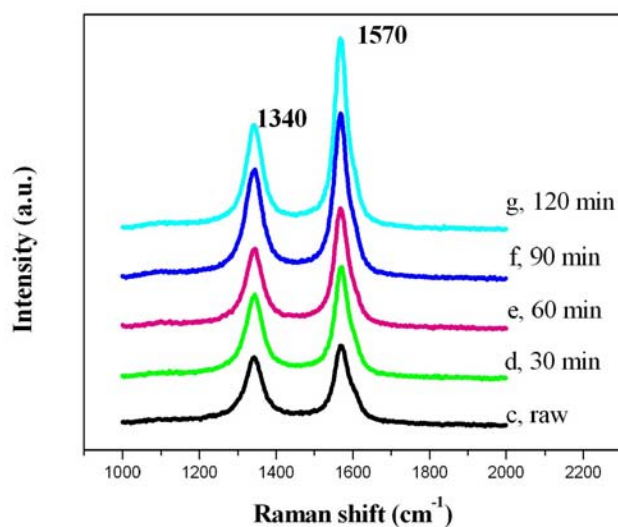


Fig. 4-18 Raman analysis of raw and purified samples for 30, 60, 90, and 120 min treatments.

Since the discovery of carbon nanotubes, many efforts have been devoted to produce the highest purified carbon nanotubes [126,129,132]. It is obvious that previous chemical purifications usually removed catalysts by long time acid treatments, about 24 h or even longer. However, it was also reported that long acid treatment time would result in the break of tubes [179]. This might be that oxygen containing mineral is very efficient to dissolve metals and polyaromatic solids, such as graphites or amorphous carbons. Although the acid could dissolve polyaromatic materials, the acid in microwave digestion system can rapidly absorb microwave energy and quickly dissolve metal particles in very short time to prevent the damages of tubes.

Different from the chemical treatment, many kinds of physical methods were provided, such as ultrasonically assisted filtration or oxidation combing with acid treatment [125,133]. However, metal catalysts embedded in the tip could not be eliminated by ultrasonication. Besides high efficiency, the other advantage of digestion method is to eliminate the catalyst embedded in tubes.

4.3.3 Summary

Microwave digestion method was successfully developed in our previous work with the advantages of high efficiency, easy operation, short time, damages free on CNTs and little consumption in reagents. However, residual catalyst amount of ECR-synthesized MWCNTs after purification was still high. Investigated in this work is the purification efficiency of MWCNTs synthesized by thermal chemical vapor deposition with different parameters by using TGA, SEM, TEM and Raman spectroscopy and MWCNTs of high purity and fast treatment are expected. The results show that the purification efficiency increases with increasing acid treatment time but the most important parameter might be the diameter of carbon nanotubes. Microwave digestion method has excellent prospect to yield carbon nanotubes of high purity if carbon nanotubes are small and uniform in diameter. The amount of residual catalysts in purified samples was lowered to only 1.75% for 10 min digestion at 210°C and 1.03% for 120 min digestion. In conclusion, microwave digestion may have great potential in mass purification. Large amount of purified CNTs with high quality would be applied to more intrinsic studies and industrial applications.

4.4 Reaction Model of Microwave-Assisted Purification of MWCNTS

4.4.1 TEM analysis and tube opening

As shown in Fig. 4-19(a)-(e), HRTEM images of MWCNTs prepared at different experiment conditions from raw samples (Fig. 4-19(a)) to purified CNTs for various treatment time (Fig. 4-19(b)-(e)) show structural variations in the apex of tubes. Fig. 4-19(a) shows that the tip of unpurified CNTs was mainly closed and usually encapsulated with metal particles by several graphene layers. Figure 4-19(b) presents a partially open-edged CNT obtained by short-time purification treatment. The arrow indicated the location of initial oxidation where a small piece of graphene layers was peeled off and this implies the position of defects or strain-inducing pentagonal rings near the tip. The encapsulated metal particle seems to be removed simultaneously once the tube was opened. This result suggests that nano-sized metal particle may have very high reactivity with acids at high temperature, and the tip-opening process would be the rate-determining step because there are no remaining metal catalysts found in already opened tubes after purification. In other words, metal catalysts will be etched away immediately once they got in touch with nitric acids after the caps of CNTs were opened. In Fig. 4-19(c), (d), and (e), it was obvious that graphite layers near the tip with high curvature have been further etched away by increasing treatment time, but wall structures around the opening have not been damaged during purification. As shown in Fig. 4-19(e), the embedded catalyst at the apex has been completely removed and the tube has larger opening than that of short treatment time. Fig. 4-20, the low-magnification TEM image, reveals that there is no remarkable damage on the tubular wall of CNTs after purification (see arrow in the picture).

These results of TEM analysis provide an acceptable mechanism to explain the tube-opening processes in microwave assisted purification. According to these results, it is obvious that the tip of CNTs was opened first and then catalysts were dissolved in

acid in microwave-assisted purification processes. As is well known, carbon nanotubes are composed of flat sp^2 graphenes (hexagonal network sheets) rolled into seamless hollow cylinders with diameter ranging from 1 nm to about 50 nm. The length of nanotubes exceeds tens micrometer, and their ends are capped with curved graphene layers. It is also known that graphite hexagonal sheet can be given the three-dimensional shapes by the introduction of rings other than hexagons. The geometry introduced by the presence of other rings clearly follows Euler's theorem, which relates the number of vertices, edges and faces of an object, and is very useful to tell what the presence of rings does to the geometry and how many are necessary to close the surfaces. According to this theorem, at least 12 pentagons are necessary to close the hexagonal network of a nanotube; i.e. typically six pentagons at each end of nanotube. Every pentagon at the tip introduces a positive curvature to a hexagonal lattice, and the strain is localized around the pentagon to call as topological defect. The arrangement of this topological defect on the tip not only determines the local strain field but also indicates the position of initial oxidation at the tip and, as we know, the oxidation of CNTs will occur there quite easily [181]. According to this discussion and the TEM analysis in our experiments, it is apparent that microwave purification, like other processes, will open CNTs first, and then etches metal catalysts away to accomplish simultaneous opening and purification of CNTs. However, the reason why this technique are highly efficient even under the same CNTs opening procedures of CNTs needs further investigations.

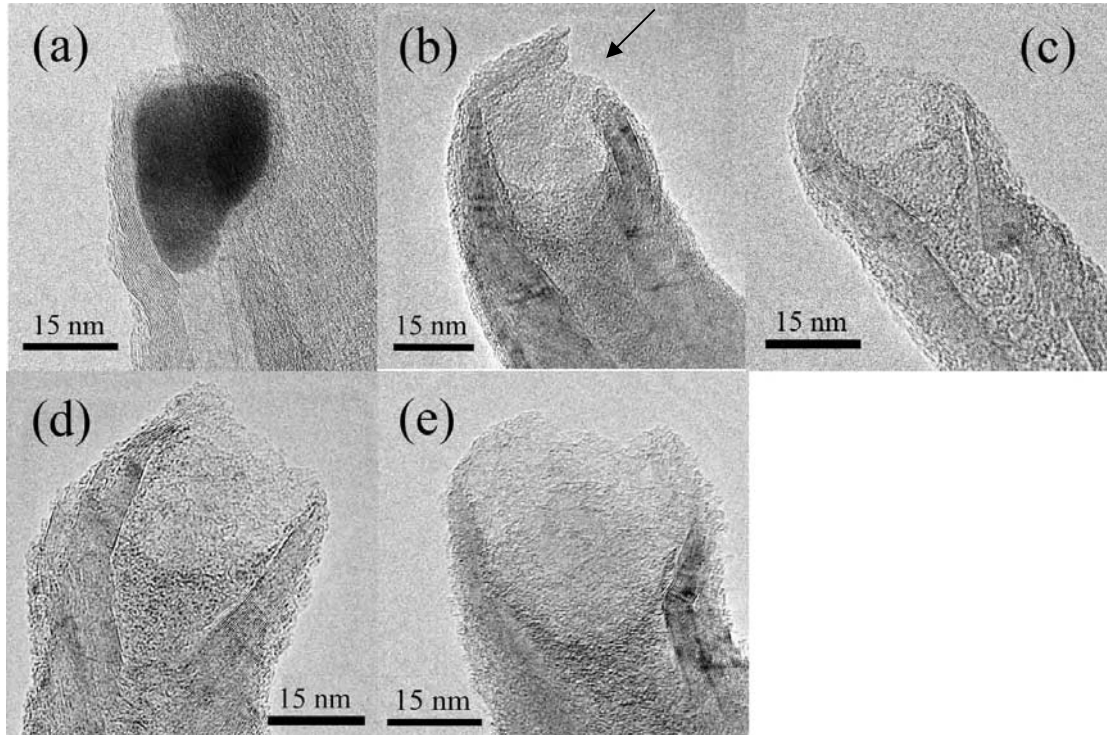


Fig. 4-19(a)-(e) High resolution TEM images of the unpurified (a) and purified (b)-(e) carbon nanotubes at the tip.

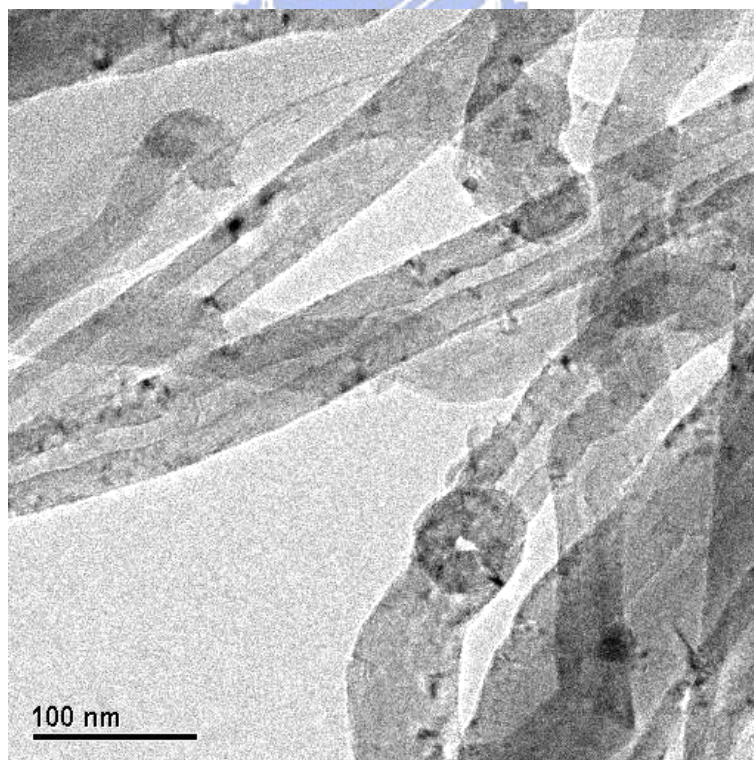


Fig. 4-20 Low magnification TEM image of tubular wall structure of the purified carbon nanotubes.

4.4.2 TGA analysis and purification efficiency

Figure 4-21 presents the relationship of residual catalyst amount with microwave-assisted processing time. The amount of residual catalysts decreased with increasing treatment time and the contents of catalysts rapidly dropped from 10.39 wt% in the raw sample to 1.52 wt% after 10 min treatment in acids at 120°C when the power of microwave was increased from 100 to 500W. The total processing time including 5 min to ramp up to working temperature and 10 min for isothermal processing.

Comparing to those conventional long-time boiling-acid methods, for example, stirred the as-prepared CNTs in 3M nitric acid and refluxed at 60°C for 24 hours, then followed finally by reflux in 5M HCl solution at 120°C for 6 hours, [129] or annealed raw CNTs in air and then purified them in HCl for 24 hours to remove metal particles, [126] and a combination method to oxidize CNTs with 2.8N HNO₃ for 6-24 hours, then in air at 550°C for 10 min and vacuum annealing at 1600°C for 3 hours, [130] our experiment results reveal that microwave-assisted purification might be the most efficient method ever reported in CNT purification. The short purification time is not only an advantage to produce industrially purified CNTs with higher efficiency but also a good news to provide scientifically damage-free CNTs of high purity for research because CNTs with long nitric-acid treatment may suffer from major drawbacks which would damage the wall structure of tubes or even break down CNTs into small pieces [126].

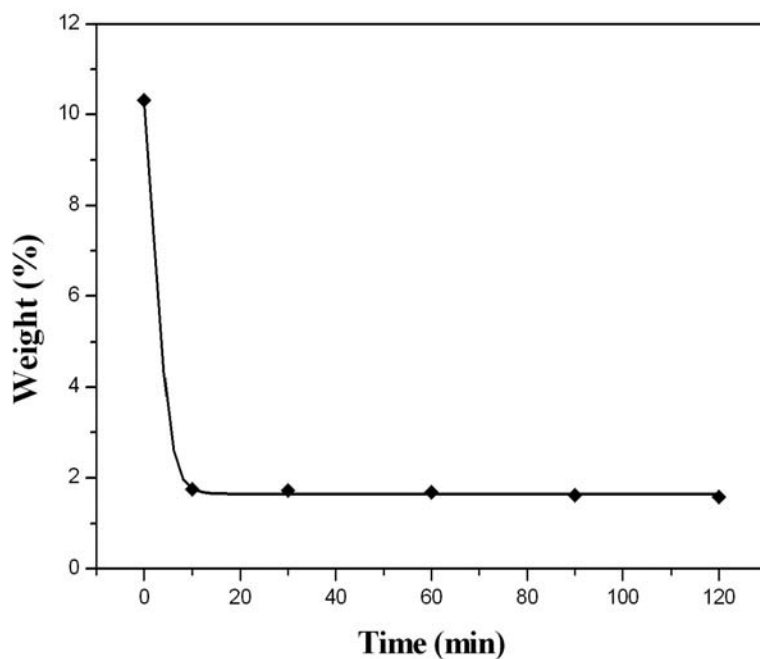
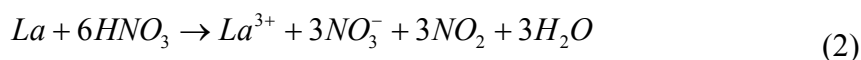
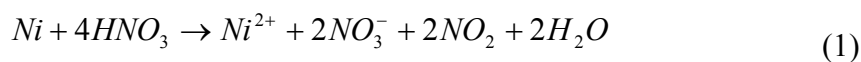


Fig. 4-21 The relationship between the amount of residual catalysts in CNTs and processing time.

4.4.3 Microwave assisted technique and reaction model

In this paper, we made an effort of using microwave heating to purify the as-prepared MWCNTs and the results showed that it was an extremely highly efficient method to eliminate metallic catalysts embedded in carbon nanotubes. Reactions of metal catalysts of La and Ni with nitric acid are



In comparison with those traditional methods which need longer treatment time even 2 or 3 days, the microwave-assisted purification method can remove metallic particles in relatively short time, only 15 min to remove almost 85 wt% catalysts in the as-prepared carbon nanotubes. The possible mechanism to explain why microwave-assisted purification can achieve such high efficiency is discussed below.

It is well known that microwaves are electromagnetic waves including the components of electric and magnetic field. These two components of electromagnetic waves will rapidly change their molecular motion in directions and furthermore result in the effect of warming and heating on objects. This is because molecules, semi-solid or liquid, cannot immediately respond to the variation of the electromagnetic fields in direction and hence creates the effect of molecular friction. Microwave dielectric heating, also referred to as microwave heating or dielectric heating, has been reported that the significant accelerations in reaction rate were achieved in a conventional microwave oven [182,183]. These results have attracted considerable attention on reactions accelerated by dielectric heating and thereby more multi-function microwave ovens were designed for industry or laboratory. Organic reactions, such as hydrolysis, esterification, etherification, substitution reactions and Diels-Alder reactions have been extensively investigated by microwave heating process. Additionally, various aspects of inorganic and polymer chemistry have also been studied. Recently, rapid synthesis of metallic nanostructures in solution under microwave heating has attached considerable attention as a new promising synthesis method. Gold spherical nanoparticles, [184] polygonal plates, [185,186] nanorods and nanowires [187,188] were efficiently synthesized under microwave heating owing to thermal and non-thermal effects caused by microwave irradiation. In addition, many kinds of silver nanostructure were also successfully produced by microwave heating method [186,189].

The reason why microwave-assisted heating could achieve such high reaction rate than traditional methods might be due to thermal and non-thermal effects. Thermal effects have been described as rapid heating, hot spots or hot surface at solid-liquid interface. In the case of rapid heating effects, the acceleration in reaction rate can be significantly increased if the microwave energy is mostly absorbed by reactants

themselves, for example, metal catalysts, not by absorbents, such as solvent. It means that the selective heating of metal catalysts embedded in the tube's tip can be achieved in microwave-assisted heating to accelerate the etching rate of catalysts in acid faster than that in other methods.

In other cases with solids involved in the reaction system, there are local hot spots or hot surfaces on solid-liquid interfaces while the bulk temperature still remained low. The formation of hot spots or hot surfaces has been reported to accelerate the reduction of metallic precursors and the nucleation of nano-particles metal in the synthesis of metallic nanostructure [190]. Non-thermal effects were reported by Laurent et al. that microwave energy might lower the activation Gibbs free energy of reactions [191]. According to these, microwave-assisted method heats reactants rapidly and creates hot surface on solid-liquid interfaces while the bulk temperature still remained low to achieve high chemical reaction rate.

Although microwave heating can accelerate the reaction rate, another important factor in our experiment to significantly accelerate the reaction rate might be that catalysts at the apex of CNTs can be heated by themselves to higher temperature than tubes or solvents by absorbing the energy of microwave radiation. The temperature of unpurified CNTs could reach approximately 1850°C after 4 seconds of microwave radiation; however, carbon black and purified CNTs only reached 500-650 °C after 10 seconds of radiation when microwave radiation was applied both on purified and unpurified CNTs in ultrahigh vacuum [192]. It is commonly known that the temperature increase is accomplished by the reaction rate increase, because higher temperature implies higher average kinetic energy of molecules and more collisions per unit time. In general, most chemical reactions approximately doubles its rate per 10°C increase in temperature. For this reason, the higher the temperature at the apex of CNTs, the higher purification rates of metal catalysts. In addition to the absorption

of microwave energy by metal catalysts embedded in unpurified CNTs, the pure cobalt and copper powders can also be heated up very fast in the microwave oven, about 700°C in 1-2 minutes, but there is no temperature rise for solid copper bar, even exposed in microwave field for 10 minutes. Nickel powders can be heated up to 384°C within 1 minute in microwave [193,194]. These results imply that the smaller the size of metallic particles, the higher the temperature of them when exposed in microwave field. This can not only ensure the previous explanation that metallic nanoparticles might be heated in microwave field but also attract a lot of interests on microwave sintering of metallic powders [195].

Microwave adsorption in metal resulting in rapid heating might be mainly due to magnetic resonance and interfacial electric polarization [196,197]. Magnetic resonance adsorption occurs when microwave field couples with internal magnetic moments of ferromagnetic particles, such as Fe, Co, and Ni [196]. Interfacial electric polarization adsorption occurs when microwave radiation interacts with charge multiples at the interface [196,197]. Therefore, it is believed that Ni catalysts in CNTs are ferromagnetic and adsorb microwave via magnetic resonance to reach higher temperature in extremely short time than traditional boiling method and result in high reaction rate. Interfacial dipoles within boundaries between catalysts and carbon shells absorb more microwave energy when crystallites are nanometer-size instead of micron size, since the smaller size of catalysts would have greater interfacial polarization effects [198].

According to the former discussion and experiments, we conclude that metallic nano-particles in microwave digestion system can absorb electromagnetic wave energy and be heated by themselves to form a local hot area at the tip end and by combining with hot-surface effects around the CNTs' tip-liquid interface, result in significant reaction rate acceleration to etch away the cap of tubes and metal catalysts

to accomplish the purification of CNTs.

Although the actual temperature gradient at the tip of individual CNT in acid solution is hard to measure at present and still needs further investigation, it is believed that the temperature at the apex of unpurified CNTs might reach at least three times higher than that of side wall of CNTs or solvent and result in the purification rate acceleration. We suggest a possible reaction model of microwave assisted purification, as shown in Fig. 4-22(a)-(e). Figure 4-22(a) represents the state of CNTs without microwave irradiation applied on them, where the temperature of CNTs remain low without hot surfaces around the apex of CNTs. As microwave is applied on CNTs (Fig. 4-22(b)), the nano-sized metallic catalysts in the tip absorb the energy of microwave irradiation and the temperature of catalysts increase to higher temperature than that of the bulk. The local hot area is also produced near the tip at the same time because of the formation of hot surface in the solid-liquid interface. These two phenomena result in local high temperature around the tip of CNTs, and the local high temperature results in reaction rate acceleration of pentagonal rings and metal catalyst with nitric acid in Fig. 4-22(c) and (d). Finally, as shown in fig. 4-22(e), the tip of CNTs is opened and the metallic catalyst embedded in tubes is also eliminated in this process, but the opening of CNTs increases with increasing treatment time in microwave-assisted purification system (shown in Fig. 4-22(f)).

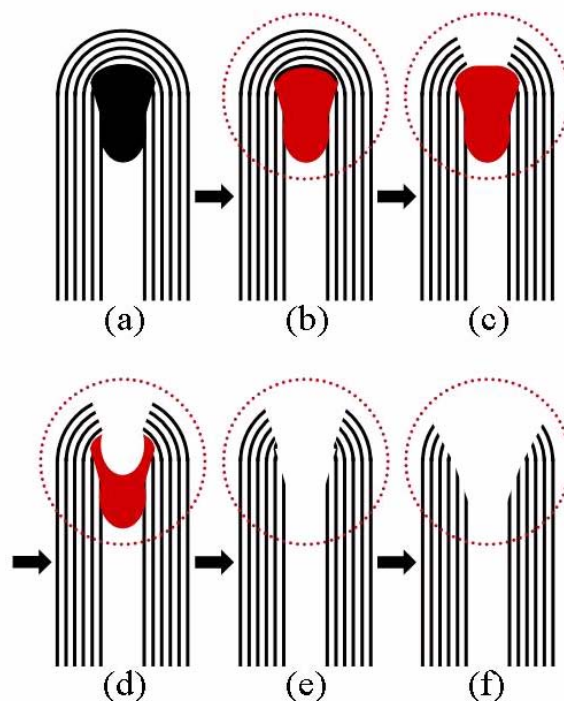
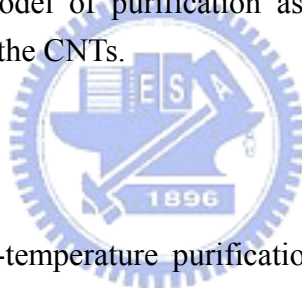


Fig. 4-22(a)-(f) Reaction model of purification assisted by microwave dielectric heating for the CNTs.



4.4.4 Summary

A high-efficiency and low-temperature purification processing technique for the raw MWCNTs sample has been significantly developed. The contents of metallic catalysts in the as-prepared MWCNTs can be effectively eliminated from 10.39 wt% to 1.515 wt% within 15 minute purification time at 120°C. A possible reaction model was apparently proposed to describe this reaction, that is, the nano-scale metallic catalysts embedded at the tip end of MWCNTs could absorb microwave radiation energy in electromagnetic field by magnetic resonance and interfacial electric polarization, and then form a localized hot area to combine with hot-surface effects around the tip-liquid interface of CNTs and significantly accelerate the reaction rate in the wall of CNTs near the tip.

Although microwave technology has been extensively applied in our daily life, there might be a great potential in microwave chemistry to apply microwave radiation

energy on traditional chemical reaction processes. However, further intensive studies are expected to acquire complete understandings of the microwave-assisted chemical reaction.



Chapter 5 Coating Pt Particles on CNTs as DMFC

Electrode Using Microwave Heating Method

5.1 Experiment Procedures to Synthesize Pt Catalyst on MWCNTs

Commercial raw multi-walled carbon nanotubes (MWCNTs) with the diameter ranging from 40~60 nm were used in this study. Raw CNTs were first purified by microwave-assisted purification reported in our previous works to eliminate metal catalysts [199,200]. Chloroplatinic acid (H_2PtCl_6) dissolved in 30 mL ethylene glycol (EG), EtOH, isopropyl-alcohol and purified MWCNTs sample were put into a 100 mL Teflon microwave closed vessels.

The prepared mixture was ultrasonically treated for 10 min and then put into the temperature-controlled microwave heating system (Milestone, 2.45GHz). The microwave power was set at 500W. The temperature of microwave vessels was controlled by ATC-400CE Milestone temperature control systems. A thermocouple was installed in a standard Milestone reference vessel to detect the temperature.

The microwave solution temperature was ramped up the setting temperature within 90 sec, and then the polyol reaction proceeded at different setting temperature isothermally with various program-controlled time. The experimental conditions are summarized in Table 5-1.

After microwave polyol procedure, the suspension was filtered with 0.1 μm PTFE (poly-(tetrafluoroethylene)) membrane in deionized water. Rinsing with alcohol and DI water, and boiling in 80°C water for 60 min, then drying for 8 h, the products were obtained.

The morphology of Pt catalysts dispersed on MWCNTs was characterized by FEI Nova 200 scanning electron microscopy (SEM). The size and distribution of Pt nanoparticles dispersed on CNTs were analyzed by a JEOL JSM-2010 high-resolution

transmission electron microscopy (HRTEM). X-ray diffraction (XRD) analysis was carried out on a Shimadzu XRD-6000 diffractometer system equipped with a Cu K α radiation ($\lambda = 1.54056 \text{ \AA}$) to calculate the mean particle size of Pt particles. X-ray photoelectron spectroscopy (XPS, VG Scientific Microlab 310F) analysis was carried out by using an Al K α (1486.6 eV) X-ray source to analyze compositions and chemical bounding change. The loading amount of Pt on CNTs was estimated by using a thermogravimetric analysis (TGA, Q500 Thermogravimetric Analyzer,) with the rate of 20°C /min from 30°C to 800°C at the air flow rate of 60 sccm.

Table 5-1 Summary of the experiment conditions.

Carbon nanotubes	MWCNTs, 40~60 nm in diameter
Platinum precursor	H ₂ PtCl ₆ , 3.5x10 ⁻³ M
Stabilizer	poly(vinylpyrrolidone) (PVP), MW=8000, 58000, 1300000
Surfactants	sodium dodecyl sulfate (SDS)
Temperature	40 to 180°C
Reaction time	90sec to 90min
Solvent	ethylene glycol (EG), EtOH, and isopropyl-alcohol
Microwave power	250W/per vessel
Microwave frequency	2.45 GHz

5.2 The effects of solutions on Pt particles synthesis

As shown in Fig. 5-1~5-3, samples were prepared at the condition for only Pt precursor dissolving in EG without any stabilizer or surfactants, and heated to 40, 60, and 80°C for 10 min by microwave dielectric heating system. It is obvious that there are no Pt particles precipitated in these three samples under such conditions. Fig. 5-4~5-6 show the results of XRD analysis, and it is clear that there are no Pt signals in these three samples, but only the peak of CNTs appears at about 26.5° of 2 θ . These results of XRD analysis completely agree with SEM images shown in Fig. 5-1~5-3.

But a large amount of catalyst particles with diameter about 200~300 nm appeared when deionized water was added into the reactant mixture and heated to 80°C for 10 min, as shown in Fig. 5-7. The XRD result shown in Fig. 5-8 also confirms that strong Pt signals appear in this sample at 2θ of 39.6°, 46.1°, 67.4°, 81.2°, 85.6° corresponding to the reflection planes of (111), (200), (220), (311), and (222) respectively. The signals are consistent with face-centered cubic structure of Pt.

These results indicate that water could help the precipitation of Pt particles, but the particles size is incredibly huge without the addition of stabilizer, such as PVP. PVP was reported to be adsorbed on the particle surface to form a stable complex and result in the continuous growth of Pt particles and determine the product morphology [201]. On the contrary, the concentration of Pt precursor was decreased to 10^{-6} M and the results show that there are no Pt particles found in these contrast groups.

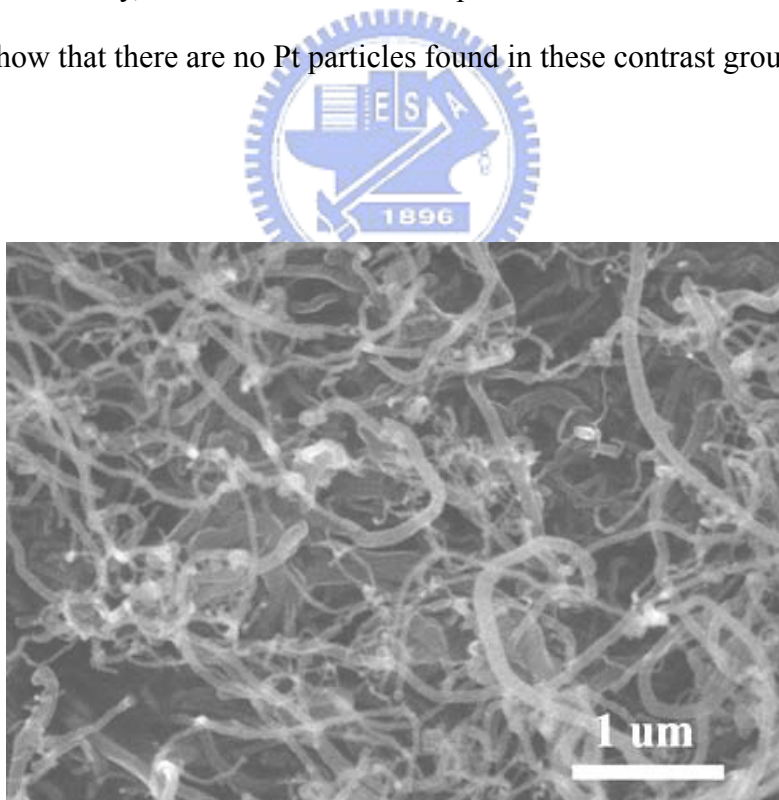


Fig. 5-1 SEM image of sample prepared at 40°C in EG.

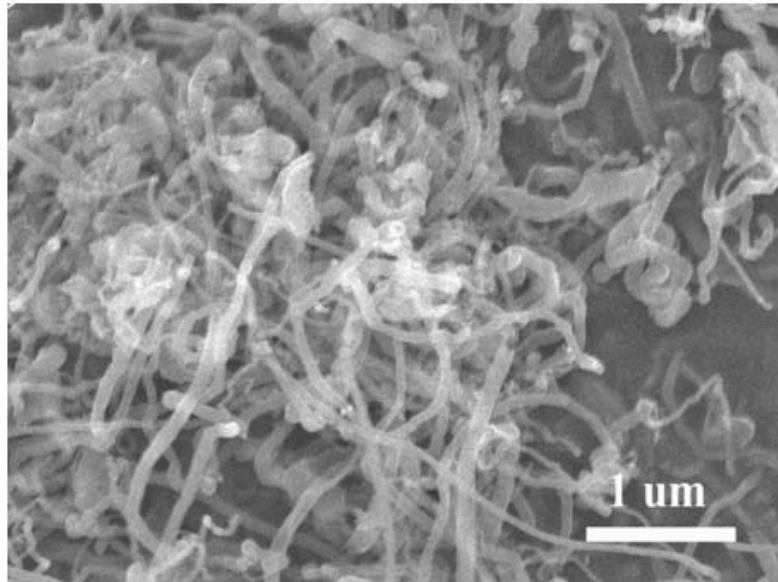


Fig. 5-2 SEM image of sample prepared at 60°C in EG.

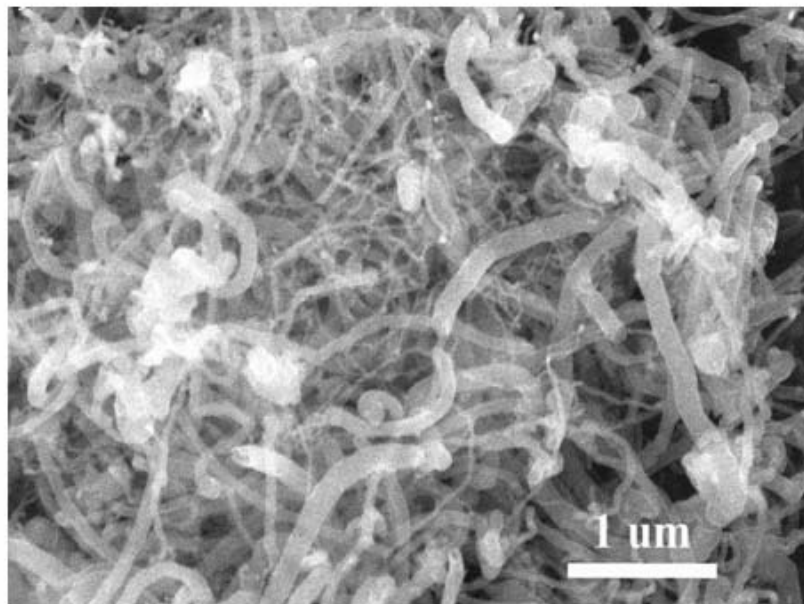


Fig. 5-3 SEM image of sample prepared at 80°C in EG.

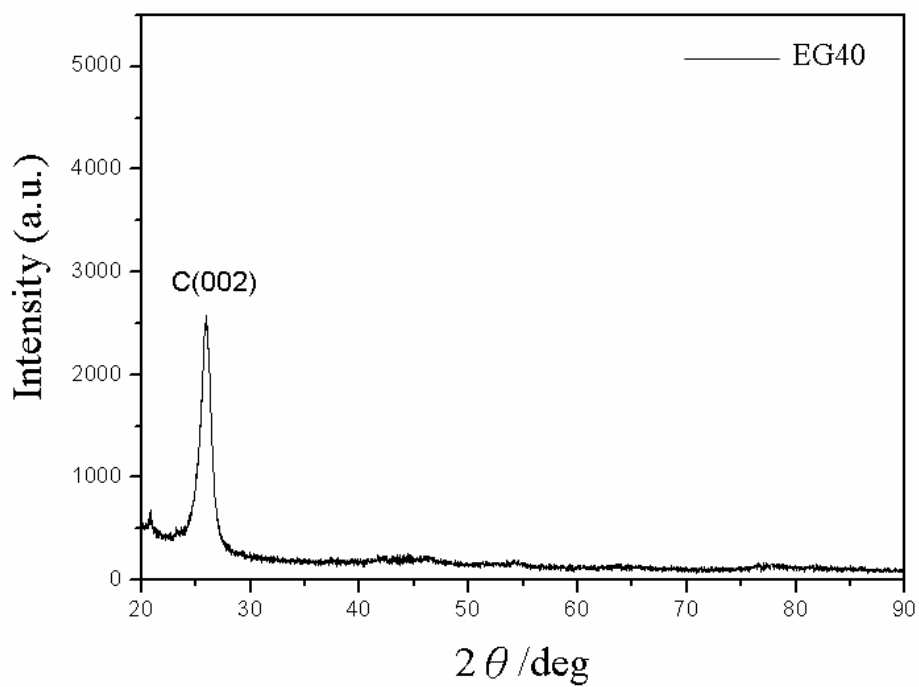


Fig. 5-4 XRD spectrum of sample prepared at 40°C in EG.

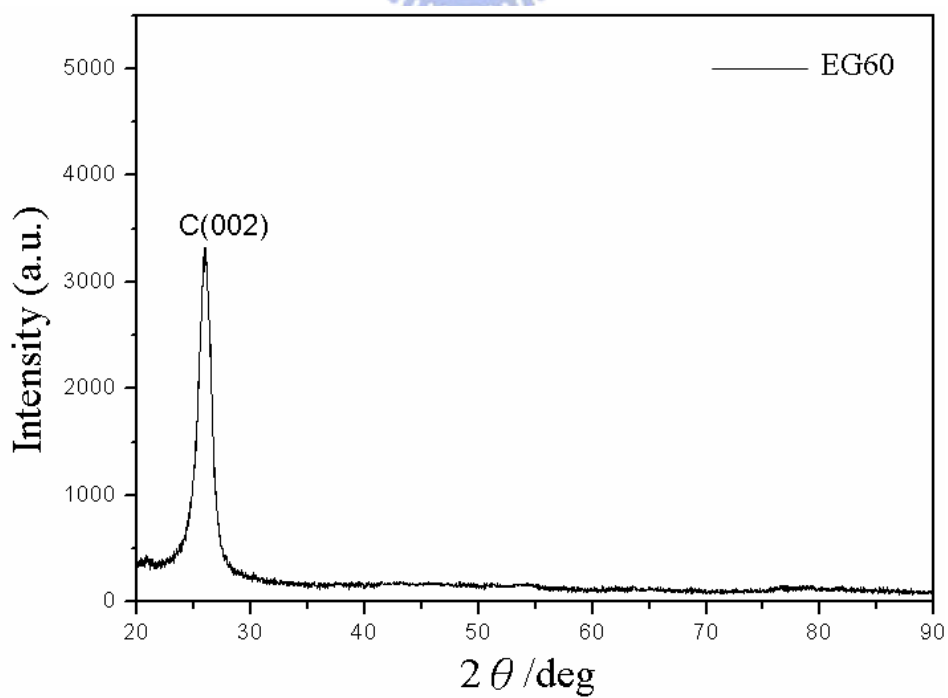


Fig. 5-5 XRD spectrum of sample prepared at 60°C in EG.

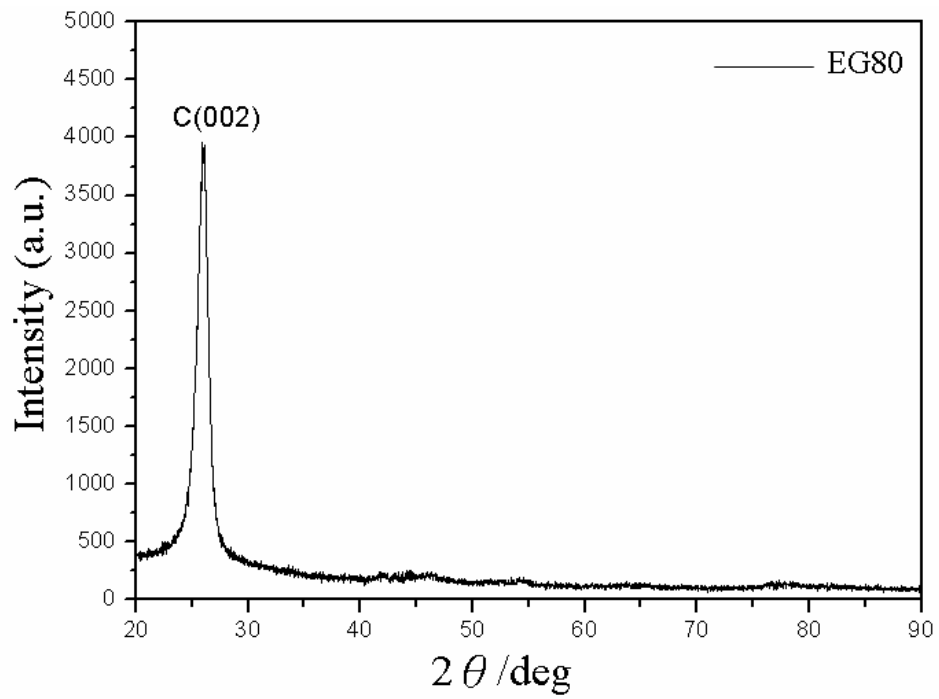


Fig. 5-6 XRD spectrum of sample prepared at 80°C in EG.



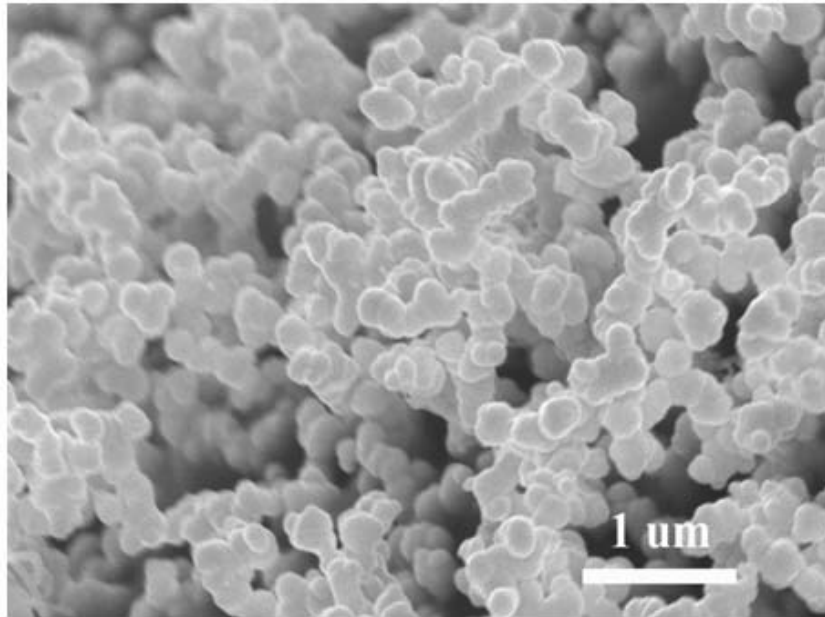


Fig. 5-7 SEM image of sample prepared at 80°C in EG with the addition of D.I. water.

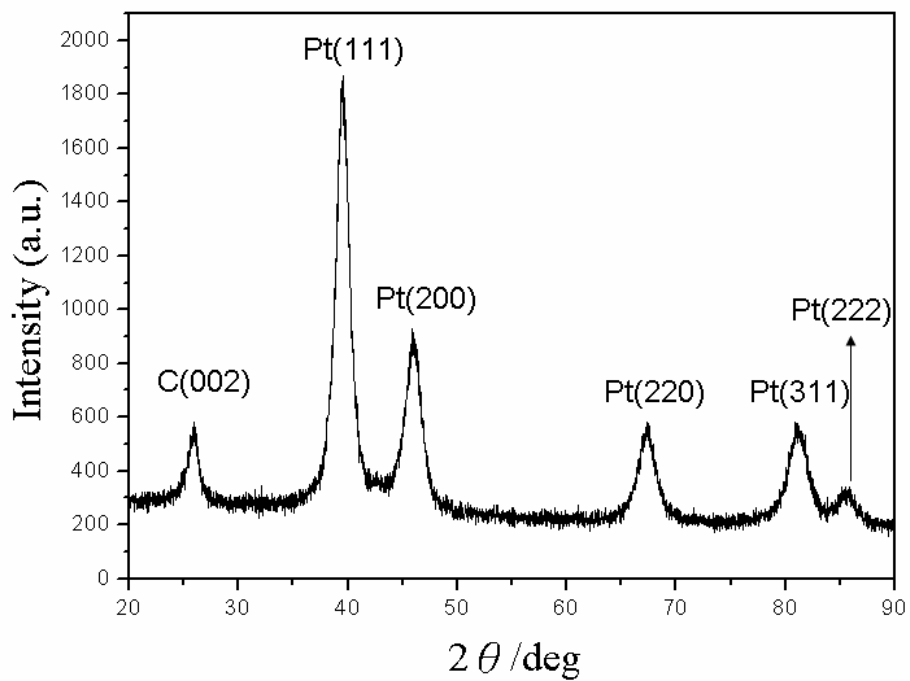


Fig. 5-8 XRD spectrum of sample prepared at 80°C in EG and D.I. water.

On the other hand, the EG was replaced by EtOH, and PVP-1300 was mixed in solution. Shown in Fig 5-9 are that Pt particles about 30~50 nm in size are dispersed on CNTs at 60°C and 80°C, and no Pt particles appeared in samples at 40°C. The XRD results shown in Fig. 5-10~5-12 also confirm that both samples of 60 and 80°C have Pt peaks, and there are no Pt signals in the sample of 40°C. Although particle size has reduced from hundreds to tens of nanometers in EtOH and shows the tendency of decreasing size with decreasing temperature as shown in Fig. 5-9 (b) and (c), the size is still too large.

Figure 5-13 (a)-(c) show that there are no Pt particles precipitated on CNTs when the solution was replaced by isopropyl-alcohol at reaction temperatures of 40, 60 and 80°C. This result showed that the isopropyl-alcohol might not be suitable for Pt particle precipitation.



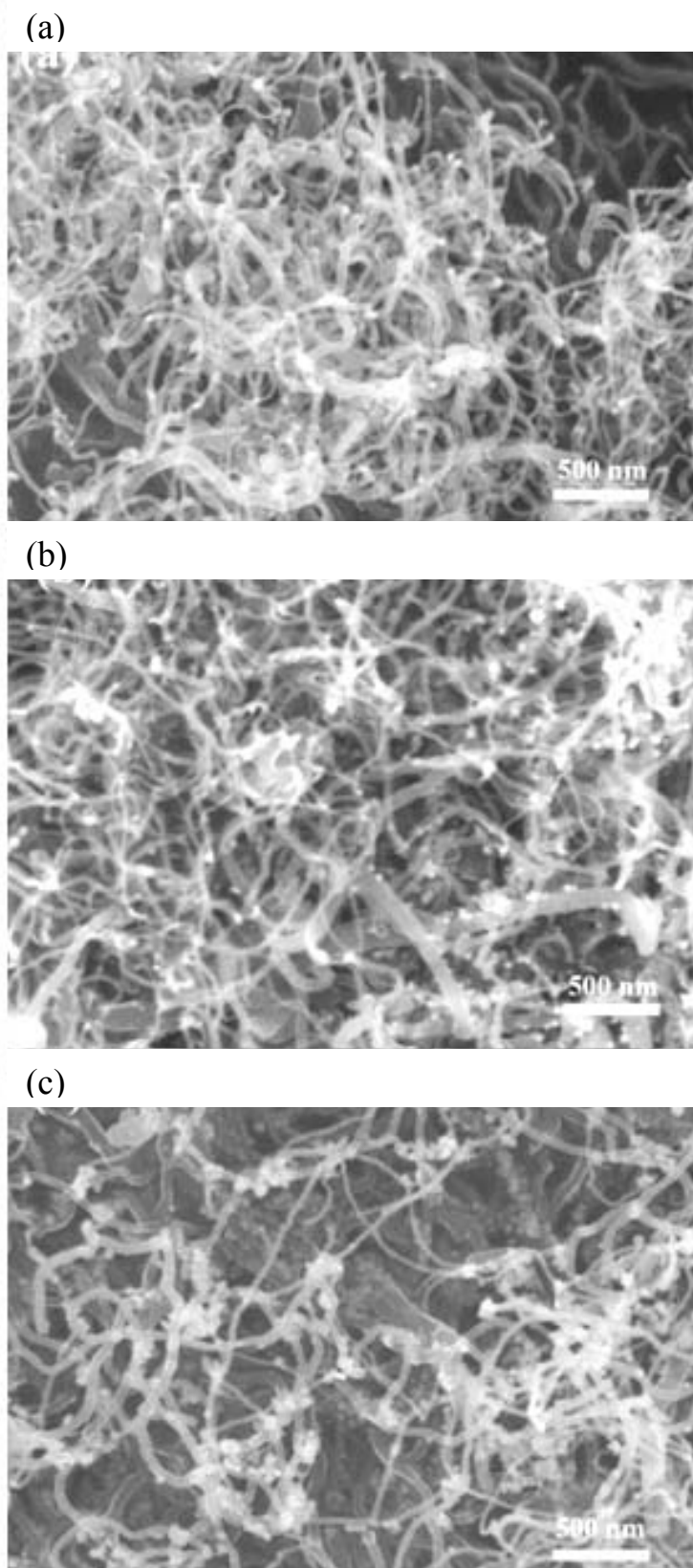


Fig. 5-9 SEM images of Pt catalyst synthesized on MWCNTs at different temperature in EtOH/water with PVP. (a) 40°C (b) 60°C (c) 80°C.

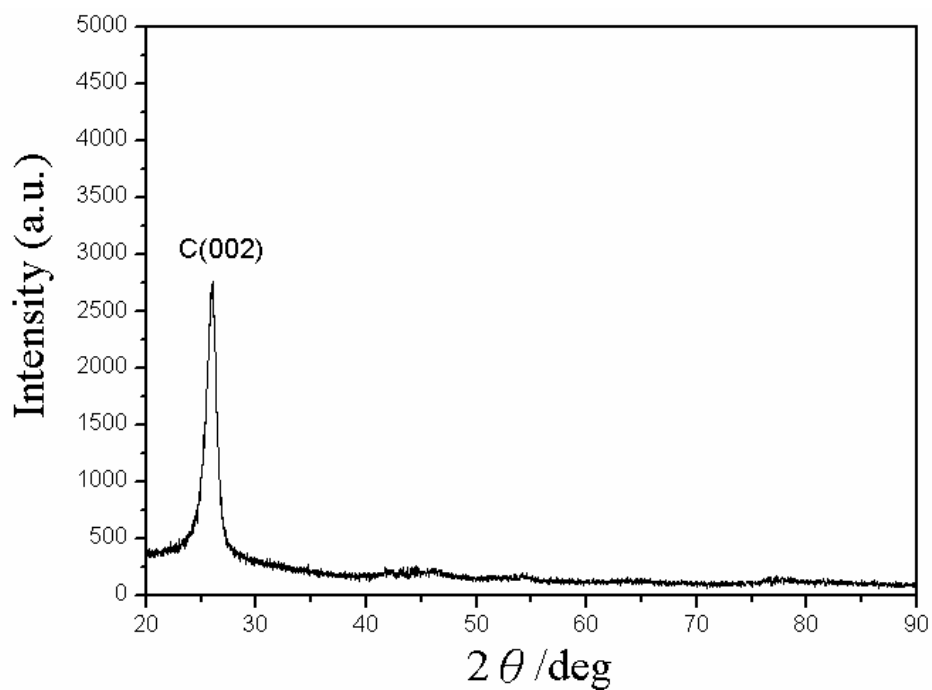


Fig. 5-10 XRD spectrum of Pt catalyst synthesized on MWCNTs at 40°C in EtOH/water solution with PVP.

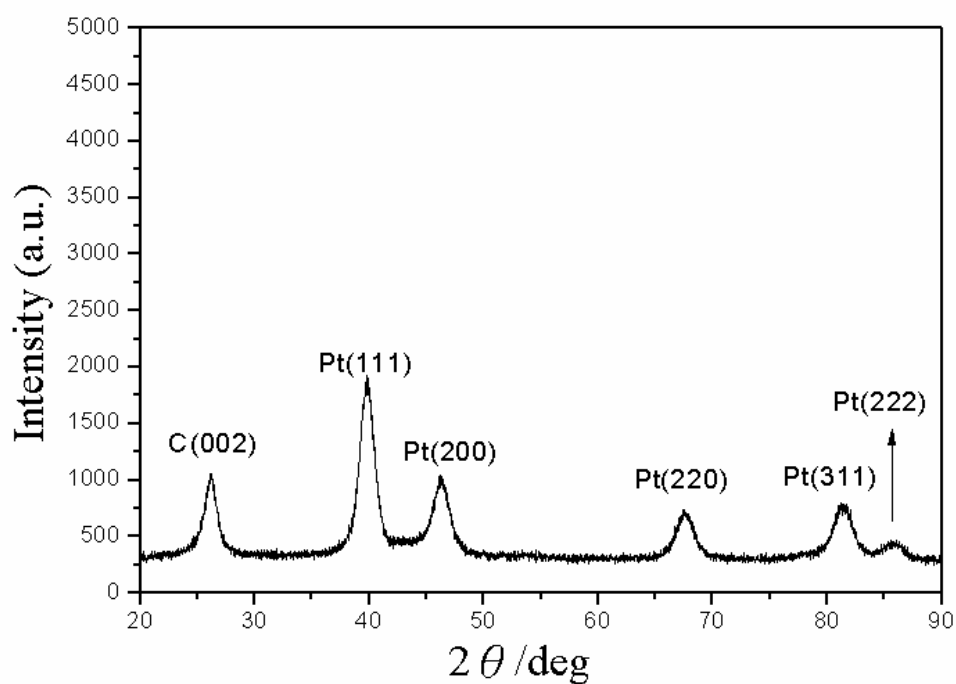


Fig. 5-11 The XRD spectrum of Pt catalyst synthesized on MWCNTs at 60°C in EtOH/water solution with PVP.

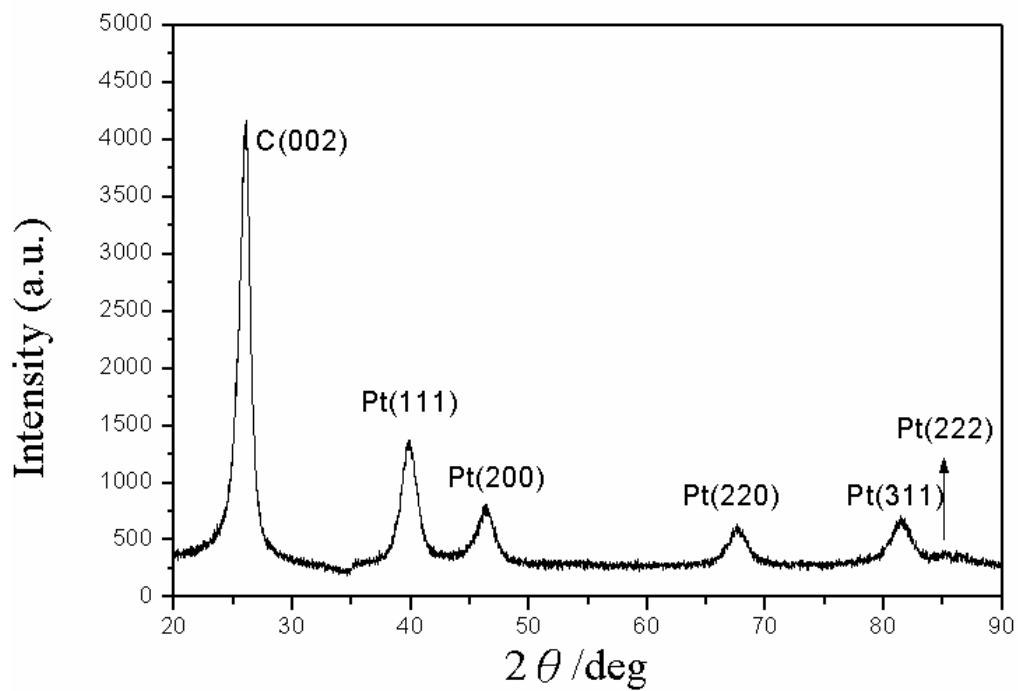


Fig. 5-12 XRD spectrum of Pt catalyst synthesized on MWCNTs at 80°C in EtOH/water solution with PVP.



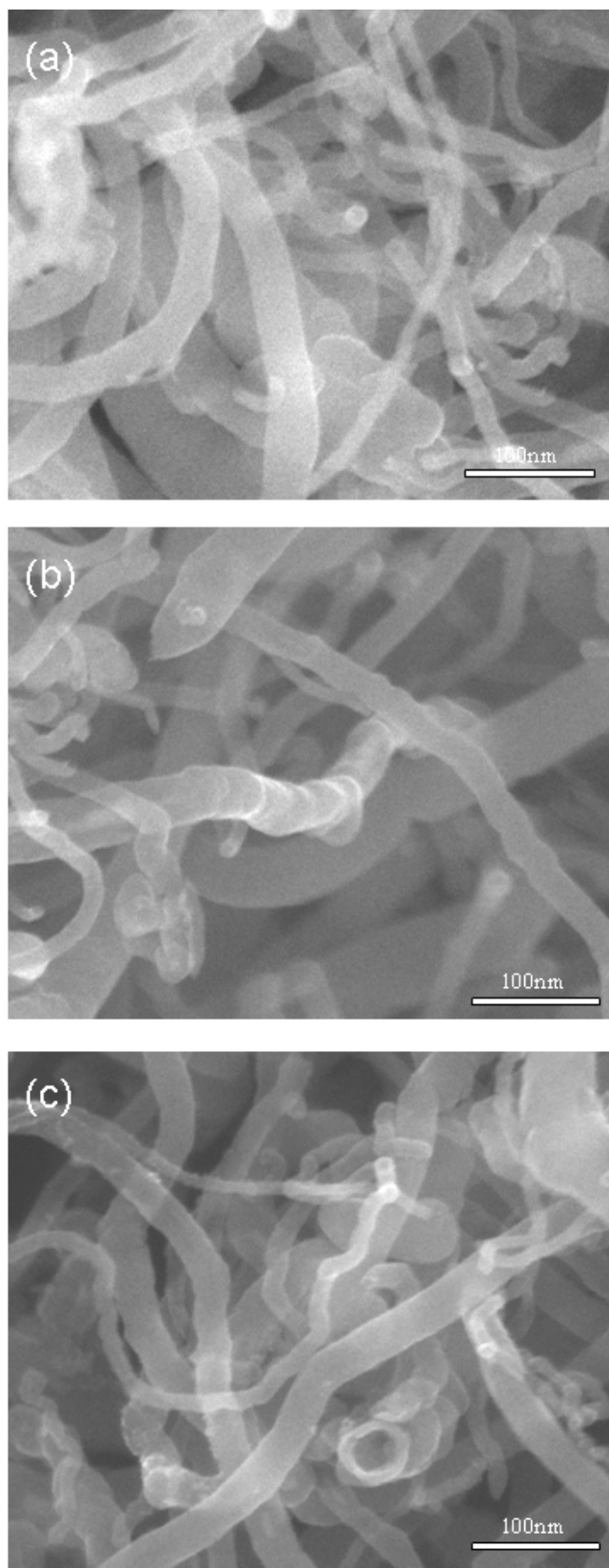
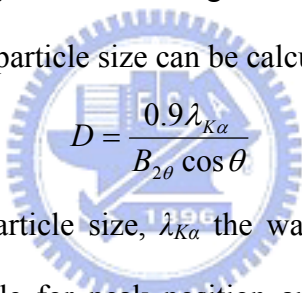


Fig. 5-13 SEM images of Pt catalyst synthesized on MWCNTs at different temperature in isopropyl-alcohol. (a) 40°C (b) 60°C (c) 80°C.

5.3 The effect of PVP molecular weight on particle size and dispersion

Nonasized Pt catalysts were successfully synthesized on CNTs for many times in the experiments, as shown in Fig. 5-14. Pt precursor was dissolved in EG solution with PVP of different molecular weights (MW=8000, 58000, and 1300000) to study the effect of PVP molecule weight on Pt particle synthesis, as shown in Fig. 5-14(a)-(c) respectively. Then solutions were heated to 160°C for 30 min. The XRD result shown in Fig. 5-15 also confirms that strong Pt signals appear in all samples at 2θ of 39.6°, 46.1°, 67.4°, 81.2°, 85.6° corresponding to reflection planes of (111), (200), (220), (311), and (222) respectively. Signals are consistent with face-centered cubic structure of Pt.

According to the XRD analysis shown in Fig. 5-15 and Scherrer equation based on the Pt (111) peak, the average particle size can be calculated by


$$D = \frac{0.9\lambda_{K\alpha}}{B_{2\theta} \cos \theta}$$

where D is the average Pt particle size, $\lambda_{K\alpha}$ the wavelength of the incident X-ray (1.5406Å), 2θ the Bragg angle for peak position and $B_{2\theta}$ is the half width at the maximum peak. The average Pt particle sizes in Fig. 5-14(a)-(c) calculated by this equation are 4.3, 4.3, and 4.4nm respectively. For smaller particles, it was reported that the adsorption strength of H, OH and CO on catalyst surface increased with decreasing particle diameter, and the specific activity of oxygen reduction is lowered [202].

The results reveal that particles of suitable size can be synthesized under this condition with PVP of various molecular weights and the peak intensity of Pt particles implies better crystalline structure. Although the particle size and size distribution seem to meet the requirements of the experiment groups, the Pt particle distribution on CNTs is not uniform. Possible reason of this phenomenon might be that the surface

of CNTs is hydrophobic and is difficult for Pt particles to be highly dispersed on. Several efforts have been thrown upon the fictionalization of the surface of CNTs [203], but the processes either take too long treatment time and waste more energy, or destruct the structure of CNTs to result in low mechanical strength required for fuel cell cycle operation.



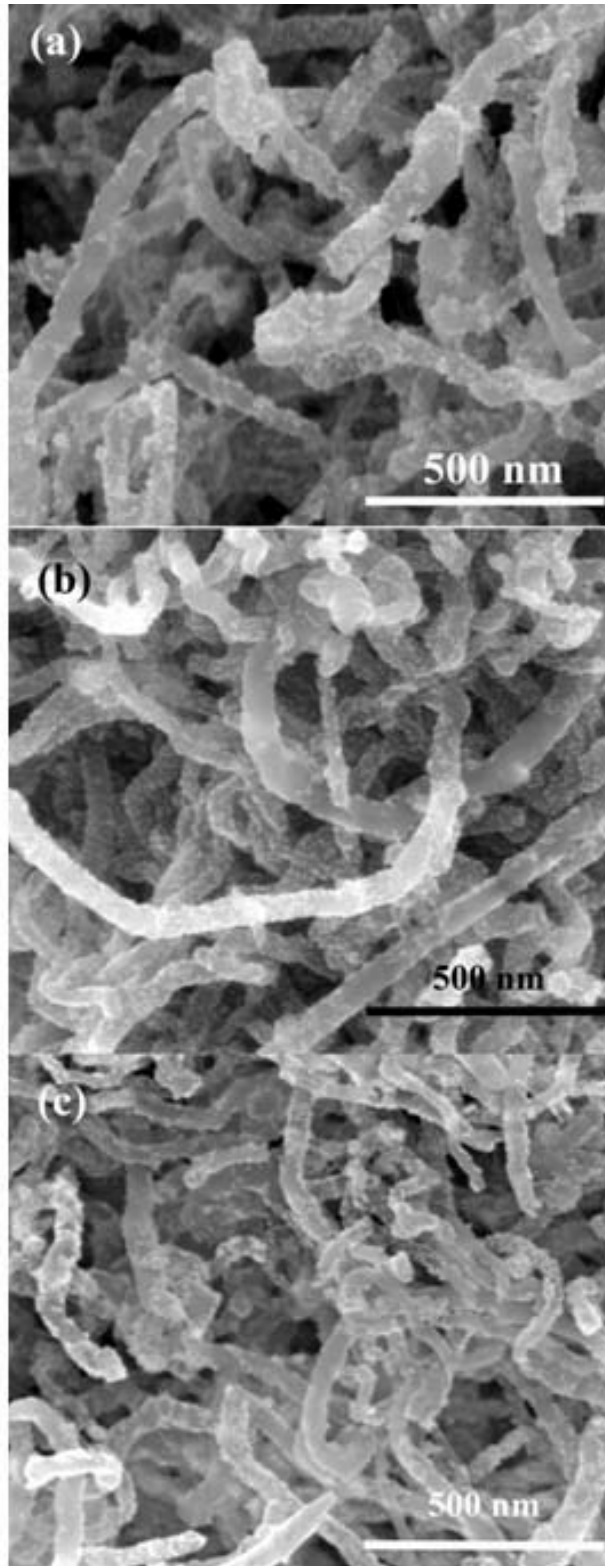


Fig. 5-14 SEM images of Pt nanoparticles synthesized on MWCNTs by heating the solution to 160°C for 30 min with PVPs of different molecular weights (a) PVP MW=8000, (b) 58000 (c) 130000.

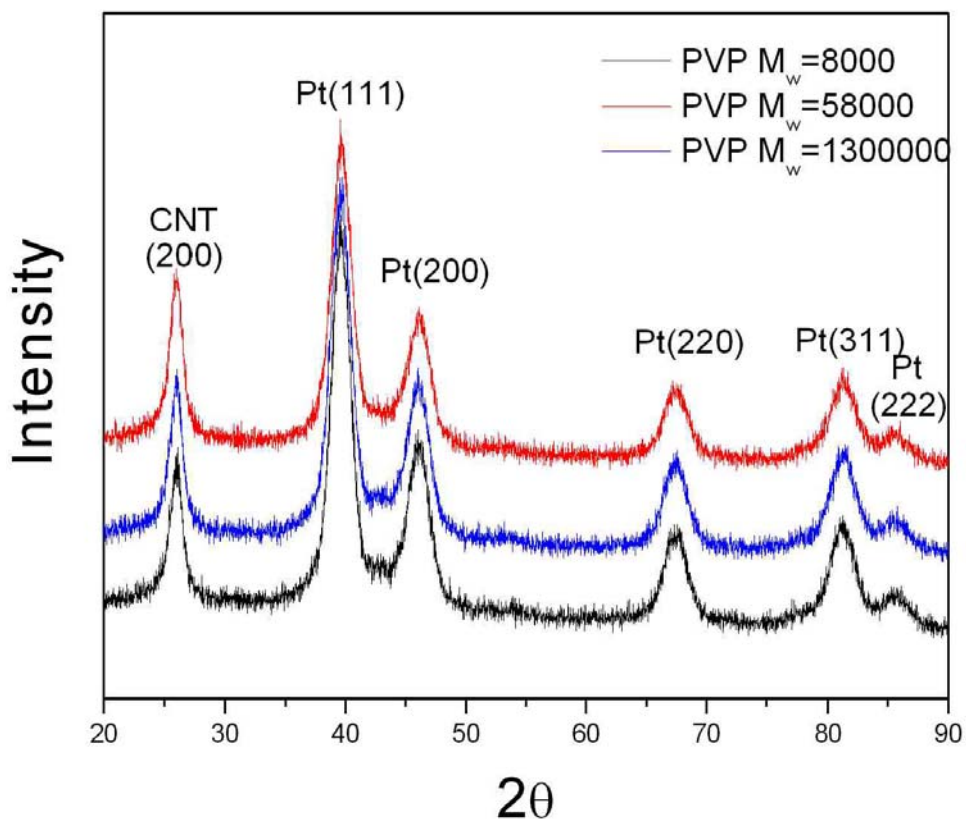


Fig. 5-15 XRD spectrum of Pt nanoparticles synthesized on MWCNTs by heating the solution to 160°C for 30 min with different molecular weight of PVP.

5.4 The Effect of SDS on Pt particle dispersion

According to the previous results, SDS was chosen to add in the following experiment groups to increase the dispersion of Pt on CNTs. The experiment conditions were the same as previously mentioned, but SDS was added in all samples (SDS/PVP=1:1). PVP used in the experiment groups were 8000, 58000, 1300000 in molecular weights. Besides, the mixtures of PVP of different molecular weight (8000/58000, 58000/1300000, 8000/1300000, at the ratio of 1:1) were also used to verify the effect on Pt particle size or distribution.

The SEM images were shown in Fig. 5-16 of (a) PVP MW=8000, (b) 58000 (c) 1300000. It is apparent that monolayer of Pt particles of small size and uniform size distribution are highly dispersed on each CNT, no matter what the diameter of CNTs

is and the PVP molecule weight is.

The results of XRD analysis are shown in Fig. 5-17. Strong Pt characteristic peaks appear in all samples to indicate that PVP can help Pt precipitation on CNTs when SDS was added in these samples. The mean particle size shown in Fig. 5-16 are 4.4 nm, 4.3 nm, and 4.3nm respectively, which were calculated by Scherrer equation based on the Pt (111) peak of all samples in Fig. 5-17. Figure 5-18 shows the HRTEM image of highly Pt-dispersed CNTs. Pt particles with uniform size are evidently attached on CNTs side by side even without multilayer stacking.

Figure 5-19 shows the SEM analysis results when PVP of different molecule weights were mixed together and added into solutions with SDS in the ratio of (a) 8000:58000=1:1, (b) 58000:1300000=1:1 (c) 1300000:8000=1:1. It can be realized that all CNTs are covered by monolayer of uniform-sized Pt particles, no matter what the diameter of CNTs is. The mean particle size calculated by equation and XRD peak width of Pt (111) shown in Fig. 5-20 are 4.0nm, 4.2nm, and 4.3nm respectively.

The HRTEM images are shown in Fig. 5-21, and it is clear that Pt particles with uniform size can be dispersed on each CNT, even though the diameters of CNTs are different from each other. The results indicate that molecule weight of PVP is not an effective factor to control the particle size or dispersion of Pt particles in the microwave dielectric heating system. On the other hand, SDS shows an effective way to disperse Pt particles on CNTs for PVP of high and low molecular weights during these experiments.

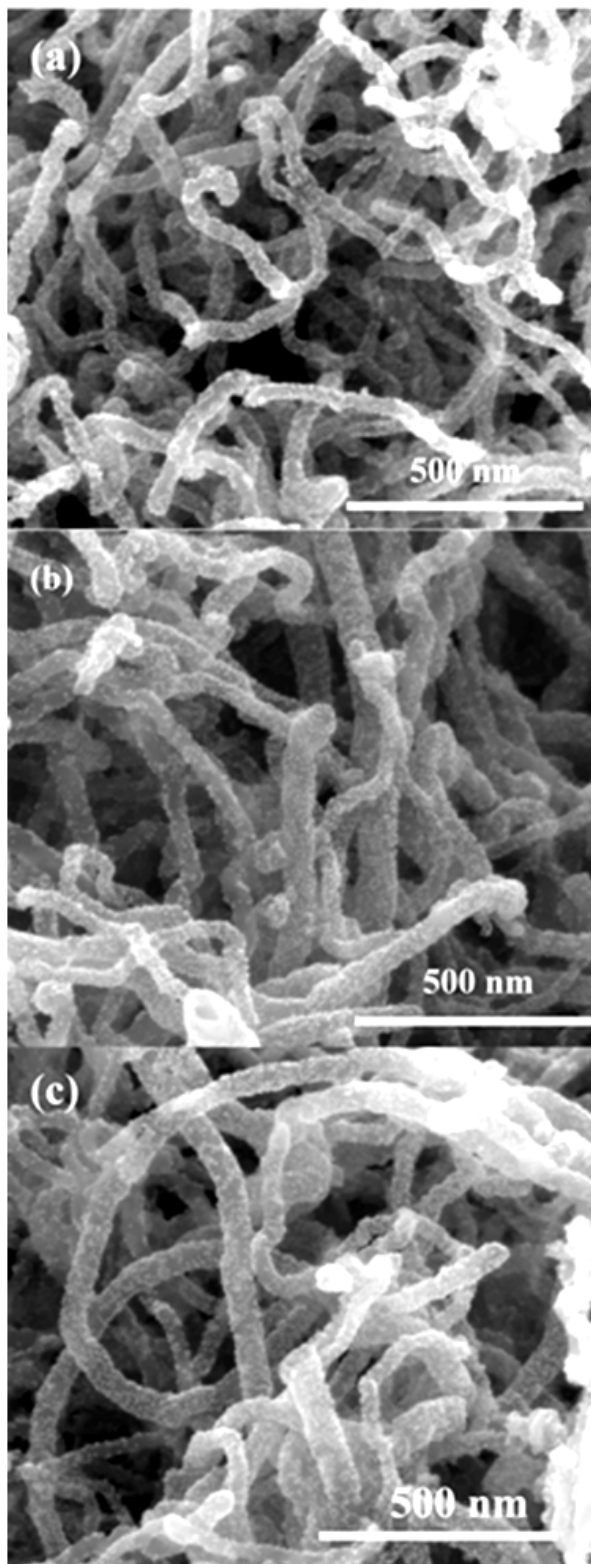


Fig. 5-16 SEM images of Pt nanoparticles synthesized on MWCNTs with PVPs of different molecular weights and the addition of SDS. (a) PVP MW=8000, (b) 58000 (c) 130000.

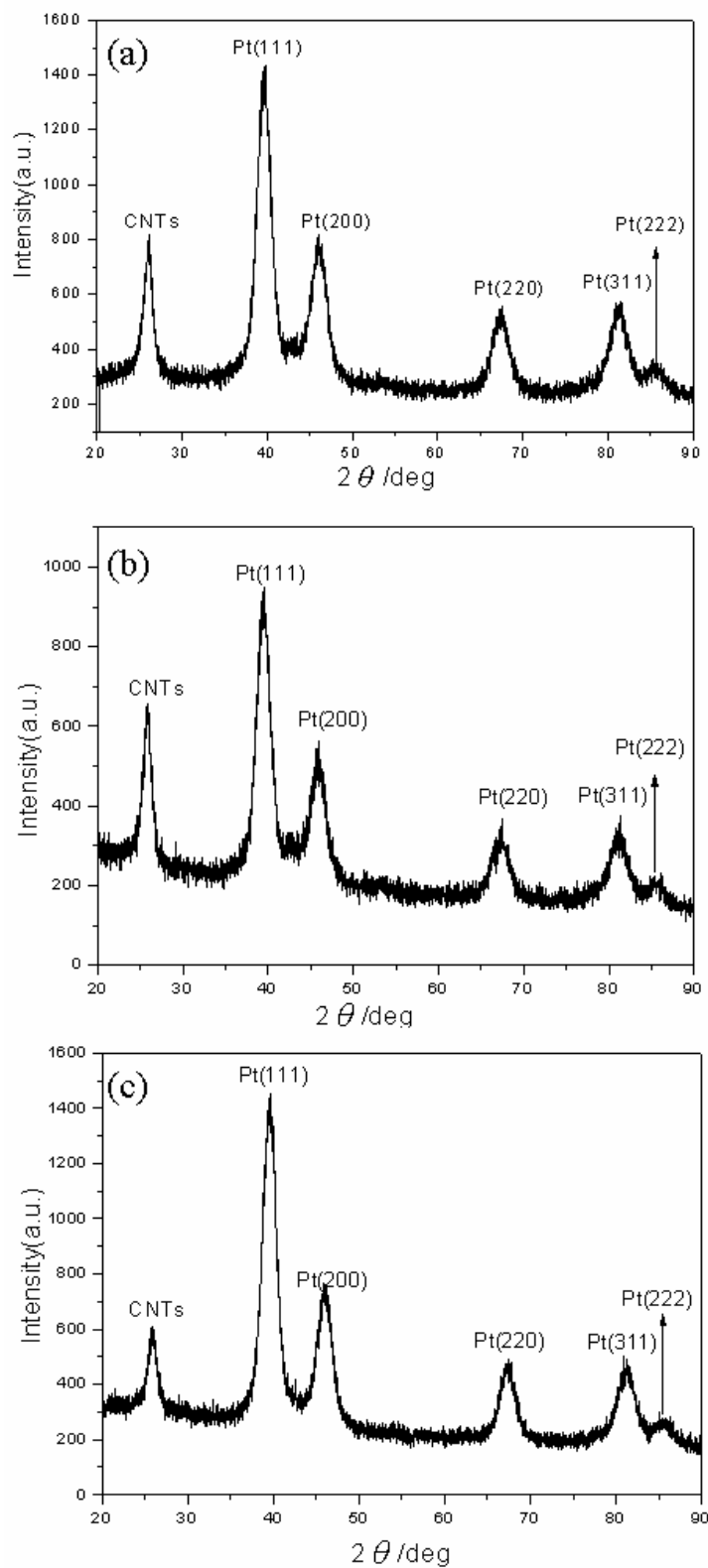


Fig. 5-17 XRD spectrums of Pt nanoparticles synthesized on MWCNTs with PVPs of different molecular weights and the addition of SDS. (a) PVP MW=8000, (b) 58000 (c) 1300000.

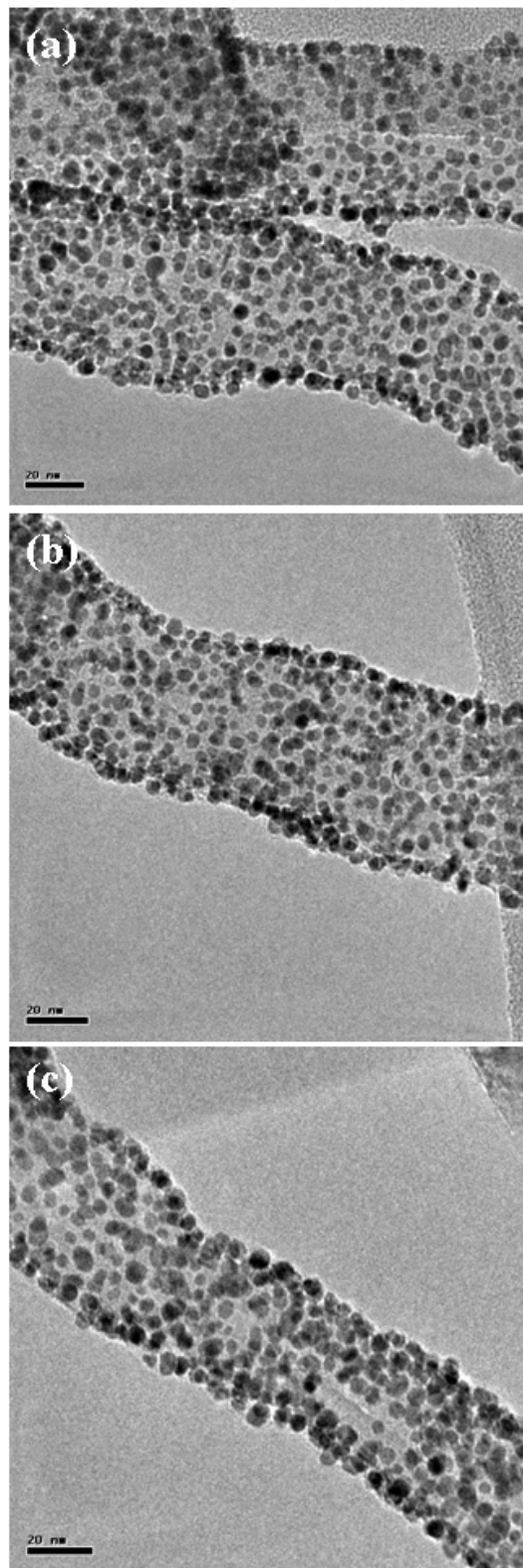


Fig. 5-18 TEM images of Pt nanoparticles synthesized on MWCNTs with PVPs of different molecular weights and the addition of SDS. (a) PVP MW=8000, (b) 58000 (c) 1300000.

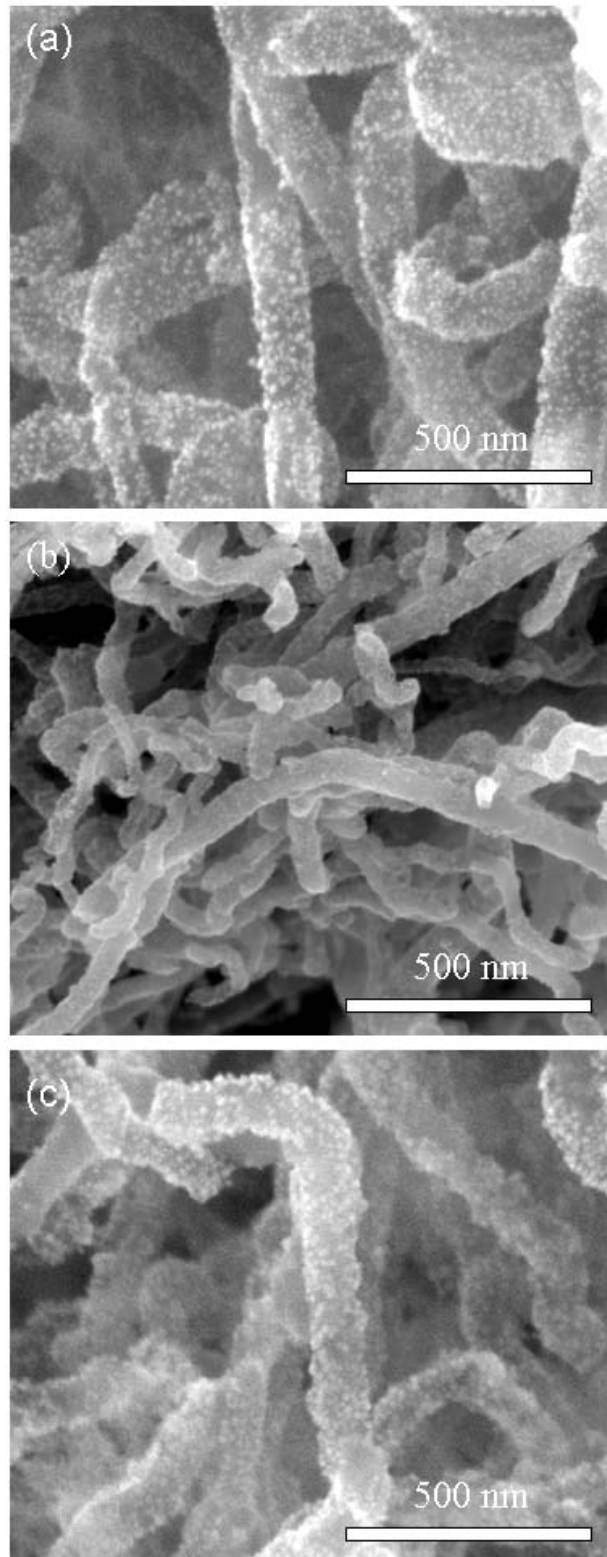


Fig. 5-19 TEM images of Pt nanoparticles synthesized on MWCNTs with PVPs of different molecular weights and the addition of SDS. (a) 8000:58000=1:1, (b) 58000:1300000=1:1 (c) 1300000:8000=1:1.

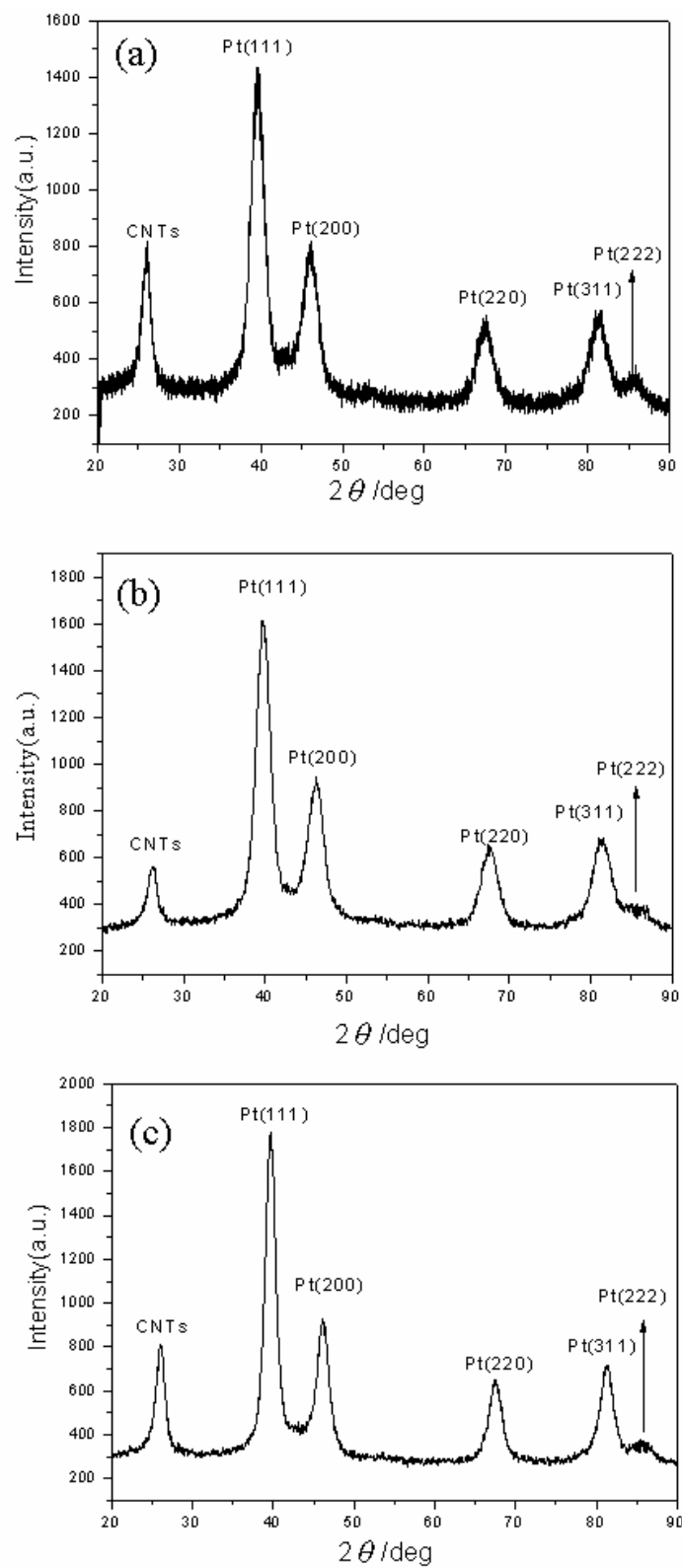


Fig. 5-20 XRD spectrums of Pt nanoparticles synthesized on MWCNTs with PVPs of different molecular weights and the addition of SDS. (a) 8000:58000=1:1, (b) 58000:130000=1:1 (c) 130000:8000=1:1.

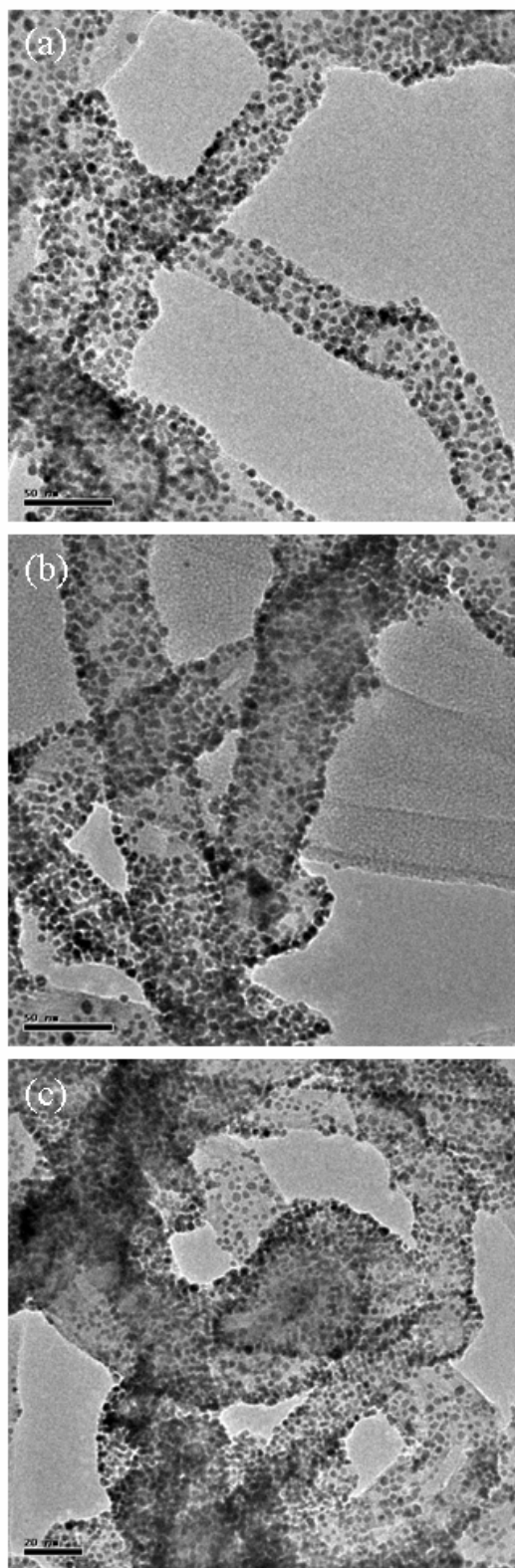


Fig. 5-21 TEM images of Pt nanoparticles synthesized on MWCNTs with PVPs of different molecular weights and the addition of SDS. (a) 8000:58000=1:1, (b) 58000:1300000=1:1 (c) 1300000:8000=1:1.

It was reported that sputtered Pt nanoparticles could also reach high dispersion of Pt on CNTs, but the disadvantage is that only several layers of CNTs on the top of surfaces can be sputtered on. Chemical methods do not have such restriction and can disperse nanoparticles on CNTs in any direction but have never been reported to reach the same high dispersion as this work. This work shows that SDS-addition can combine advantages of both physical and chemical methods to highly disperse Pt particles in any direction on CNTs. These results showed a successful way to synthesize Pt catalyst of suitable size, uniform size distribution and high dispersion on CNTs by using microwave-assisted heating method with the addition of SDS.

The mechanism to explain the role of SDS in Pt particle distribution and the loading amount can be considered in two parts shown in Fig. 5-22. First, it is well known that PVP in the solution can be adsorbed on the surface of Pt cluster to influence the growth of particle size or the shape of particles; that is, during the process a layer of PVP covers Pt particles. In the others, it has also been reported that PVP adsorption on a particle surface is strongly enhanced to about 40 times in the presence of SDS [204]. Pure PVP, in the absence of SDS, adsorbs at levels in the order of only 0.02 mg/m^2 , and to the order of 0.78 mg/m^2 as the addition of SDS. The surfactant adsorbs at the particle surface. Then PVP in turn forms a complex with the SDS micelles and the surface-adsorbed SDS will complex with the PVP molecules. This is the reason for the enhanced PVP adsorption. Next, SDS is known to be able to wrap monolayer PVP around single-walled carbon nanotubes (SWNTs) without covalent modification by chemical treatment, which could change favorable properties of tubes [205]. This means that SDS has excellent ability to attach PVP on CNTs. The reason is that SDS can adsorb chemically on CNTs, and attract PVP molecules by the electrostatic attraction between the surfactant head-group of SDS and the PVP nitrogen atom of side group.

According to these discussions, Pt nanoparticles are covered by PVP in solution and SDS wraps PVP around CNTs. It is believed that the added-SDS in this work could improve the dispersion and loading of Pt on tubes by bounding Pt-covering PVP and tubes together.

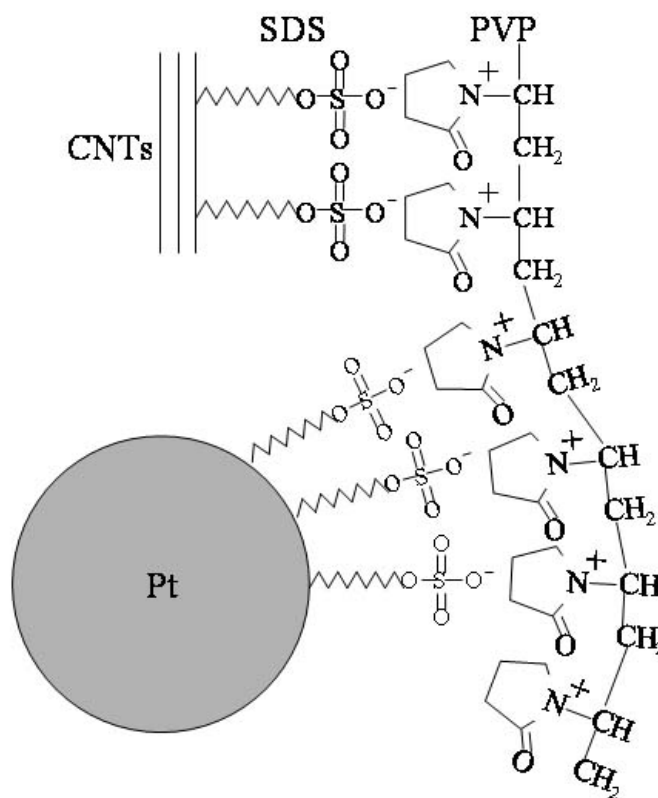


Fig. 5-22 Mechanism among Pt particle, SDS, and PVP.

5.5 The effect of temperature on loading amount of Pt

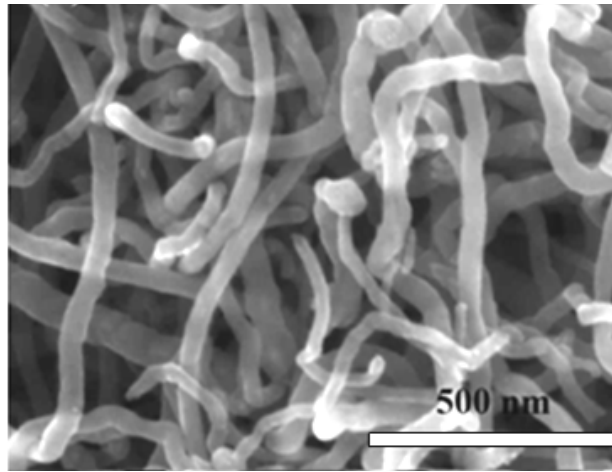
Further studies of the temperature effect in microwave heating method are shown in Fig. 5-23. The temperatures of each sample are (a)80°C, (b)100°C, (c)120°C, (d)140°C, (e)160°C and (f)180°C respectively, the same as other parameters but molecule weight of PVP was chosen as 8000 because previous results show that it makes no differences for these three PVPs and PVP of lower molecule weight has higher solubility in water and lower vaporization temperature and is easy to remove. As shown in Fig. 5-23, it is hard to find even a Pt particle in Fig. (a), and several

particles can be found in (b), but more and more particles appear from (c) to (e). The dispersion density of Pt particles both in (d) and (e) is almost the same, but much lower in Fig. (c). For the sample at 180°C, some lumps of Pt particles are occasionally observed, and this might be attributed to the aggregation at high temperature. The result tells that temperature effect on Pt particle synthesis is outstanding. Although SDS can help the dispersion on CNTs, the total amount of Pt particles during synthesis and the particle size were dominated by temperature. Only tens of temperature variation can cause such different results from 120°C to 180°C.

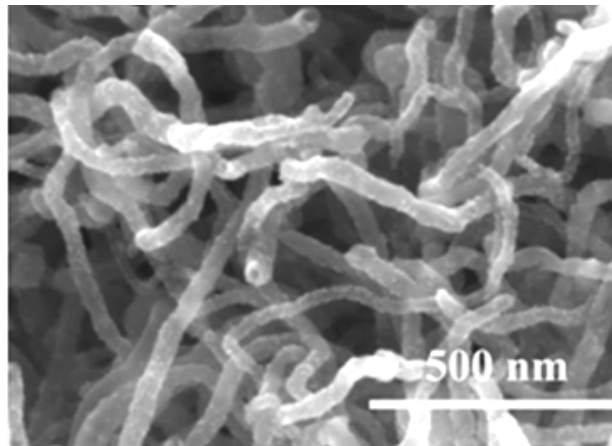
The images of HRTEM analysis are shown in Fig. 5-24, and it is hard to find Pt particles in the sample of (a)80°C, and more and more Pt particles can be seen in samples of (b)100, (c)120, (d)140, (e)160, and (f)180°C. The particle size about 4~4.5nm measured by HRTEM image completely agree with the results of XRD of samples at 100, 120, 140, 160 and about 7.6 of sample at 180 °C.

Figure 5-25 shows the XRD analysis results. There is a weak Pt signal in the sample of 80°C at 2θ of 39.6°, which agrees with the result of SEM and TEM analysis. As the temperature increase, Pt signals are becoming stronger for samples of 100 and 120°C. When the temperature is above 140°C, strongest Pt peaks appear in all samples of 140, 160 and 180°C. However, it can be found in the XRD spectrum that 7.6 nm of the Pt particle size is too big at 180°C. These results imply that temperature might be a key factor to control the amount of Pt particles dispersed on CNT, but high temperature could result in coarsening of particle size.

(a)



(b)



(c)

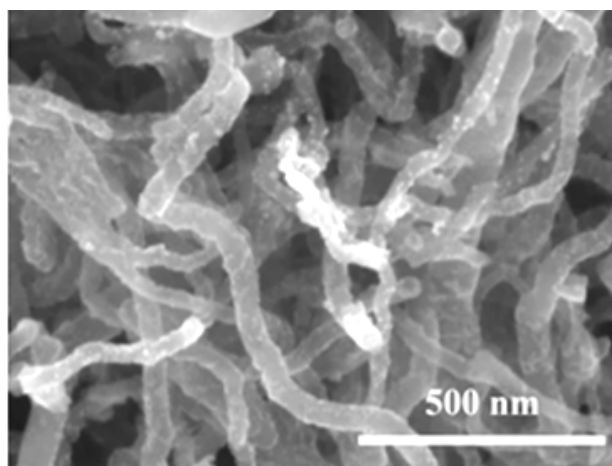
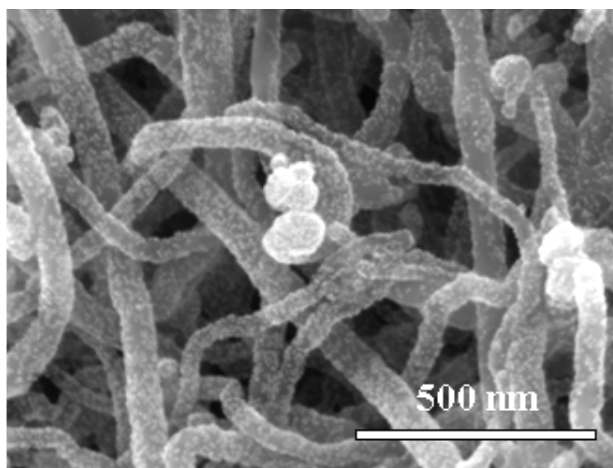
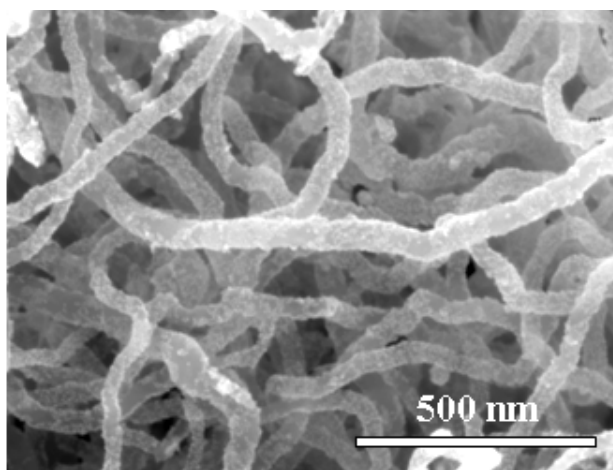


Fig. 5-23 SEM images of Pt particles synthesized on MWCNTs at different temperature for 30min. (a) 80°C (b) 100°C (c) 120°C.

(d)



(e)



(f)

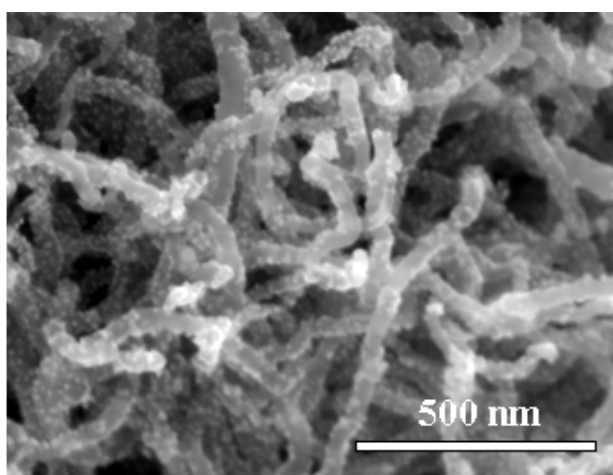
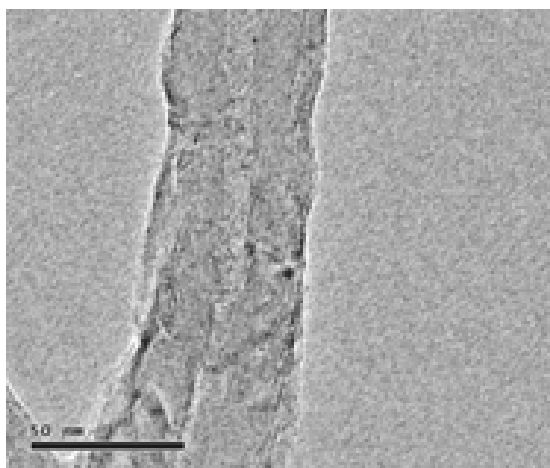
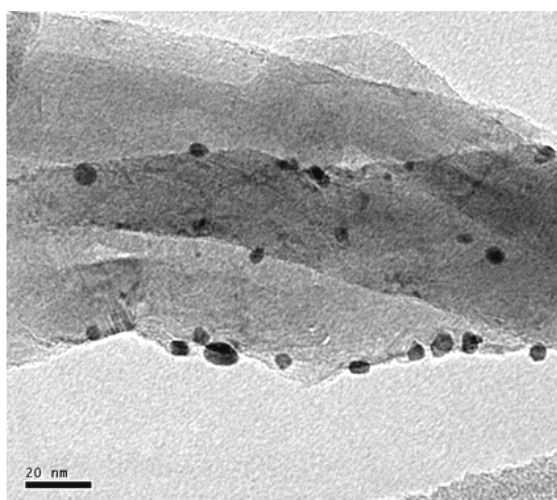


Fig. 5-23 SEM images of Pt particles synthesized on MWCNTs at different temperature for 30min. (d) 140°C (e) 160°C (f) 180°C.

(a)



(b)



(c)

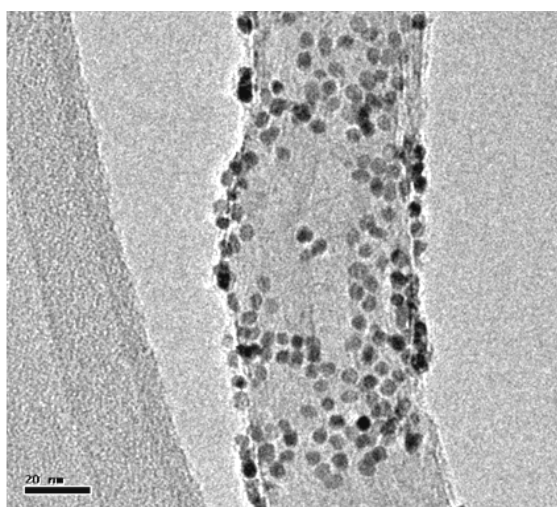
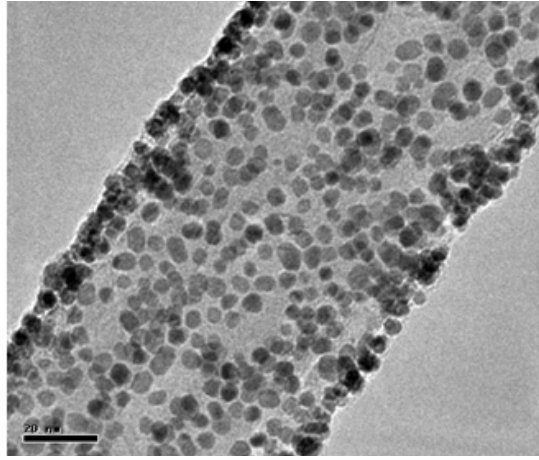
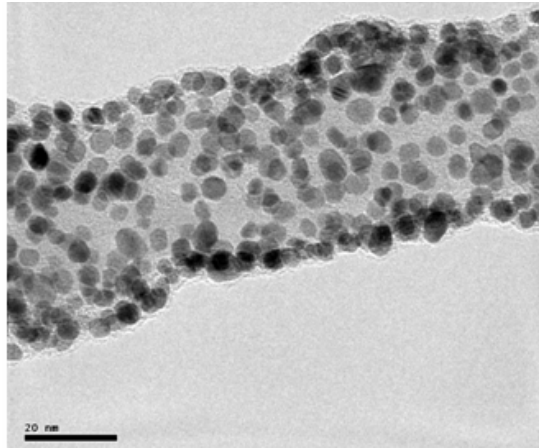


Fig. 5-24 TEM images of Pt particles synthesized on MWCNTs at different temperatures for 30min. (a) 80°C (b) 100°C (c) 120°C.

(d)



(e)



(f)

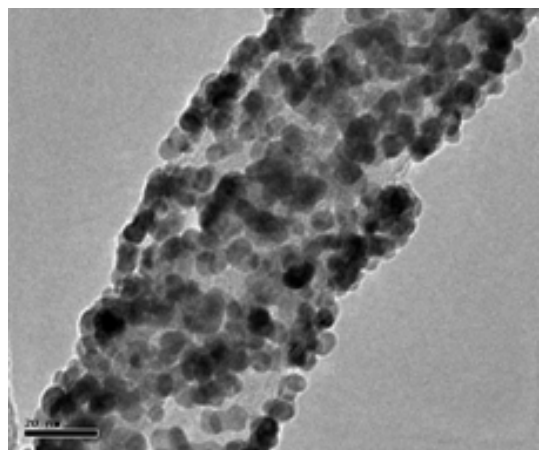


Fig. 5-24 TEM images of Pt particles synthesized on MWCNTs at different temperature for 30min. (d) 140°C (e) 160°C (f) 180°C.

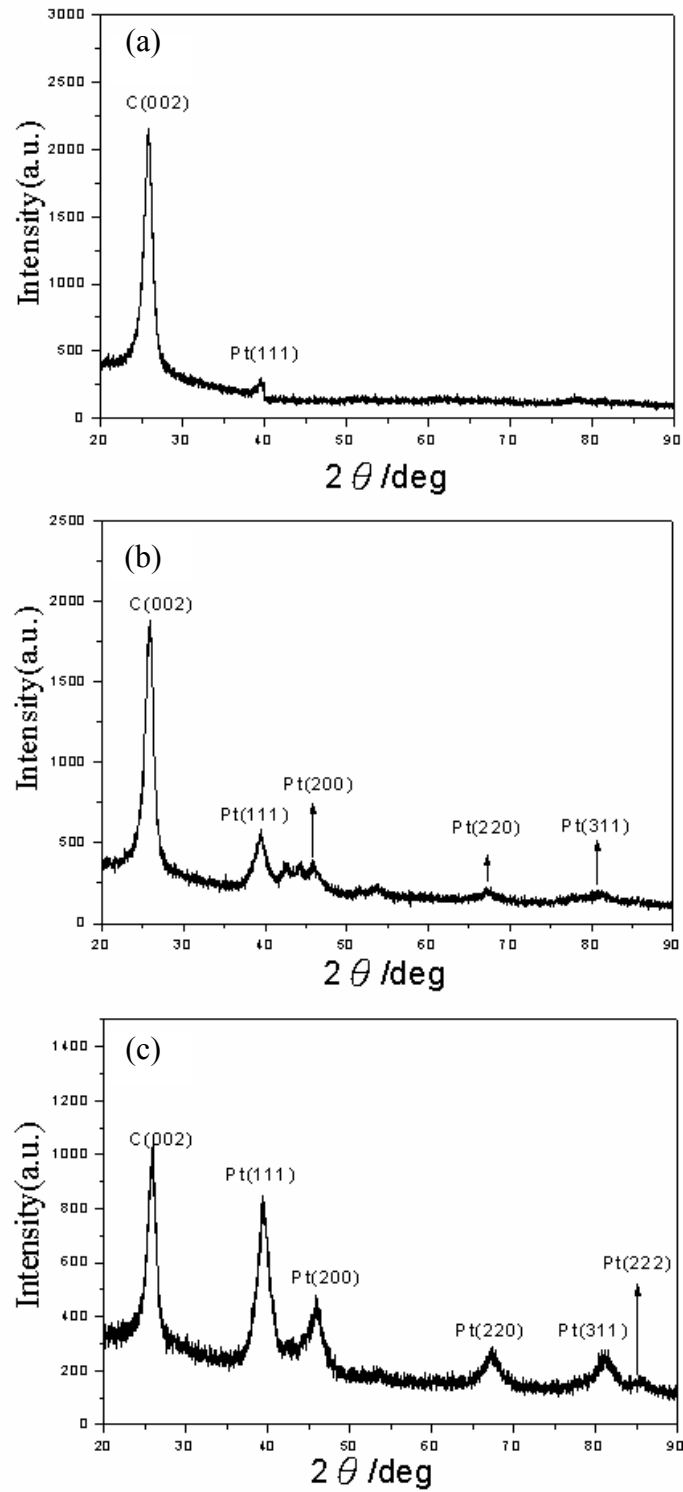


Fig. 5-25 XRD spectrums of Pt particles synthesized on MWCNTs at different temperatures for 30min. (a) 80°C (b) 100°C (c) 120°C .

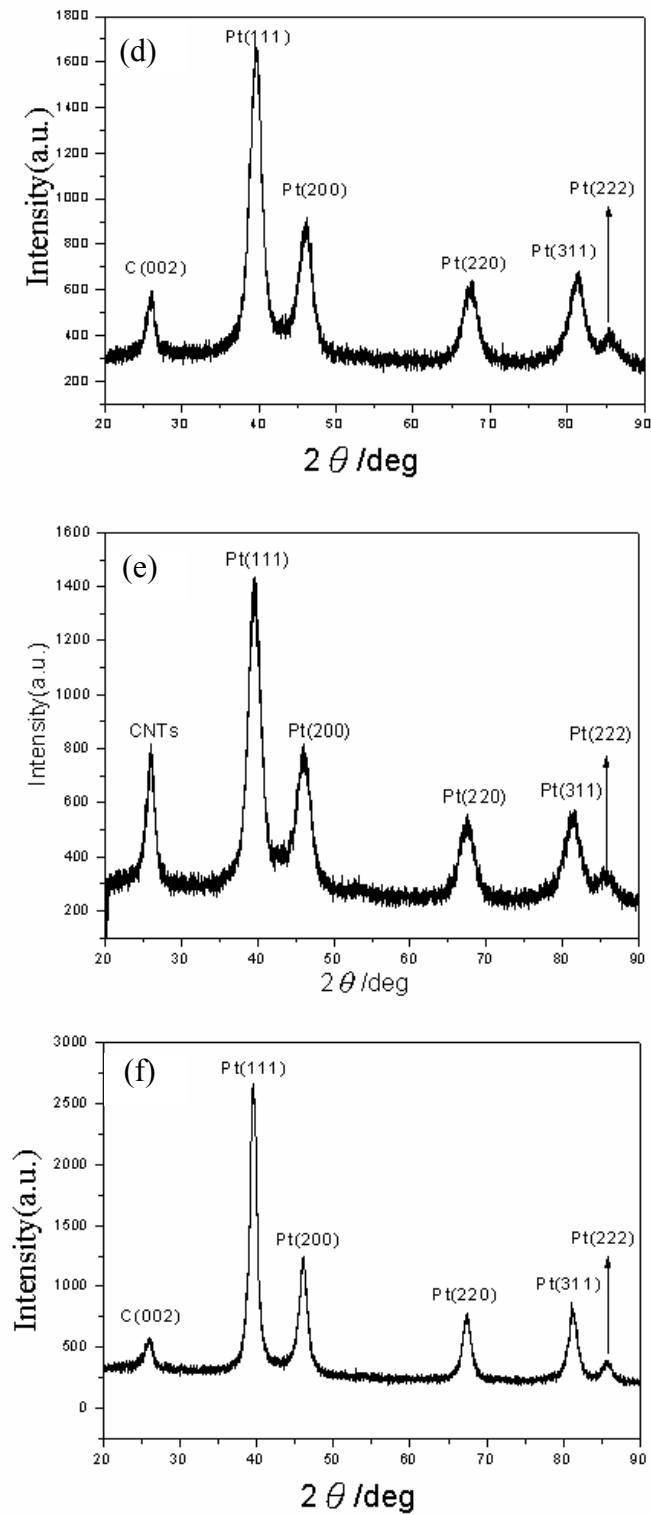


Fig. 5-25 XRD spectrums of Pt particles synthesized on MWCNTs at different temperature for 30min. (d) 140°C (e) 160°C (f) 180°C.

Figure 5-26 shows the Pt loading amounts at different reaction temperatures by TGA analysis. Obviously, the loading amount is low at low treatment temperature of 80°C and increases with increasing temperature to 140°C which has the largest loading amount of 54.64 wt %. When the temperature keeps increasing to 180°C, the loading amount slightly decrease to 51.12 wt % possibly by the aggregation or coarsening of nanoparticles, and then Pt peels off form the surface of CNTs. The TGA analysis results are consistent with the SEM, TEM and XRD analysis in Fig. 5-23~5-25. So, the reduction rate of Pt particle from chloroplatinic acid and loading amounts of Pt particle can be controlled by synthesized temperature .The reaction temperature is outstanding and seems to be the key factor to affect the loading amount of Pt particles on supports.

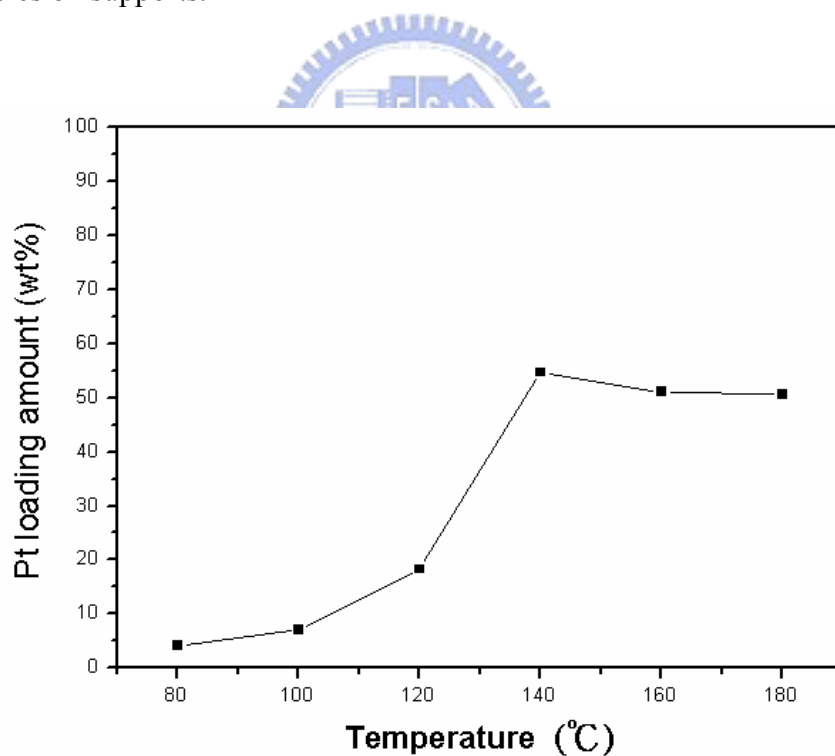


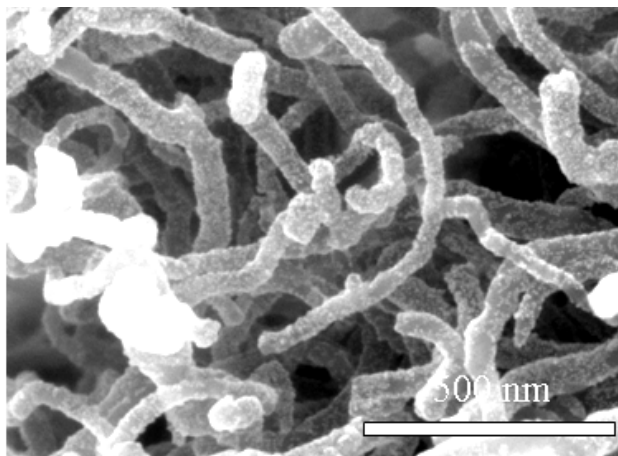
Fig. 5-26 The Pt loading amounts at different reaction temperatures.

5.6 The effect of time on Pt loading amount

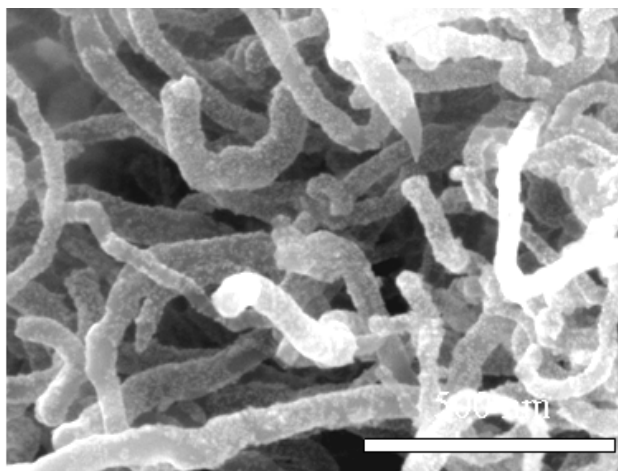
Besides the temperature effect, the effects of treatment time under constant temperature of 140°C are investigated and shown isothermally in Fig. 5-27 with time intervals of (a)1.5, (b)2, (c)5, (d)10, (e)30, and (f)90min. From the SEM images, it is apparent that Pt particles are highly dispersed on CNTs in all samples of different reaction time, even though the reaction time is as short as 1.5min. These analysis results clearly indicate that temperature might be more important than reaction time to control the dispersion of Pt particles on CNTs. Fig. 5-28 shows the HRTEM images. It is obvious that all CNTs are highly dispersed on by Pt particles in all samples, even the sample of shortest treatment. However, for too long treatment time of about 90 min, the disadvantages are not only time and energy consuming but also the double layer or multilayer of Pt particles stacking on the first layer that results in the Pt peeling off from tube surfaces by internal stress, which can be found occasionally and is shown in Fig. 5-28(f).

Figure 5-29 shows the XRD results of samples of different reaction time. Pt signals are equally intense in all samples of different time and the mean particle size calculated by the equation and Pt (111) peak in all samples are 4.1nm, 4.4nm, 4.5nm, 4.5nm, 4.5nm, and 4.3nm respectively. The results evidently point out that the particle size are almost the same in spite of reaction time variation under constant temperature without coarsening and are not affected by increasing reaction time. Comparing to the temperature effect discussed previously, XRD results show again that reaction temperature not only dominates the dispersion of Pt particles, but also the particle size of Pt.

(a)



(b)



(c)

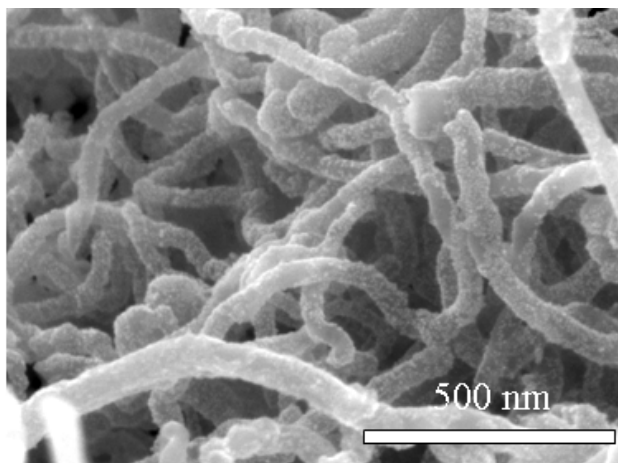
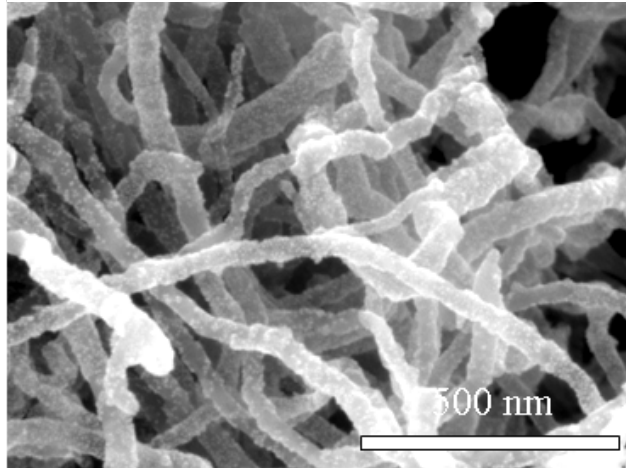
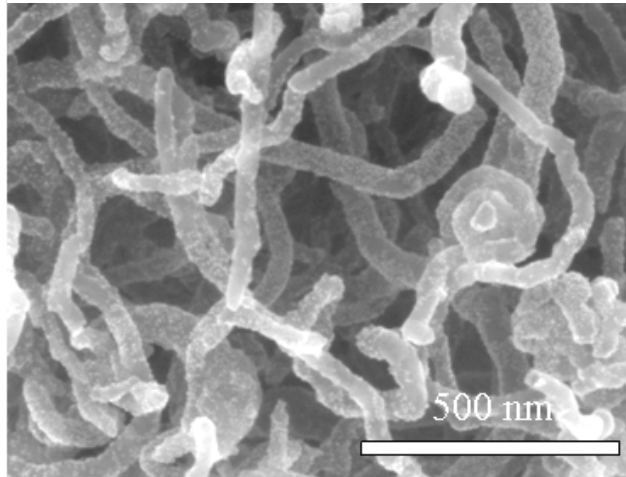


Fig. 5-27 SEM images of Pt particles synthesized on MWCNTs of different reaction time at 140°C. (a) 1.5min (b) 2min (c) 5min.

(d)



(e)



(f)

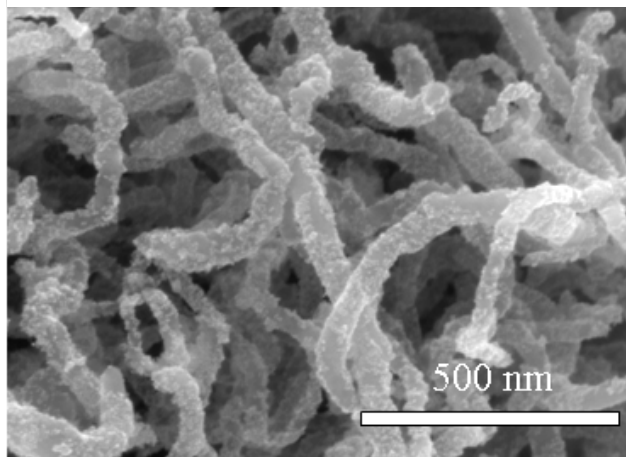
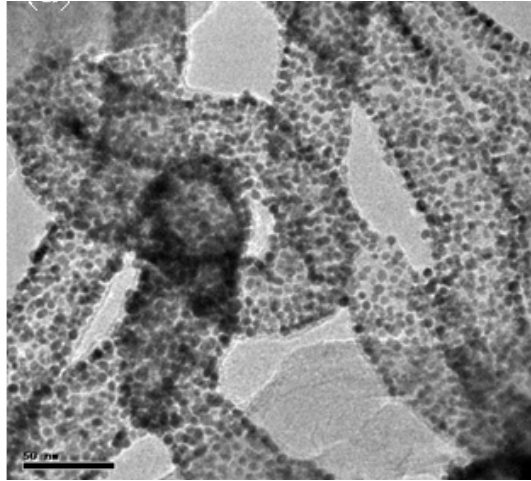
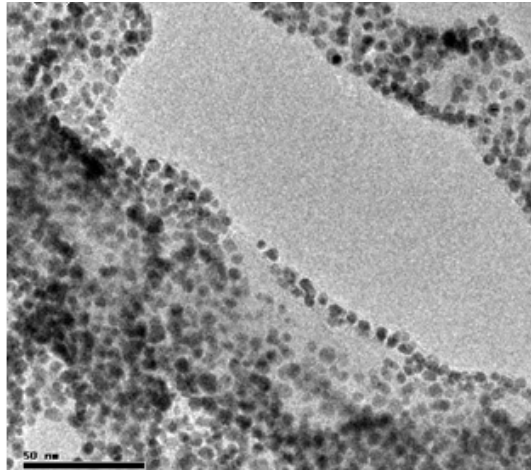


Fig. 5-27 SEM images of Pt particles synthesized on MWCNTs of different reaction time at 140°C. (d) 10 min (e) 30min (f) 90min.

(a)



(b)



(c)

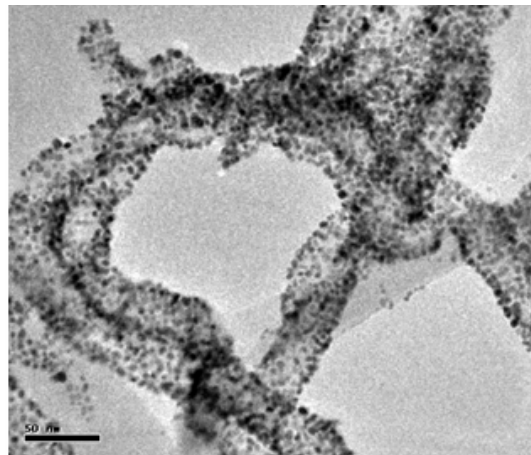
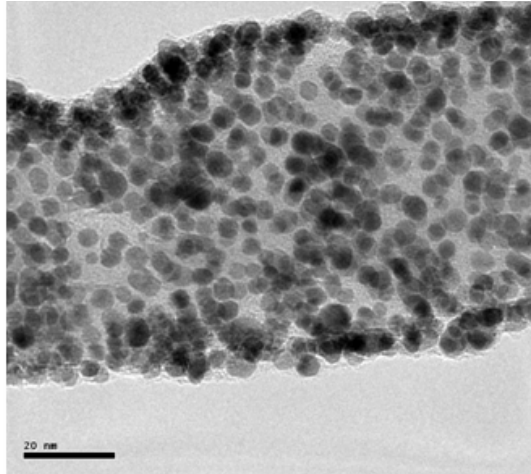
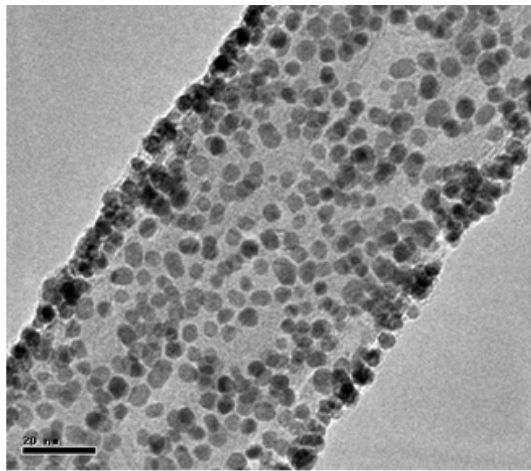


Fig. 5-28 TEM images of Pt particles synthesized on MWCNTs of different reaction time at 140°C. (a) 1.5min (b) 2min (c) 5min.

(d)



(e)



(f)

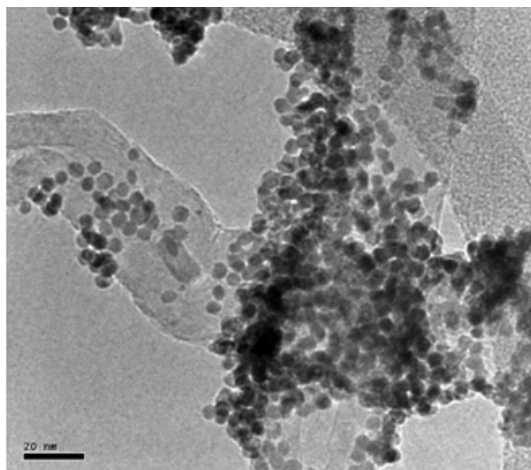


Fig. 5-28 TEM images of Pt particles synthesized on MWCNTs of different reaction time at 140°C. (d) 10 min (e) 30min (f) 90min.

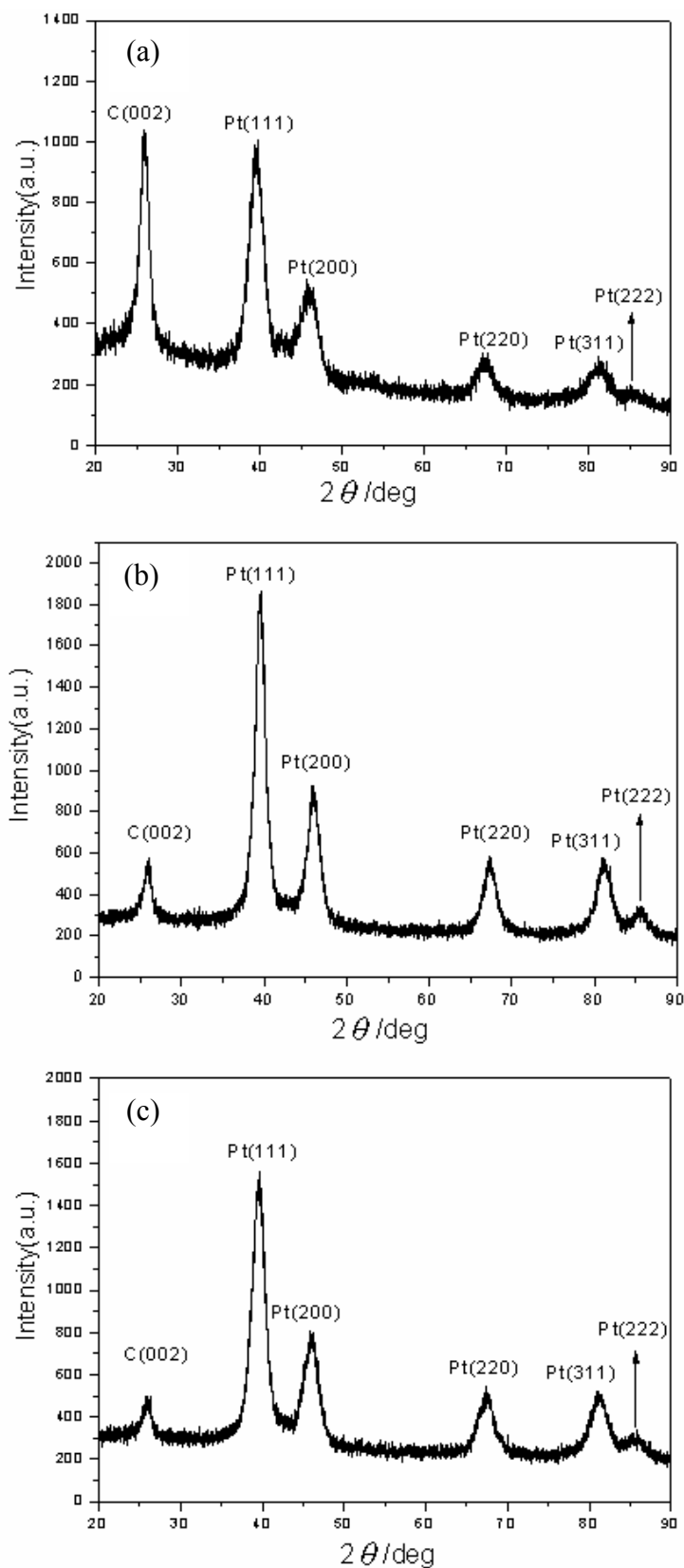


Fig. 5-29 XRD spectrums of Pt particles synthesized on MWCNTs of different reaction time at 140°C . (a) 1.5min (b) 2min (c) 5min.

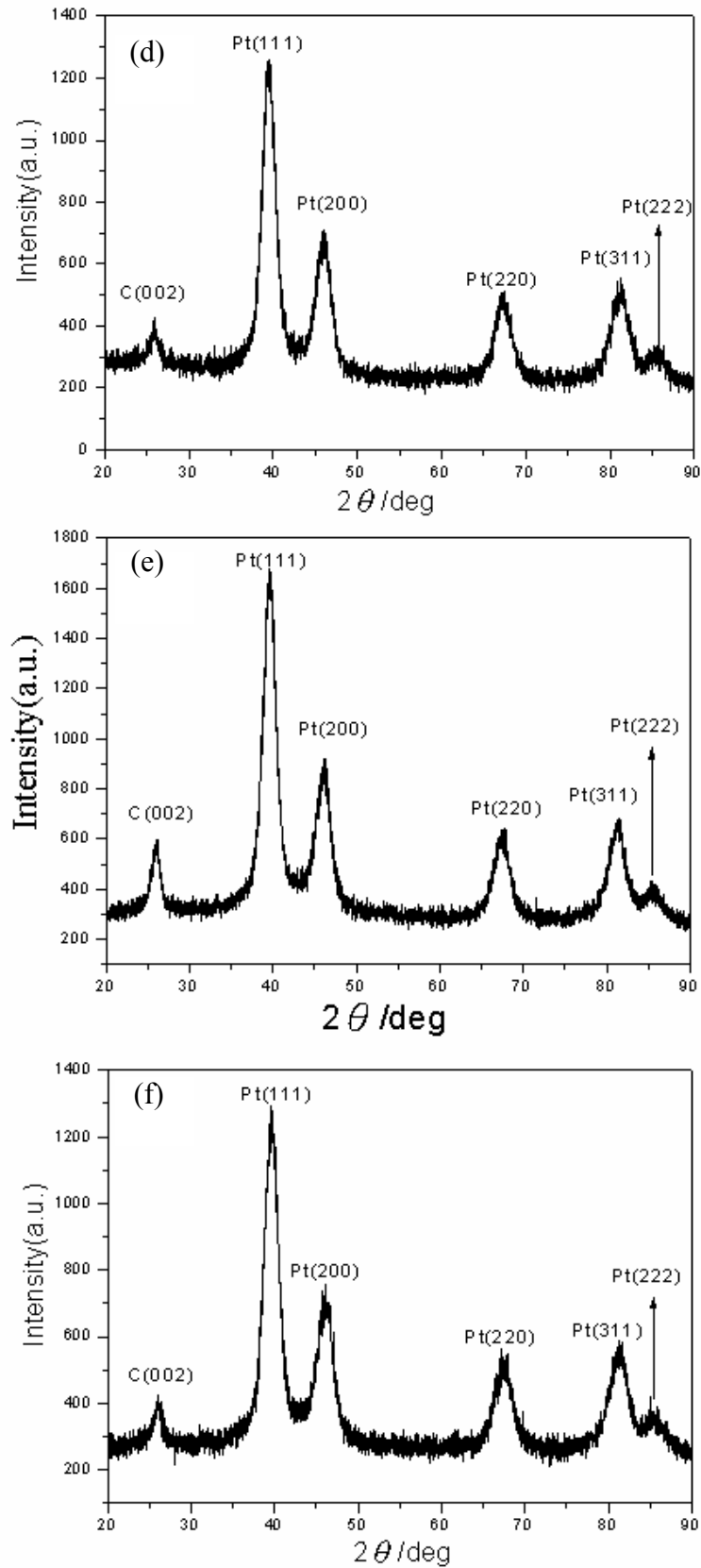


Fig. 5-29 XRD spectrums of Pt particles synthesized on MWCNTs of different reaction time at 140°C . (d) 10 min (e) 30min (f) 90min.

The TGA analysis results of Pt loading amount with different reaction time are shown in Fig. 5-30. This curve shows that the loading amount can achieve 52.1 wt % as soon as the temperature reaches 140°C for 1.5 min of heating time. As the isothermal time increases, the loading amount of Pt on CNTs slightly increases. When the isothermal time is set up to 90 min, the loading amount can rise to 60 wt%. However, it has been known that the disadvantages of long time treatment are not only time and energy consuming but also the appearance of double layers or triple-layers of Pt particles stacking layer by layer.

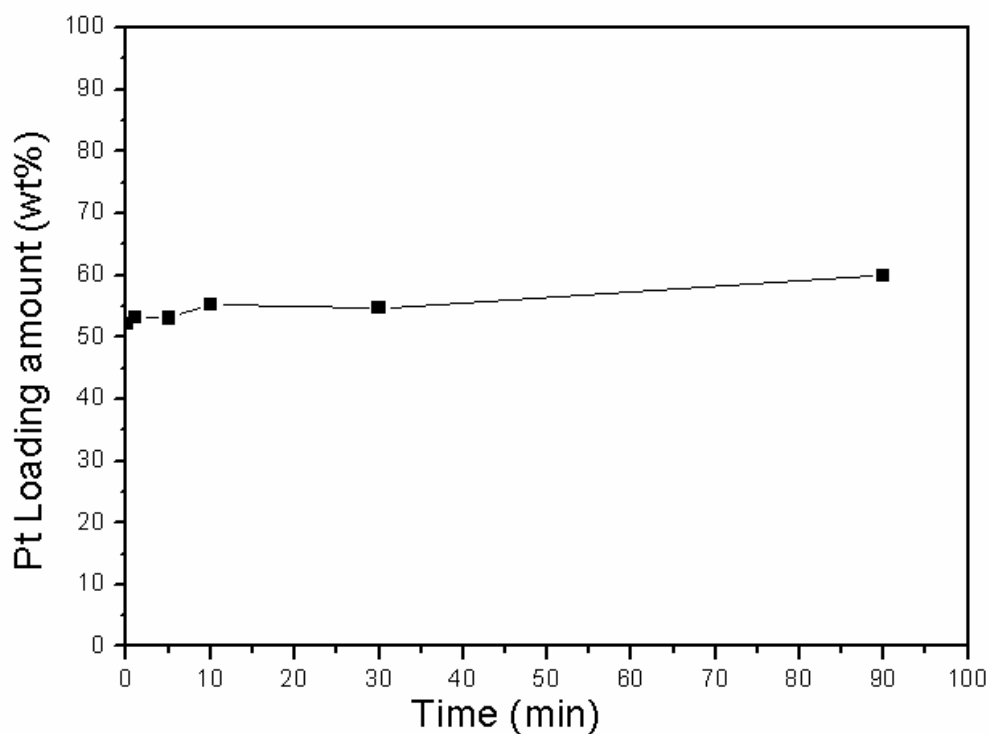


Fig. 5-30 Pt loading amount of different reaction time.

Figure 5-31 is the histogram of Pt particle size distribution obtained from the enlarged HRTEM images of well-dispersed Pt particles on CNTs. The total sampling amount is 2868 particles. This diagram shows the narrow size distribution of Pt clusters supported on CNTs in which diameter distribution of about 47% particles ranges between 4 and 5 nm and only a few particles are larger than 6nm or smaller than 3 nm. The average particle size is 4.3 nm by statistic calculation.

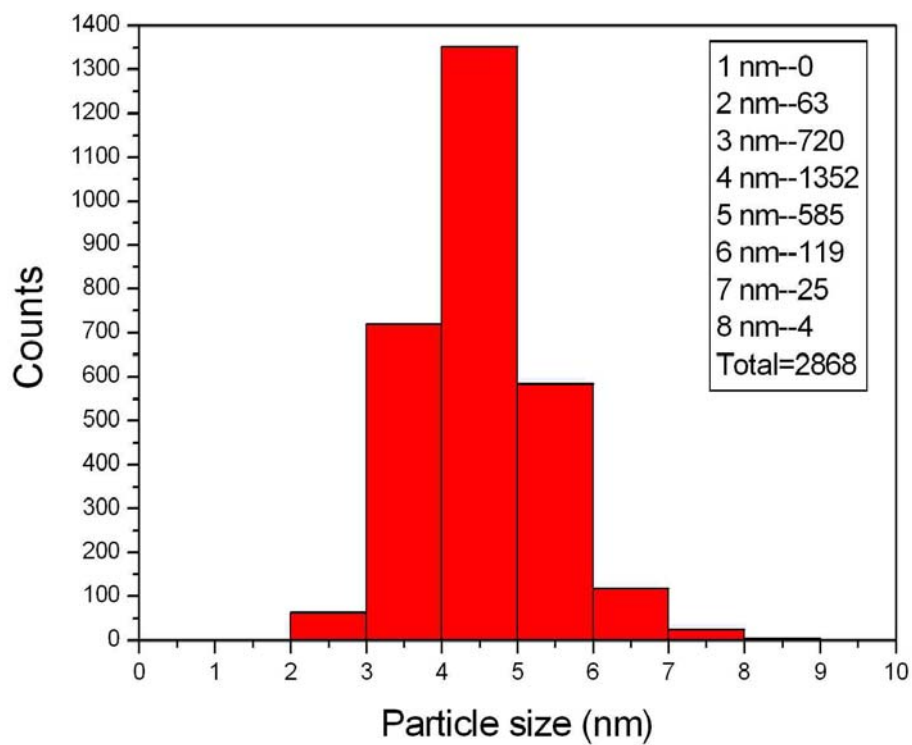


Fig. 5-31 Particle size distribution of Pt nanoparticles.

Fig. 5-32 is the high magnification SEM image of Pt-dispersed spiral MWCNTs. CNTs were synthesized on Si substrate by thermal CVD method with Fe catalyst. It can be seen that Pt particles are uniformly and highly dispersed on straight and spiral MWCNTs.

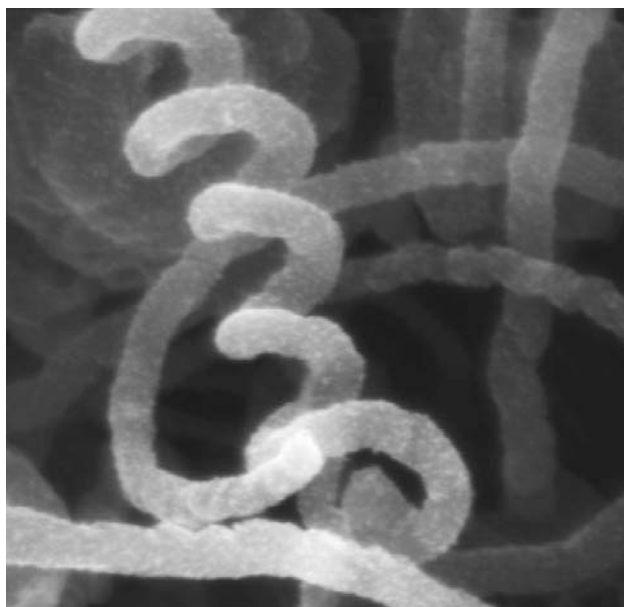


Fig. 5-32 High magnification SEM image of Pt-dispersed spiral CNTs.

Fig. 5-33 shows the cross-sectional image of MWCNTs with sputtered Pt particles. This cross-section was cut by FIB, as shown in Fig. (a). In Fig. (b), it is clearly shown that the sputtered Pt can be found in the upper layers of CNTs; however, in the inner layers marked by red line, CNTs are shelled by upper layers and can't be dispersed on Pt particles by sputtering method. Fig. 5-34 is the cross-sectional image of CNTs cut by FIB. Pt particles were dispersed by microwave-assisted polyol method. CNTs were dried and dispersed on carbon tape and cut for cross-section in the edge. It is evident that each tube, compared to that of sputtering method, is fully covered by Pt particles in all directions, regardless of upper or inner layers.

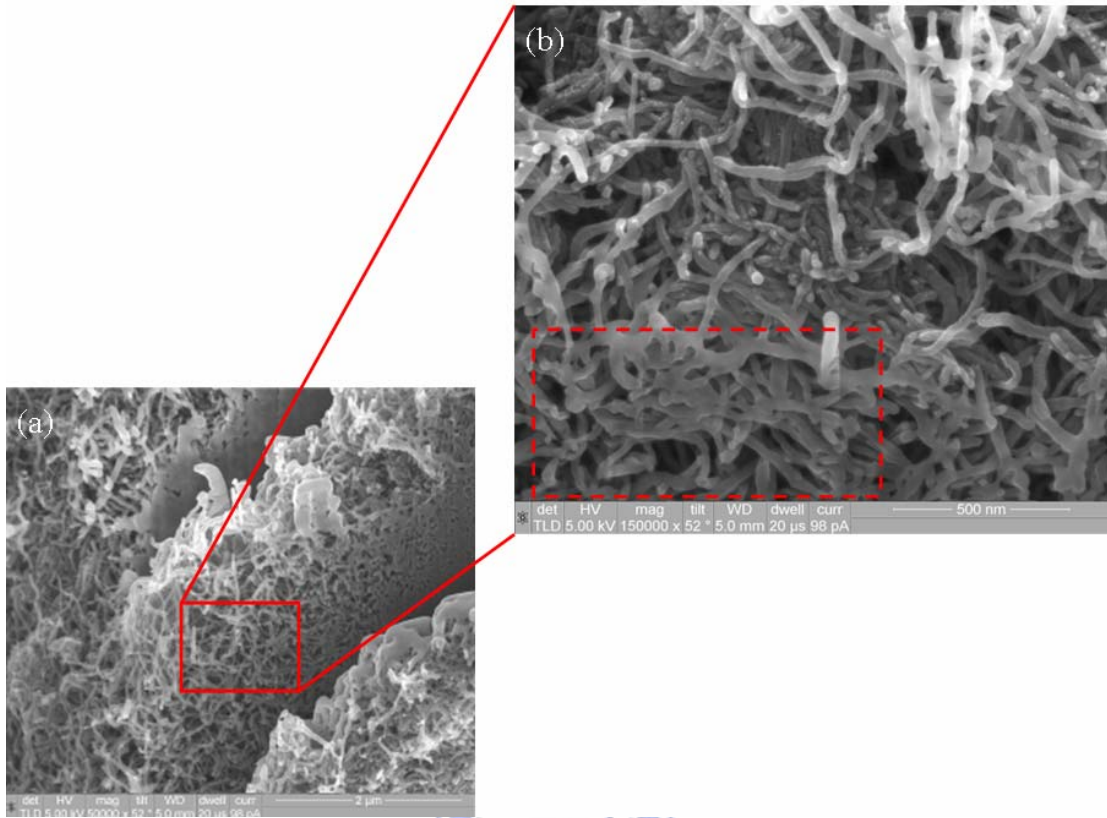


Fig. 5-33 Cross sectional images of Pt-sputtered MWCNTs.

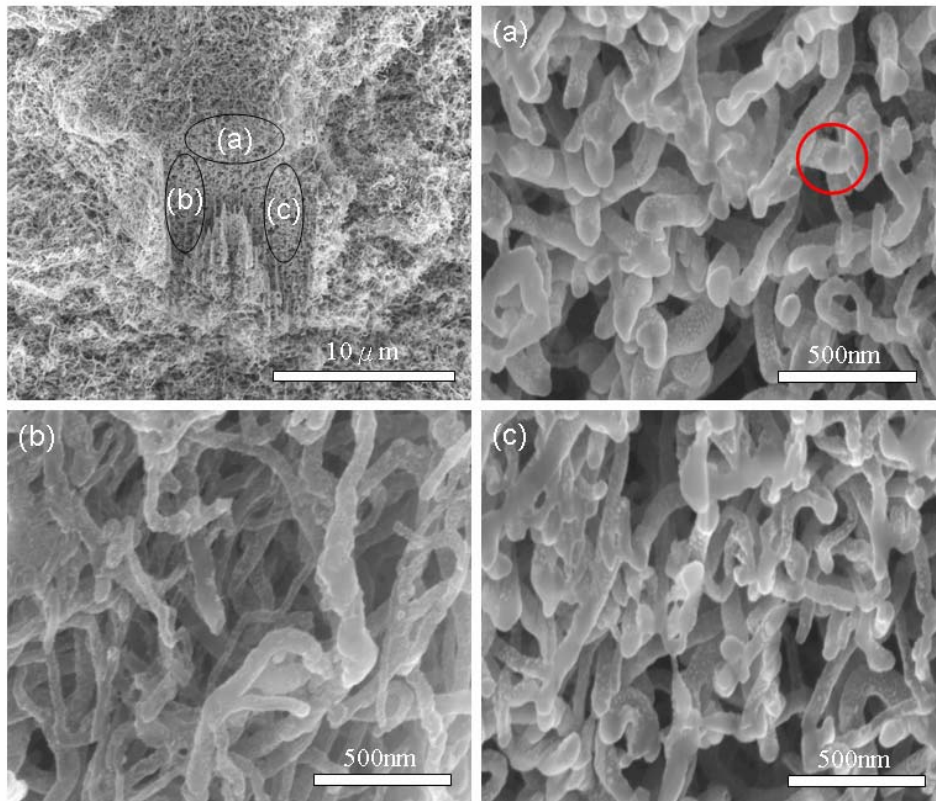


Fig. 5-34 Cross sectional images of highly Pt-dispersed MWCNTs by microwave assisted polyol method.

Figure 5-35 shows the XPS spectrum of Pt 4f peak of the microwave synthesized Pt particles on MWCNTs. The Pt 4f peak consisted of two pairs of signals and the most intense peak (4f7/2 at 71.2 and 4f5/2 at 74.5 eV) can be assigned to metallic Pt. A weak peak appeared at 72.5 eV could be regarded as the chemical state of Pt(II) in Pt(OH)₂, and the other peak at 76.0eV might be halides. Chen et al. [206] reported a method to synthesize Pt catalyst on MWCNTs by polyol processes but without the addition of PVP, which has been reported to stabilize Pt particles preventing oxidation during synthesis. The XPS analysis result in their report showed an intense Pt oxidation state of PtO in the Pt catalyst; however, there is no such oxidation state found in our XPS analysis spectrum. This result indicates that surfaces of Pt particles during synthesis still need protection to prevent nanoparticles from oxidation.

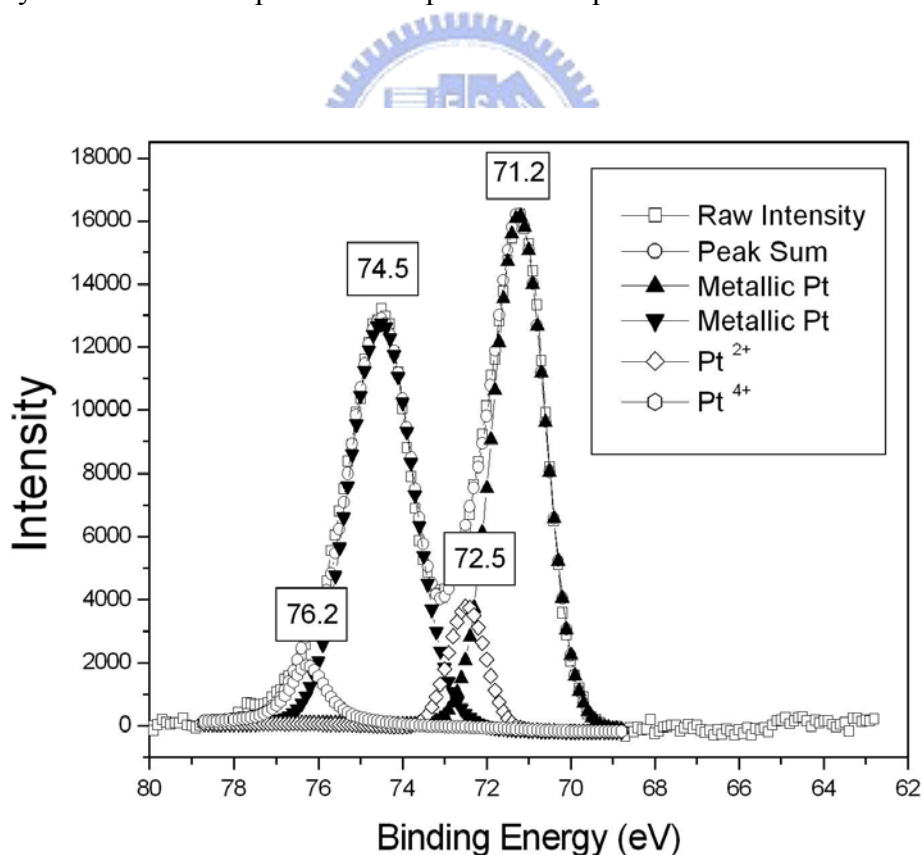


Fig. 5-35 XPS spectrum of Pt 4f peak of the microwave synthesized Pt particles on MWCNTs.

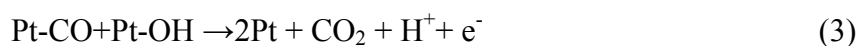
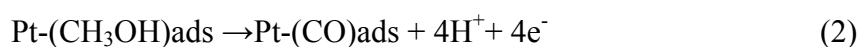
5.7 Electrochemical properties of Pt/MWCNTs electrode

The electrocatalytic activity of Pt catalyst was tested by cyclic voltammetry (CV) in electrolyte of 1.0M H₂SO₄ with a scan rate of 100 mV/s and is shown in Fig. 5-36. In the voltages between -0.2 and 0.2 V, several sharp peaks can be shown. H-adsorption and H-desorption peaks are observed during cathodic potential sweep. The H-desorption peaks between -0.2 and 0.2 V are also observed under anodic sweep [207]. By using the charge passed for H-adsorption Q_H, surface area of Pt (S_{Pt}) can be estimated from the equation below [208],

$$S_{Pt}/\text{cm}^2 = Q_H/210 (\mu\text{C}/\text{cm}^2) \quad (1)$$

The constant 210 in equation (1) is the surface charge density of Pt. Each electrode was taken with a triangular potential sweep (100 mV/s) between -0.2 and 1.1 V (vs. SCE) in 1 M H₂SO₄ solution to determine the surface area of Pt. Therefore, the calculated active surface area of Pt from Fig. 5-36 is 128 m²/g.

Shown in Fig. 5-37 are electrocatalytic activities of Pt/MWCNTs electrodes in methanol solution measured in a deaerated 2.0 M CH₃OH + 1.0 M H₂SO₄ solution between 0 and 1.0 V at the scan rate of 100 mV/s. Methanol-oxidation current peaks which represent the reactions of equation (2) and (3) [209] are clearly observed at 0.75 V in the anodic sweep and at 0.5 V in the cathodic sweep from all samples,



The current density of methanol oxidation of microwave-synthesized Pt/ MWCNTs at 0.75V is 138 mA/cm², which is higher than the previous results in our research team. Pt nanoparticles dispersed on MWCNTs by highly efficient microwave polyol method show higher utility than traditional method through mass efficiency comparison. This may be attributed to the high Pt surface area and the presence of open-end MWCNTs, in which Pt nanoparticles can uniformly be dispersed on MWCNTs in larger amount.

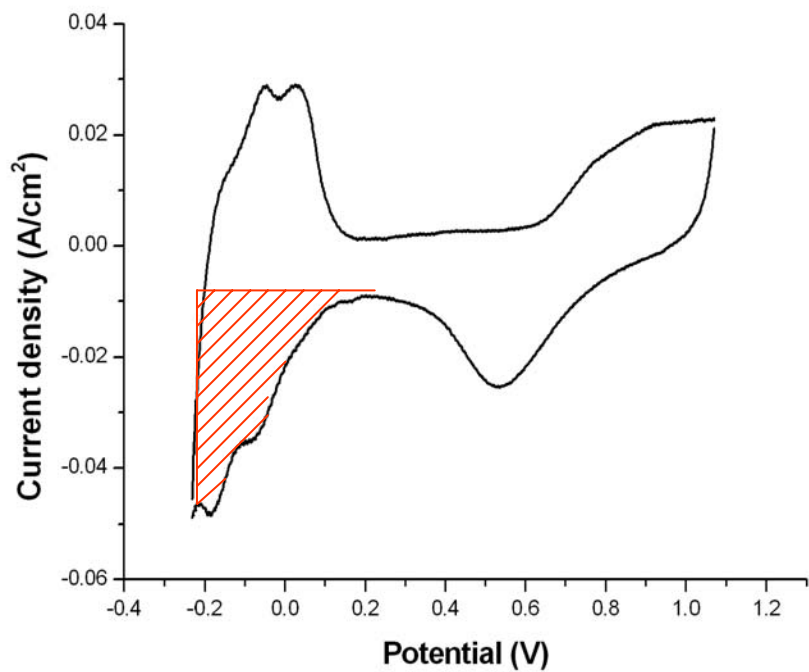


Fig. 5-36 The electrocatalytic activity of Pt catalyst was tested by cyclic voltammetry (CV) in electrolyte of 1.0M H₂SO₄.

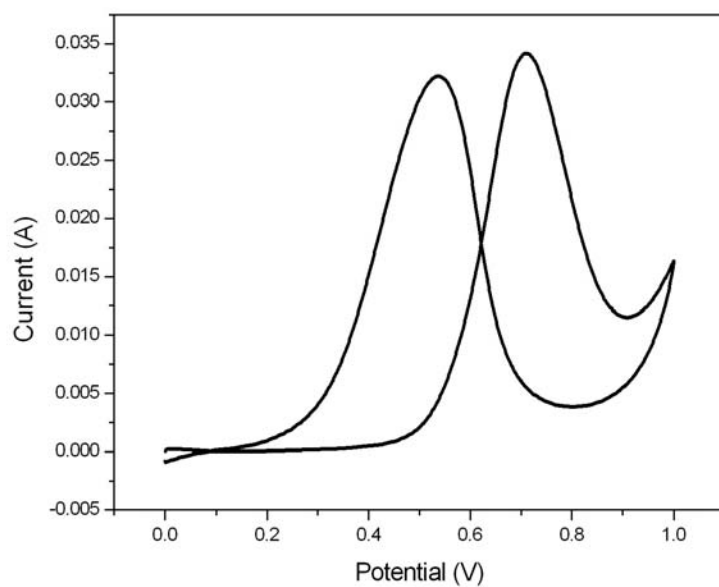


Fig. 5-37 Electrocatalytic activities of Pt/MWCNTs electrodes.

5.8 Conclusions of Microwave-assisted synthesis Pt/MWCNTs electrode

Pt nanoparticles on CNTs were prepared by rapid and uniform microwave heating, which provided a more homogeneous temperature gradient for the quick nucleation and growth of Pt particles. The effects of temperature and time on the synthesis of Pt in microwave-assisted methods were clarified by individual careful control of the two factors, and the results, first reported by this work, showed the domination of temperature over the reaction time. Pt/CNTs electrocatalysts with suitable narrow distribution size and highly dispersed Pt nanoparticles were synthesized by a one-step microwave-assisted polyol method by adding proper amount of SDS to the synthesis solution. It was found that SDS in the solution could be used as a good agent to wrap a lot of PVP-adsorbed Pt nanoparticles around MWCNTs side by side without particle agglomeration, and the loading of Pt on CNTs could exceed 50 wt%, higher than the 20 wt% or below of conventional or other microwave methods without SDS addition. The synthesis method proposed in this paper is simple and fast, and has great potential to be developed for the preparation of other high loading supported metal and alloy systems.

Chapter 6 Conclusions

First part presented in the research is purification of MWCNTs. The MWCNTs of high yield and no damage are obtained by microwave heating system with acid treatment. In the microwave system, acid rapidly absorbs microwave heat and energy and completely dissolve metals for purification without damage and of high quality. The processing time of the microwave-assisted and acid treated system to dissolve metals in MWCNTs is below one hour. After purification, the amounts of residual catalyst metals in samples reduced from 30wt% to 5.15wt% for ECR-synthesized MWCNTs. The results show that multi-walled carbon nanotubes of no damage and with metals about 5wt% are obtained.

Investigated of purification efficiency of MWCNTs synthesized by thermal chemical vapor deposition with different parameters by using TGA, SEM, TEM and Raman spectroscopy and MWCNTs of high purity are expected. The results show that the purification efficiency increases with increasing acid treatment time. The amount of residual catalysts in purified samples was reduced to 0.1% after digestion for 90 min at 210°C. Microwave heating method has excellent prospect to yield carbon nanotubes of high purity if carbon nanotubes are small and uniform in diameter. In conclusion, microwave heating method may have great potential in mass purification. Large amount of purified CNTs with high quality would be applied to more intrinsic studies and industrial applications.

The contents of metallic catalysts in the as-prepared MWCNTs can be effectively eliminated from 10.39 wt% to 1.515 wt% within 15 minute purification time at 120°C of 250W power. A possible reaction model was apparently proposed to describe this reaction, that is, the nano-scale metallic catalysts embedded at the tip end of MWCNTs could absorb microwave radiation energy in electromagnetic field by

magnetic resonance and interfacial electric polarization, and then form a localized hot area to combine with hot-surface effects around the tip-liquid interface of CNTs and significantly accelerate the reaction rate in the wall of CNTs near the tip.

Although microwave technology has been extensively applied in our daily life, there might be a great potential in microwave chemistry to apply microwave radiation energy on traditional chemical reaction processes. However, further intensive studies are expected to acquire complete understandings of the microwave-assisted chemical reaction.

In the second part of this thesis, Pt nanoparticles on CNTs were prepared by rapid and uniform microwave heating, which provided a more homogeneous temperature gradient for the quick nucleation and growth of Pt particles. The effects of temperature and time on the synthesis of Pt in microwave-assisted methods were clarified by individual careful control of the two factors, and the results, first reported by this work, showed the domination of temperature over the reaction time. Pt/CNTs electrocatalysts with suitable narrow distribution size and highly dispersed Pt nanoparticles were synthesized by a one-step microwave-assisted polyol method by adding proper amount of SDS to the synthesis solution. It was found that SDS in the solution could be used as a good agent to wrap a lot of PVP-adsorbed Pt nanoparticles around MWCNTs side by side without particle agglomeration, and the loading of Pt on CNTs could exceed 50 wt%, higher than the 20 wt% or below of conventional or other microwave methods without SDS addition. The synthesis method proposed in this paper is simple and fast, and has great potential to be developed for the preparation of other high loading supported metal and alloy systems.

References

- [1] M. S. Dresselhaus, G. Dresselhaus, P. C. Eklund, Boston (1996).
- [2] R. Saito, G. Dresselhaus, M. S. Dresselhaus, Imperial College Press, London (1998).
- [3] <http://smalley.rice.edu/images/allotropes.jpg>
- [4] R. Saito, M. Fujita, G. Dresselhaus, M. S. Dresselhaus, Appl. Phys. Lett. 60 (1992) 2204.
- [5] M. S. Dresselhaus, G. Dresselhaus, and R. Saito, Carbon, 33 (1995) 883.
- [6] S. Iijima, T. Ichihashi, Y. Ando, Nature 356 (1992) 776.
- [7] L. Chico, V.H. Crespi, L.X. Benedict, S.G. Louie, M.L. Cohen, Phys Rev Lett 76 (1996) 971.
- [8] J. M. Bonard, H. Kind, T. Stöckli, L. O. Nilsson, Solid State Electronics 45 (2001) 893.
- [9] E. T. Thostenson, Z. Ren, T. W. Chou, Composites Science and Technology 61 (2001) 1899.
- [10] K. Tanaka, K. Okahara, M. Okada, T. Yamabe, Chem. Phys. Lett. 191 (1992) 469.
- [11] S. Iijima, Nature 354 (1991) 56.
- [12] D. Bernaerts, M. Op De Beek, S. Amelinckx, J. Van Landuyt, G. Van Tendeloo, Philos. Mag. A 74 (1996) 723.
- [13] X. F. Zhang, X. B. Zhang, G. Van Tendeloo, S. Amelinckx, M. Op de Beek, J. Van Landuyt, J. Cryst. Growth 130 (1993) 3.
- [14] N. Hamada, S.-I. Sawada, A. Oshiyama, Phys. Rev. Lett. 68 (1992) 1579.
- [15] X. Blase, L.X. Benedict, E.L. Shirley, S.G. Louie, Phys. Rev. Lett. 72 (1994) 1878.

- [16] J.W. Mintmire, C.T. White, *Carbon* 33 (1995) 893.
- [17] C.L. Kane, E.J. Mele, *Phys. Rev. Lett.* 78 (1997) 1932.
- [18] P.R. Wallace, *Phys. Rev.* 71 (1947) 622.
- [19] J.W.G. Wildöer, L.C. Venema, A.G. Rinzler, R.E. Smalley, C. Dekker, *Nature* 391 (1998) 59.
- [20] T.W. Odom, J.L. Huang, P. Kim, C.M. Lieber, *Nature* 391 (1998) 62.
- [21] L.C. Venema, J.W.G. Wildöer, C. Dekker, A.G. Rinzler, R.E. Smalley, *Appl. Phys.* A 66 (1998) S153.
- [22] T.W. Odom, J.L. Huang, P. Kim, C.M. Lieber, *J. Phys. Chem. B* 104 (2000) 2794.
- [23] L.C. Venema, J.W.G. Wildöer, J.W. Janssen, S.J. Tans, H.L.J. Temminck Tuinstra, L.P. Kouwenhoven, C. Dekker, *Science* 283 (1999) 52.
- [24] P. Kim, T.W. Odom, J.-L. Huang, C.M. Lieber, *Phys. Rev. Lett.* 82 (1999) 1225.
- [25] S.J. Tans, A.R.M. Verschueren, C. Dekker, *Nature* 393 (1998) 49.
- [26] R. Martel, T. Schmidt, H.R. Shea, T. Hertel, Ph. Avouris, *Appl. Phys. Lett.* 73 (1998) 2447.
- [27] M. Bockrath, D.H. Cobden, P.L. McEuen, N.G. Chopra, A. Zettl, A. Thess, R.E. Smalley, *Science* 275 (1997) 1922.
- [28] S.J. Tans, M.H. Devoret, H. Dai, A. Thess, R.E. Smalley, L.J. Geerligs, C. Dekker, *Nature* 386 (1997) 474.
- [29] S.J. Tans, M.H. Devoret, R.J.A. Groeneveld, C. Dekker, *Nature* 394 (1998) 761.
- [30] M. Bockrath, D.H. Cobden, J. Lu, A.G. Rinzler, R.E. Smalley, L. Balents, P.L. McEuen, *Nature* 397 (1999) 598.
- [31] A. Bachtold, C. Strunk, J.-P. Salvetat, J.-M. Bonard, L. Forró, T. Nussbaumer, C. Schönenberger, *Nature* 397 (1999) 673.
- [32] H.T. Soh, C.F. Quate, A.F. Morpurgo, C.M. Marcus, J. Kong, H. Dai, *Appl. Phys.*

- Lett. 75 (1999) 627.
- [33] C. Schönenberger, A. Bachtold, C. Strunk, J.-P. Salvetat, L. Forró, Appl. Phys. A 69 (1999) 283.
- [34] J. Kong, C. Zhou, A. Morpurgo, H.T. Soh, C.F. Quate, C. Marcus, H. Dai, Appl. Phys. A 69 (1999) 305.
- [35] K. Liu, M. Burghard, S. Roth, P. Bernier, Appl. Phys. Lett. 75 (1999) 2494.
- [36] P.L. McEuen, M. Bockrath, D.H. Cobden, Y.-G. Yoon, S.G. Louie, Phys. Rev. Lett. 83 (1999) 5098.
- [37] H. Dai, E.W. Wong, C.M. Lieber, Science 272 (1996) 523.
- [38] L. Langer, V. Bayot, E. Grivei, J.-P. Issi, J.P. Heremans, C.H. Olk, L. Stockman, C. Van Haesendonck, Y. Bruynseraede, Phys. Rev. Lett. 76 (1996) 479.
- [39] T.W. Ebbesen, H.J. Lezec, H. Hiura, J.W. Bennett, H.F. Ghaemi, T. Thio, Nature 382 (1996) 54.
- [40] B.I. Yakobson, C.J. Brabec, J. Bernholc, Phys. Rev. Lett. 76 (1996) 2511.
- [41] B.I. Yakobson, G. Samsonidze, G.G. Samsonidze, Carbon 38 (2000) 1675.
- [42] M.M.J. Treacy, T.W. Ebbesen, T. M. Gibson, Nature 381 (1996) 678.
- [43] E.W. Wong, P.E. Sheehan, C.M. Lieber, Science 277 (1997) 1971.
- [44] D.A. Walters, L.M. Ericson, M.J. Casavant, J. Liu, D.T. Colbert, K.A. Smith, R.E. Smalley, Appl. Phys. Lett. 74 (1999) 3803.
- [45] M.-F. Yu, O. Lourie, M.J. Dyer, K. Moloni, T.F. Kelly, R.S. Ruoff, Science 287 (2000) 637.
- [46] M.-F. Yu, B.S. Files, S. Arepalli, R.S. Ruoff, Appl. Phys. Lett. 84 (2000) 5552.
- [47] [http:// 140.114.18.223/~heshih/diamond/nanotube.html](http://140.114.18.223/~heshih/diamond/nanotube.html) (2000).
- [48] Ajayan, P. M. and Zhou, O. Z., Carbon Nanotubes, 80 (2001) 391
- [49] Baughman, R. H., Zakhidov, A. A., and de Heer, W. A., Science, 297 (2002) 787
- [50] D.Rotman, Natuur & Techniek, 70 (2002) 30

- [51] S. Iijima, *Nature* 354 (1991) 56.
- [52] T.W. Ebbesen, P.M. Ajayan, *Nature* 358 (1992) 220.
- [53] S. Iijima, T. Ichihashi, *Nature* 363 (1993) 603.
- [54] D.S. Bethune, C.H. Klang, M.S. de Vries, G. Gorman, R. Savoy, J. Vazquez, R. Beyers, *Nature* 363 (1993) 605.
- [55] J. Abrahamson, P.G. Wiles, B.L. Rhoades, *Carbon* 37 (1999) 1873.
- [56] P.A. Thrower, *Carbon* 37 (1999) 1677.
- [57] X.K. Wang, X.W. Lin, V.P. Dravid, J.B. Ketterson, R.P.H. Chang, *Appl. Phys. Lett.* 66 (1995) 2430.
- [58] H. W. Kroto, J. R. Heath, S. C. O'Brien, R. F. Curl, R. E. Smalley, *Nature* 318 (1985) 162.
- [59] T. Guo, P. Nikolaev, A. Thess, D. T. Colbert, R. E. Smalley, *Chem. Phys. Lett.* 243 (1995) 49.
- [60] T. Guo, P. Nikolaev, A.G. Rinzler, D. Tománek, D.T. Colbert, R.E. Smalley, *J. Phys. Chem.* 99 (1995) 10694.
- [61] A. Thess, R. Lee, P. Nikolaev, H. Dai, P. Petit, J. Robert, C. Xu, Y.H. Lee, S.G. Kim, A.G. Rinzler, D.T. Colbert, G.E. Scuseria, D. Tománek, J.E. Fischer, R.E. Smalley, *Science* 273 (1996) 483.
- [62] A.G. Rinzler, J. Liu, H. Dai, P. Nikolaev, C.B. Huffman, F.J. Rodriguez-Macias, P.J. Boul, A.H. Lu, D. Heymann, D.T. Colbert, R.S. Lee, J.E. Fischer, A.M. Rao, P.C. Eklund, R.E. Smalley, *Appl. Phys. A* 67 (1998) 29.
- [63] B. I. Yakobson, R. E. Smalley, *Am. Sci.* 85 (1997) 324.
- [64] P.L. Walker Jr, J.F. Rakszawski, G.R. Imperial, *J. Phys. Chem.* 63 (1959) 133.
- [65] M.S. Kim, N. M. Rodriguez, R.T.K. Baker, *J. Catal.* 131 (1991) 60.
- [66] M. José-Yacamán, M. Miki-Yoshida, L. Rendón, J.G. Santiesteban, *Appl. Phys. Lett.* 62 (1993) 657.

- [67] V. Ivanov, J.B. Nagy, P. Lambin, A. Lucas, X.B. Zhang, X.F. Zhang, D. Bernaerts, G. Van Tendeloo, S. Amelinckx, J. Van Landuyt, *Chem. Phys. Lett.* 223 (1994) 329.
- [68] K. Hernadi, A. Fonseca, J.B. Nagy, D. Bernaerts, J. Riga, A. Lucas, *Synthetic Metals* 77 (1996) 31.
- [69] A. Fonseca, K. Hernadi, P. Piedigrosso, J.-F. Colomer, K. Mukhopadhyay, R. Doome, S. Lazarescu, L.P. Biro, Ph. Lambin, P.A. Thiry, D. Bernaerts, J.B. Nagy, *Appl. Phys. A* 67 (1998) 11.
- [70] P. Nikolaev, M.J. Bronikowski, R.K. Bradley, F. Rohmund, D.T. Colbert, K.A. Smith, R.E. Smalley, *Chem. Phys. Lett.* 313 (1999) 91.
- [71] J. Kong, A.M. Cassell, H. Dai, *Chem. Phys. Lett.* 292 (1998) 567.
- [72] M. Ge, K. Sattler, *Appl. Phys. Lett.* 64 (1994) 710.
- [73] G. Che, B.B. Lakshmi, C.R. Martin, E.R. Fisher, R.S. Rouff, *Chem. Mater.* 10 (1998) 260.
- [74] R. T. K. Baker, P. S. Harris, *Chem. Phys. Carbon* 14 (1978) 83.
- [75] S.B. Sinnott, R. Andrews, D. Qian, A.M. Rao, Z. Mao, E.C. Dickey, F. Derbyshire, *Chem. Phys. Lett.* 315 (1999) 25.
- [76] R. Andrews, D. Jacques, A.M. Rao, F. Derbyshire, D. Qian, X. Fan, E.C. Dickey, J. Chen, *Chem. Phys. Lett.* 303 (1999) 467.
- [77] R.T.K. Baker, *Carbon* 27 (1989) 315.
- [78] The first reference to microwave temperature-jump experiments can be found in 1967. Later an improved modification of this method was reported E F Caldin and J P Field, *J Chem Soc Faraday Trans I*, 78 (1982)1923
- [79] S W Liu and J P Wightman, *J Appl Chem Biotechnol*, 21 (1971)168
- [80] R N Gedye, W Rank and K C Westaway, *Can J Chem*, 69 (1991) 706
- [81] R Hicks and G Majetich, *J Microwave Power Electromagn Eng*, 30 (1995) 27

- [82] F. Fievet, J. P. Lagier, B. Blin, B. Beaudoin, M. Fiflarz, *Solid State Ionics*, 32/33 (1989)198.
- [83] a) P.-Y. Silvert, R. Herrera-Urbina; N. Duvauchelle, V. Vijayakrishnan, K. Tekaiia-Elhsissen, *J. Mater. Chem.*, 6 (1996) 573; b) P.-Y. Silvert, R. Herrera-Urbina, K. Tekaiia-Elhsissen, *J. Mater. Chem.*, 7 (1997) 293.
- [84] M. S. Hedge, D. Larcher, L. Dupont, B. Beaudoin, K. Tekaiia-Elhsissen, J. M. Tarascon, *Solid State Ionics*, 93 (1997) 33.
- [85] Y. Wada, H. Kuramoto, T. Sakata, H. Mori, T. Sumida, T. Kitamura, S. Yanagida, *Chem. Lett.*, 28 (1999) 607.
- [86] W. Tu, H. Liu, *J. Mater. Chem.*, 10 (2000) 2207.
- [87] Z. L. Jiang, Z. W. Feng, X. C. Shen, *Chin. Chem. Lett.*, 12 (2001) 551.
- [88] M. Tsuji, M. Hashimoto, T. Tsuji, *Chem. Lett.*, 31 (2002) 1232.
- [89] I. Pastoriza-Santos, L. Liz-Marz_n, *Langmuir*, 18 (2002) 2888.
- [90] S. Komarneni, D. Li, B. Newalkar, H. Katsuki, A. S. Bhalla, *Langmuir*, 18 (2002) 5959.
- [91] R. He, X. Qian, J. Yin, Z. Zhu, *J. Mater. Chem.*, 12 (2002) 3783.
- [92] R. He, X. Qian, J. Yin, Z. Zhu, *Chem. Phys. Lett.*, 369 (2003) 454.
- [93] F. K. Liu, C. J. Ker, Y. C. Chang, F. H. Ko, T. C. Chu, B. T. Dai, *Jpn. J. Appl. Phys. Part 1*, 42 (2003) 4152.
- [94] M. Tsuji, M. Hashimoto, Y. Nishizawa, T. Tsuji, *Chem. Lett.*, 32 (2003) 1114.
- [95] Y. J. Zhu, X. L. Hu, *Chem. Lett.*, 32 (2003) 1140.
- [96] R. Harpeness, A. Gedanken, A. M. Weiss, M. A. Slifkin, *J. Mater. Chem.*, 13 (2003) 2603.
- [97] T. Yamamoto, Y. Wada, T. Sakata, H. Mori, M. Goto, S. Hibino, S. Yanagida, *Chem. Lett.*, 33 (2004) 158.
- [98] M. Tsuji, Y. Nishizawa, M. Hashimoto, T. Tsuji, *Chem. Lett.*, 33 (2004) 370.

- [99] W. X. Chen, J. Zhao, J. Y. Lee, Z. L. Liu, *Chem. Lett.*, 33 (2004) 474.
- [100] F. Liu, Y. Chang, F. Ko, and T. Chu, *Mater. Lett.*, 58 (2004) 373.
- [101] Y. J. Zhu, X. L. Hu, *Mater. Lett.*, 58 (2004) 1517.
- [102] M. Tsuji, M. Hashimoto, Y. Nishizawa, T. Tsuji, *Mater. Lett.*, 58 (2004) 2326.
- [103] M. Tsuji, M. Hashimoto, Y. Nishizawa, T. Tsuji, *Hoshasen Kagaku, Radiation Chem.*, 77 (2004) 8
- [104] T. Yamamoto, H. Yin, Y. Wada, T. Kitamura, T. Sakata, H. Mori, S. Yanagida, *Bull. Chem. Soc. Jpn.*, 77 (2004) 757.
- [105] O. Palchik, R. Kerner, A. Gedanken, A. M. Weiss, M. A. Slifkin, V. Palchik, J. *Mater. Chem.*, 11 (2001) 874.
- [106] Y. Wada, H. Kuramoto, J. Anand, T. Kitamura, T. Sakata, H. Mori, S. Yanagida, *J. Mater. Chem.*, 11 (2001) 1936.
- [107] T. Yamamoto, Y. Wada, H. Yin, T. Sakata, H. Mori, S. Yanagida, *Chem. Lett.*, 31 (2002) 964.
- [108] T. Ding, J. Zhang, S. Long, J. Zhu, *Microelectron. Eng.*, 66 (2003) 46.
- [109] H. Grisar, O. Palchik, A. Gedanken, V. Palchik, M. A. Slifkin, A. M. Weiss, *Inorg. Chem.*, 42 (2003) 7148.
- [110] Z. L. Liu, X. Y. Ling, J. Y. Lee, X. D. Su, L. M. Gan, *J. Mater. Chem.*, 13 (2003) 3049.
- [111] Z. L. Liu, J. Y. Lee, W. X. Chen, M. Han, L. M. Gan, *Langmuir*, 20 (2004) 181.
- [112] R. Harpeness, A. Gedanken, *Langmuir*, 20 (2004) 3431.
- [113] *Microwave-Enhanced Chemistry: Fundamentals, Sample Preparation, Applications* (Eds.: H. M. Kingston, S. J. Haswell), American Chemical Society, Washington DC, 1997.
- [114] S. A. Galema, *Chem. Soc. Rev.*, 26 (1997) 233.

- [115] R. Andrews, D. Jacques, D. Qian, E. C. Dickey, *Carbon* 39 (2001) 1681.
- [116] P. X. Hou, S. Bai, Q. H. Yang, C. Lin, H. M. Cheng, *Carbon* 40 (2002) 81.
- [117] M. Yumura, S. Ohshima, K. Uchida, Y. Tasaka, Y. Kuriki, F. Ikazaki, Y. Saito, S. Uemura, *Diamond and Relat. Mater.* 8 (1999) 785.
- [118] Y. Saito, K. Hamaguchi, K. Hata, K. Tohji, A. Kasuya, Y. Nishina, K. Uchida, Y. Tasaka, F. Ikazaki, M. Yumura, *Ultramicroscopy* 73 (1998) 1.
- [119] Y. Ando, X. Zhao, H. Kataura, Y. Achiba, K. Kaneto, M. Tsuruta, S. Uemura, S. Iijima, *Diamond and Relat. Mater.* 9 (2000) 847.
- [120] Y. S. Park, Y. C. Choi, K. S. Kim, D. C. Chung, D. J. Bae, K. H. An, S. C. Lim, X. Y. Zhu, Y. H. Lee, *Carbon* 39 (2001) 655.
- [121] S.C. Tsang, P.J.F. Harris, M.L.H. Green, *Nature* 362(1993) 520.
- [122] T. Y. Ebbesen, P. M. Ajaya, F. H. Liou, H. Hiura, K. Tangaki, *Nature* 367(1997) 519.
- [123] K. Tohji, H. Takahashi, Y. Shinoda, N. Shimizu, B. Jeyadevan, I. Matsuoka, Y. Saito, A. Kasuya, S. Ito, Y. Nishina, *J. Phys. Chem. B* 101(1997) 1974.
- [124] B. Liu, T. Wagberg, E. Olssen, R. Yang, H. Li, S. Zhang, H. Yang, G. Zou, B. Sundqvist, *Chem. Phys. Lett.* 321(2000)365.
- [125] K.B. Shelimov, R. O. Esenaliev, A. G. Rinzler, C. B. Huffman, R. E. Smalley, *Chem. Phys. Lett.* 282(1998) 429.
- [126] J. M. Moon, K. H. An, Y. H. Lee, Y. S. Park, D. J. Bae, G. S. Park, *J. Phys. Chem. B* 105(2001) 5677.
- [127] M. Zhang, M. Yudasaka, A. Koshio, S. Iijima, *Chem. Phys. Lett.* 349 (2001) 25.
- [128] D. Chattopadhyay, I. Galeska, F. Papadimitrakopoulos, *Carbon* 40 (2002) 985.
- [129] X. H. Chen, C. S. Chen, Q. Chen, F. Q. Cheng, G. Zhang, Z. Z. Chen, *Materials Lett.* 57(2002) 734.
- [130] H. Kajiura, S. Tsutsui, H. Huang, Y. Murakami, *Chem. Phys. Lett.* 364 (2002)

586.

- [131] S. Bandow, A. M. Rao, K. A. Williams, A. Thess, R. E. Smalley, P. C. Eklund, J. Phys. Chem. B, 101 (1997) 8839.
- [132] Y. Ando, X. Zhao, S. Inoue, S. Iijima, Journal of Crystal Growth 237-239 (2002) 1926.
- [133] I. W. Chiang, B. E. Brinson, A. Y. Huang, P. A. Willis, M. J. Bronikowski, J. L. Margrave, R. E. Smalley, R. H. Hauge, J. Phys. Chem. B 105 (2001) 8297.
- [134] US EPA Method 3051, "Microwave-Assisted Acid Digestion of Sediments, Sludges, Soils and Oils", Washington DC, (1994)
- [135] K. A. Mauritz, C. J. Hora, A. J. Hopfinger, Advances in Chemistry 187 (1980) 124
- [136] H. L. Yeager, A. J. Steck, Electrochem. Soc. 128 (1981) 1880
- [137] A. Eisenberg, B. Hird, R. B. Moore, "A new multiplet-cluster model for the morphology of random ionomers", Macromolecules 23 (1990) 4098
- [138] T. D. Gierke, G. E. Munn, F. C. Wilson, J. Polym. Sci. 19 (1981) 1687
- [139] G. B. Butler, K. F. O'Driscoll, G. L. Wilkes, Chem. Phys. C 34 (1994) 325
- [140] A. Eisenberg and H. L. Yeager, ACS Symp. Ser. No. 180, American Chemical Society: Washington, DC, (1982) pp. 1-6, 41-63,
- [141] L. A. Utracki and R. A. Weiss, ACS Symp. Ser. No. 395; American Chemical Society: Washington, DC, (1989) 401
- [142] A. Eisenberg and M. King, Ion-Containing Polymers: Physical Properties and Structure, Vol. 2, (1977) 163
- [143] W. Y. Hsu, T. D. Gierke, Macromolecules 15 (1982) 101
- [144] A. V. Anantaraman, C. L. Gardner, "Studies on ion-exchange membranes. Part 1. Effect of humidity on the conductivity of Nafion®", J. Electroanal. Chem. 414 (1996) 115

- [145] C. S. Kim, Y. G. Chun, D. H. Peck, D. R. Shin, “ A novel process to fabricate membrane electrode assemblies for proton exchange membrane fuel cells “ Int. J. Hydrogen Energy 23 (1998) 1045
- [146] D. Bevers, N. Wagner, M. VonBradke, “ Innovative production procedure for low cost PEFC electrodes and electrode/membrane structures “ Int. J. Hydrogen Energy 24 (1998) 57
- [147] L. Giorgi, E. Antolini, A. Pozio, E. Passalacqua, “Influence of the PTFE content in the diffusion layer of low-Pt loading electrodes for polymer electrolyte fuel cells ”, Electrochim. Acta 43, (1998) 3675
- [148] H. S. Wroblowa, Y. C. Pan, G. J. Razumnet, Electroanal. Chem. 69, 195, 1976.
- [149] A. J. Appleby, M. J. Savy, Electroanal. Chem., 92 (1978) 15
- [150] R. W. Zurilla, R. K. Sen, E. J. Yeager, Electrochem. Soc. 125 (1978) 1103
- [151] Gruver, G. A.; Pascoe, R. F.; Kunz, H. R. J. Electrochem. Soc. 127 (1980) 1219
- [152] M. C. Lefebvre, Z. Qi, P. G. Pickup, ” Electronically Conducting Proton Exchange Polymers as Catalyst Supports for Proton Exchange Membrane Fuel Cells. Electrocatalysis of Oxygen Reduction, Hydrogen Oxidation, and Methanol Oxidation”, J. Electrochem. Soc. 146 (1999) 2054
- [153] J. Shan, P. G. Pickup, ” Characterization of polymer supported catalysts by cyclic voltammetry and rotating disk voltammetry ”, Electrochim. Acta 46 (2000) 119
- [154] I. D. Raistri, Symposium on Diaphragms, Separators, and Ion-Exchange Membranes, Pennington, NJ (1986) 172
- [155] S. Srinivasan, D. J. Manko, H. Koch, M. A. Enayetullah, A.J. Appleby, “Recent advances in solid polymer electrolyte fuel cell technology with low platinum loading electrodes ”, J. Power Sources, 29 (1990) 367
- [156] S. Hirano, J. Kim, S. Srinivasan, ” High performance proton exchange

- membrane fuel cells with sputter-deposited Pt layer electrodes”, *Electrochim. Acta* 42 (1997) 1587
- [157] S. Y. Cha, W. M. Lee, ” Performance of Proton Exchange Membrane Fuel Cell Electrodes Prepared by Direct Deposition of Ultrathin Platinum on the Membrane Surface”, *J. Electrochem. Soc.* 146 (1999) 4055
- [158] A. Hamnett, “Mechanism and electrocatalysis in the direct methanol fuel cell “, *Catal. Today* 38 (1997) 445
- [159] S. Wasmus, A. Kuver, “Methanol oxidation and direct methanol fuel cells: a selective review”, *J. Electroanal. Chem.* 461 (1999) 14
- [160] T. Matsumoto, T. Komatsu, K. Arai, T. Yamazaki, M. Kijima, H. Shimizu, Y. Takasawa, J. Nakamura, “Reduction of Pt usage in fuel cell electrocatalysts with carbon nanotube electrodes”, *Chem. Commun.* 7 (2004) 840
- [161] W. Y. Yu, W. X. Tu, H. F. Liu, *Langmuir* 15 (1999) 6.
- [162] W. X. Tu, H. F. Liu, *Chem. Mater.* 12 (2000) 564.
- [163] V. Mehta, J. S. Cooper, *J. Power Sources* 114 (2003) 32.
- [164] E. Antolini, *Mater. Chem. Phys.* 78 (2003) 563.
- [165] T. S. Armadi, Z. L. Wang, T. C. Green, A. Henglein, M. A. El-Sayed, *Science* 272 (1996) 1924.
- [166] J. Kiwi, M. Gratzel, *J. Am. Chem. Soc.* 101 (1979) 7214.
- [167] G. Schmid, *Chem. Rev.* 92 (1992) 1709.
- [168] M. Brust, M. Walker, D. Bethell, D. J. Schiffrin, R. Whyman, *J. Chem. Soc., Chem. Commun.* 7 (1994) 801.
- [169] K. Y. Chan, J. Ding, J. Ren, S. Cheng, K. Y. Tsang, *J. Mater. Chem.* 14 (2004) 505.
- [170] Z. L. Liu, J. Y. Lee, M. Han, W. X. Chen, L. M. Gan, *J. Mater. Chem.* 12 (2002) 2453.

- [171] Y. H. Lin, X. L. Cui, C. H. Yen, C. M. Wai, *Langmuir* 21 (2005) 11474.
- [172] K. Okitsu, A. Yue, S. Tanabe, H. Matsumoto, *Chem. Mater.* 12 (2000) 3006.
- [173] T. Fujimoto, S. Teraushi, H. Umehara, I. Kojima, W. Henderson, *Chem. Mater.* 13 (2001) 1057.
- [174] L. K. Kurihara, G. M. Chow, P. E. Schoen, *Nanostruct. Mater.* 5 (1995) 607.
- [175] F. Bonet, V. Delmas, S. Grugeon, R. H. Urbina, P. Y. Silvert, K. Tekaiia-Elhsissen, *Nanostruct. Mater.* 11 (1999) 1277.
- [176] C. L. Sun, L. C. Chen, M. C. Su, L. S. Hong, O. Chyan, C. Y. Hsu, K. H. Chen, T. F. Chang, L. Chang, *Chem. Mater.* 17 (2005) 3749.
- [177] <http://www.milestonesci.com/dig-products.php>
- [178] <http://www.tainstruments.com/product.aspx?id=20&n=1&siteid=11>
- [179] A. C. Dillon, T. Gennett, K. M. Jones, J. L. Alleman, P. A. Parilla, and M. J. Heben, *Adv. Mater.* 11 (1999) 1354.
- [180] J. F. Colomer, P. Piedigrosso, A. Fornseca, *Synth. Met.* 103 (1999) 2482.
- [181] V. Lordi, S. X. C. Ma, and N. Yao: *Surface Science* 421 (1999) 150.
- [182] R. N. Gedye, W. Rank, and K. C. Westaway: *Can. J. Chem.* 69 (1991) 706.
- [183] R. Hicks, and G. Majetich: *J. Microwave Power Electromagn. Eng.* 30 (1995) 27.
- [184] F. K. Liu, C. J. Ker, Y. C. Chang, F. H. Ko, T. C. Chu, and B. T. Dai: *Jpn. J. Appl. Phys. Part 1* 42 (2003) 4152.
- [185] M. Tsuji, M. Hashimoto, Y. Nishizawa, and T. Tsuji: *Chem. Lett.* 32 (2003) 1114.
- [186] M. Tsuji, M. Hashimoto, Y. Nishizawa, and T. Tsuji: *Radiation Chem.* 77 (2004) 8.
- [187] Y. J. Zhu, and X. L. Hu: *Chem. Lett.* 32 (2003) 1140.
- [188] F. Liu, Y. Chang, F. Ko, and T. Chu: *Mater. Lett.* 58 (2004) 373.

- [189] R. He, X. Qian, J. Yin, and Z. Zhu: *J. Mater. Chem.* 12 (2002) 3783.
- [190] M. Tsuji, M. Hashimoto, Y. Nishizawa, M. Kubokawa, and T. Tsuji: *Chem. Eur. J.* 11 (2005) 440.
- [191] R. Laurent, A. Laportene, J. Dubac, J. Berlan, S. Lefeuvre, and M. Audhuy : *J. Org. Chem.* 57 (1992) 7099.
- [192] A. Wadhawan, D. Garret, and J. M. Perez: *Appl. Phys. Lett.* 83 (2003) 2683.
- [193] J. Cheng, R. Roy, and D. Agrawal: *J. Mater. Sci. Lett.* 20 (2001) 1561.
- [194] D. Michael, P. Mingos, and D. R. Baghurst: *Chem. Soc. Rev.* 20 (1991) 1.
- [195] R. Roy, D. Agrawal, J. Cheng, and S. Gedevisanishvili: *Nature* 399 (1999) 668.
- [196] C. G. Koops: *Phys. Rev.* 83 (1951) 121.
- [197] P. A. Miles, W. B. Westphal, and A. von Hippel: *Rev. Mod. Phys.* 29 (1957) 279.
- [198] S. Ruan, B. Xu, H. Suo, F. Wu, S. Xiang, and M. Zhao: *J. Magn. Magn. Mater.* 212 (2000) 175.
- [199] C. M. Chen, M. Chen, F. C. Leu, S. Y. Hsu, S. C. Wang, S. C. Shi, C. F. Chen, *Diam. Relat. Mater.* 13 (2004) 1182.
- [200] C. M. Chen, M. Chen, Y. W. Peng, C. H. Lin, L. W. Chang, C. F. Chen, *Diam. Relat. Mater.* 14 (2005) 798.
- [201] Y. T. Kim, T. Mitani, *J. Catal.* 238 (2006) 394.
- [202] S. Mukerjee, J. McBreen, *J. Electroanal. Chem.* 448 (1998)163.
- [203] B. Xue, P. Chen, Q. Hong, J. Y. Lin, K. L. Tan, *J. Mater. Chem.* 11 (2001) 2378.
- [204] C. Ma, C. Li, *J. Colloid Interface Sci.* 131 (1989) 485
- [205] V. V. Didenko, V. C. Moore, D. S. Baskin, R. E. Smalley, *Nano Lett.* 5 (2005) 1563.
- [206] W. Chen, J. Zhao, J. Y. Lee, Z. Liu, *Mater. Chem. Phys.* 91 (2005) 124.
- [207] Minoru Umeda, Mitsuhiro Kokubo, Mohamed Mohamedi and Isamu Uchida,

Electrochimica Acta 10 (2003) 1367

[208] S.Kerkeni, E. Lamy-Pitara, J.Barbier, Catal. Today 75 (2002) 35

[209] H. Wang, T. Loffler, H. Baltruschat, J. Appl. Electrochem. 31 (2001) 759

